THE PHYSICAL SOCIETY

MEMOIRS

OF THE

COLLEGE OF SCIENCE

UNIVERSITY OF KYOTO

SERIES A

VOL. XXVII, No. 3

September 1955

KYOTO

Digitized by the Internet Archive
in 2024

https://archive.org/details/memoirs-faculty-science-kyoto-phys-astro-geophys-chem_1955-09_27_3

MEMOIRS OF THE COLLEGE OF SCIENCE, University of Kyoto, Series A,
Vol. XXVII, No. 3, Article 1, 1955

THE INFLUENCE OF VORTICES UPON THE DRAG EXPERIENCED BY AN ELLIPTIC CYLINDER MOVING THROUGH AN INVISCID LIQUID

BY

S. TOMOTIKA and H. FUJIKAWA

(*Received January 10, 1954*)

SUMMARY

Assuming the existence of a vortex-pair behind an elliptic cylinder moving with a constant velocity through an unlimited mass of an incompressible inviscid fluid in a direction perpendicular to the axis of the cylinder as well as to the major-axis of its cross-section, the drag experienced by the cylinder is discussed.

To this end, the complex velocity potential for the flow around the elliptic cylinder is first obtained in terms of elliptic coordinates, and the drag acting on the cylinder is then computed in two different ways: namely, (i) by directly summing up the fluid pressures acting on the surface of the body, and (ii) by applying the theorem of momentum to an infinite mass of fluid surrounding the cylinder.

As we should have expected, one and the same expression for the drag on the cylinder is obtained, irrespective of the method of computation.

1. Introduction

It is well known that when a cylinder with arbitrary cross-sectional shape is moving, with an appropriate velocity, through a fluid, two or more discrete vortices are created in its wake and in consequence the pressure distribution over the surface of the body differs greatly, especially in the rear part of the body, from that computed on the basis of the theory of continuous flow of an incompressible inviscid fluid.

Assuming two symmetrically disposed vortices of equal strength κ, with circulations in the senses indicated, at two points A and B in the wake of a circular cylinder as shown in Fig. 1, Föppl (**1**) and Bickley (**2**) computed independently the drag acting on a circular cylinder. The former calculated the drag by applying the theorem of momentum to an unlimited mass of fluid surrounding the body, while the latter obtained the drag by directly summing up the fluid pressures over the surface of the cylinder.

According to Bickley, the drag X experienced by a circular cylinder is expressed in the form:

$$X=2\kappa\rho\left\{u_A\frac{a^2}{c^2}\sin 2\gamma+v_A\left(1-\frac{a^2}{c^2}\right)\cos 2\gamma\right\}, \tag{1.1}$$

where u_A, v_A are the x- and y-components of the velocity of vortex A, a the radius of the cylinder, c the distance of vortices A and B from the centre O of the cylinder, 2γ the angle AOB and ρ the density of the fluid concerned.

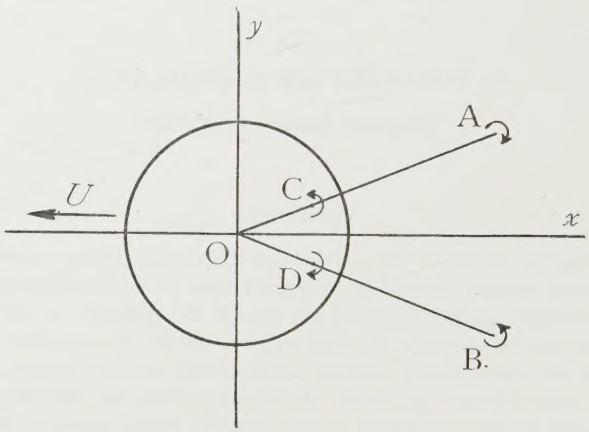

Fig. 1.

If we introduce the rectangular components of the velocities of image vortices C and D at the inverse points of A and B with respect to the circular cylinder respectively (Fig. 1), which are connected with u_A and v_A as:

$$\left.\begin{aligned} u_C&=-\frac{a^2}{c^2}(u_A\cos 2\gamma+v_A\sin 2\gamma), \\ v_C&=-\frac{a^2}{c^2}(u_A\sin 2\gamma-v_A\cos 2\gamma), \\ u_D&=u_C, \qquad v_D=-v_C, \end{aligned}\right\} \tag{1.2}$$

the expression (1.1) for X becomes

$$X=2\kappa\rho(v_A-v_C), \tag{1.3}$$

which, on taking account of the obvious relations:

$$v_A=\frac{d}{dt}(c\sin\gamma), \quad v_C=\frac{d}{dt}\left(\frac{a^2}{c}\sin\gamma\right), \tag{1.4}$$

can ultimately be written in the form:

$$X=2\kappa\rho\frac{d}{dt}\left\{\left(c-\frac{a^2}{c}\right)\sin\gamma\right\}. \tag{1.5}$$

It is to be noted here that Föppl's formula for the drag on a circular cylinder differs from the above Bickley's formula (1.5). Namely, using the same notations as above, Föppl's formula takes the form:

$$X=3\kappa\rho\frac{d}{dt}\left\{\left(c-\frac{a^2}{c}\right)\sin\gamma\right\}. \tag{1.6}$$

The cause of the discrepancy between Föppl's and Bickley's formulae was discussed by Sugawara and the senior writer in 1938 (**3**). In computing the drag experienced by a circular cylinder accompanied by a vortex-pair in its wake, both the direct method as used by Bickley of summing up the fluid pressures acting on the surface of the body and the indirect method as employed by Föppl of applying the theorem of momentum to an infinite mass of fluid surrounding the cylinder were employed.* Thus, it has been shown there that Bickley's formula is correct, but Föppl's one is erroneous.

The corresponding problem for the case of an elliptic cylinder was treated by Sanuki and Arakawa in 1931 by applying the theorem of momentum (**4**). However, the expression for the drag on a circular cylinder as deduced, as a limiting form, from their formula for the drag on an elliptic cylinder is neither in accord with Föppl's formula nor with Bickley's. In effect, in the same notations as above, their formula gives the following formula:

$$X=\kappa\rho\frac{d}{dt}\left\{\left(c-\frac{a^2}{c}\right)\sin\gamma\right\} \tag{1.7}$$

for the drag experienced by a circular cylinder.

The object of the present paper is to compute the drag acting on an elliptic cylinder moving, with a constant velocity U, through an unlimited mass of an incompressible inviscid fluid in a direction perpendicular to the axis of the cylinder as well as to the major-axis of its cross-section, by assuming the existence of a vortex-pair behind the cylinder.

For the computation of the drag on the body, two different methods are both employed as in our old paper (**3**) cited before: namely, the drag is calculated (i) by using the direct method of summing up the fluid pressures acting on the surface of the cylinder, and (ii) by applying the theorem of momentum to an infinite mass of fluid surrounding the body. Thus, as we should have expected, one and the same expression for the drag is obtained, which gives, as its limiting case, the correct Bickley's formula for the drag on a dircular cylinder. The sources of error in Sanuki and Arakawa's formula are indicated.

---

* Recently it has been found out that in our paper (**3**) cited above, there are some errors in the course of analysis developed on the basis of the theorem of momentum, but fortunately the final result there given needs no alteration. For drawing our attention to these errors, we should like to express our cordial thanks to Dr. K. Tamada. The correct analysis will be given briefly in Appendix of the present paper.

I. Calculation of the Drag by summing up the Fluid Pressures acting on an Elliptic Cylinder

2. The complex velocity potential

In the first place, we shall calculate the drag experienced by an elliptic cylinder by directly summing up the fluid pressures acting on the surface of the body. Adopting the usual artifice, we shall consider a stationary elliptic cylinder placed in a uniform stream of velocity U flowing in the positive direction of the x-axis. We consider the case where the major-axis of the ellipse lies on the y-axis, the origin of the coordinate-axes being taken at the centre of the ellipse.

Now, it is convenient to introduce the elliptic coordinates (ξ, η) connected with the rectangular coordinates (x, y) as:

$$\left.\begin{aligned} x+iy &= c\sinh(\xi+i\eta), \\ z &= c\sinh\zeta. \\ (0<\xi<\infty, \quad -\pi<\eta<\pi) & \end{aligned}\right\} \quad \text{or} \qquad (2.1)$$

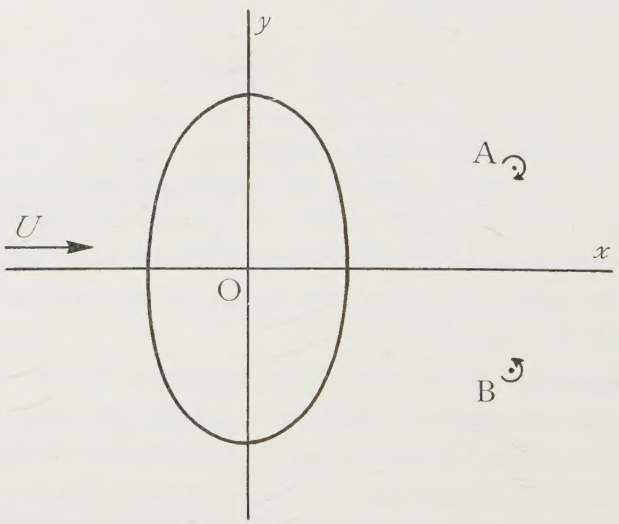

Fig. 2.

We assume that the elliptic cylinder under consideration is defined by $\xi=\xi_1$. Since the two vortices A and B, of strength κ with circulations in the senses as indicated in Fig. 2, are symmetrically situated with respect to the x-axis, we can define their positions (x_A, y_A) and (x_B, y_B) as (ξ_0, η_0) and $(\xi_0, -\eta_0)$ respectively. Thus, we have

$$\left.\begin{aligned} x_A &= x_B = c\sinh\xi_0\cos\eta_0, \\ y_A &= -y_B = c\cosh\xi_0\sin\eta_0. \end{aligned}\right\} \qquad (2.2)$$

The complex velocity potential w for the flow around the elliptic cylinder consists of two parts: one part, w_1 say, is the complex velocity potential for the continuous uniform stream past the cylinder, while the other, w_2 say, is the complex velocity potential for the vortex motion. The former can be expressed as:

$$w_1 = Uce^{\xi_1}\cosh(\zeta-\xi_1), \tag{2.3}$$

and, after several calculations, the latter can be determined as (**6**):

$$w_2 = \frac{\kappa}{2\pi i}\log\frac{\cosh(\zeta-\xi_1)-\cosh(\bar{\zeta}_0-\xi_1)}{\cosh(\zeta-\xi_1)-\cosh(\zeta_0-\xi_1)}, \tag{2.4}$$

where $\bar{\zeta}_0$ denotes the conjugate complex of ζ_0.

Thus, the required complex velocity potential w becomes

$$w = Uce^{\xi_1}\cosh(\zeta-\xi_1)+\frac{\kappa}{2\pi i}\log\frac{\cosh(\zeta-\xi_1)-\cosh(\bar{\zeta}_0-\xi_1)}{\cosh(\zeta-\xi_1)-\cosh(\zeta_0-\xi_1)}, \tag{2.5}$$

or

$$w = \frac{1}{2}Uc(e^{\zeta}+e^{2\xi_1-\zeta})+\frac{\kappa}{2\pi i}\log\frac{(e^{\zeta}-e^{\bar{\zeta}_0})(e^{\zeta}-e^{2\xi_1-\bar{\zeta}_0})}{(e^{\zeta}-e^{\zeta_0})(e^{\zeta}-e^{2\xi_1-\zeta_0})}. \tag{2.6}$$

Separating the real and imaginary parts on both sides, we have the velocity potential ϕ and the stream function ψ in the forms:

$$\phi = Uce^{\xi_1}\cosh(\xi-\xi_1)\cos\eta+\frac{\kappa}{2\pi}\left\{\tan^{-1}\frac{\sinh(\xi_0-\xi_1)\sin(\eta_0+\eta)}{\cosh(\xi-\xi_1)-\cosh(\xi_0-\xi_1)\cos(\eta_0+\eta)}\right.$$
$$\left.+\tan^{-1}\frac{\sinh(\xi_0-\xi_1)\sin(\eta_0-\eta)}{\cosh(\xi-\xi_1)-\cosh(\xi_0-\xi_1)\cos(\eta_0-\eta)}\right\}, \tag{2.7}$$

$$\psi = Uce^{\xi_1}\sinh(\xi-\xi_1)\sin\eta$$
$$+\frac{\kappa}{4\pi}\log\frac{\{\cosh(\xi-\xi_0)-\cos(\eta-\eta_0)\}\{\cosh(\xi+\xi_0-2\xi_1)-\cos(\eta+\eta_0)\}}{\{\cosh(\xi-\xi_0)-\cos(\eta+\eta_0)\}\{\cosh(\xi+\xi_0-2\xi_1)-\cos(\eta-\eta_0)\}}. \tag{2.8}$$

3. The velocities of the vortices

Making use of either of the above expressions for the velocity potential ϕ and the stream function ψ, the fluid velocity at any point not coinciding with either of the vortices can easily be obtained. Thus, if we denote the velocity components perpendicular to and along an ellipse $\xi=$const by v_ξ and v_η respectively, we have

$$v_\xi = \frac{1}{h}\frac{\partial\psi}{\partial\eta}, \qquad v_\eta = -\frac{1}{h}\frac{\partial\psi}{\partial\xi}, \tag{3.1}$$

where $h=c\sqrt{\cosh^2\xi-\sin^2\eta}$.

In order to obtain the velocity of a vortex, e.g. the vortex $(-\kappa)$ at A, itself, however, we must first subtract from ψ the stream function ψ_A due to this vortex alone. Thus, the velocity components $[v_\xi]_A$, $[v_\eta]_A$ of the vortex $(-\kappa)$ at A (ξ_0, η_0) can be obtained by differentiating $\psi-\psi_A$ by ξ and η respectively, and we have

$$
\left.\begin{aligned}
[v_\xi]_A &= \frac{1}{c\sqrt{\cosh^2\xi_0-\sin^2\eta_0}}\Big[Uce^{\xi_1}\sinh(\xi_0-\xi_1)\cos\eta_0 \\
&\quad+\frac{\kappa}{4\pi}\Big\{\frac{\sin 2\eta_0}{\cosh 2(\xi_0-\xi_1)-\cos 2\eta_0}-\frac{\sin 2\eta_0}{1-\cos 2\eta_0}+\frac{\sin 2\eta_0}{\cosh 2\xi_0+\cos 2\eta_0}\Big\}\Big], \\
[v_\eta]_A &= \frac{1}{c\sqrt{\cosh^2\xi_0-\sin^2\eta_0}}\Big[-Uce^{\xi_1}\cosh(\xi_0-\xi_1)\sin\eta_0 \\
&\quad+\frac{\kappa}{4\pi}\Big\{\frac{\sinh 2(\xi_0-\xi_1)}{\cosh 2(\xi_0-\xi_1)-1}-\frac{\sinh 2(\xi_0-\xi_1)}{\cosh 2(\xi_0-\xi_1)-\cos 2\eta_0}+\frac{\sinh 2\xi_0}{\cosh 2\xi_0+\cos 2\eta_0}\Big\}\Big].
\end{aligned}\right\} \tag{3.2}
$$

On account of the symmetry, the velocity components $[v_\xi]_B$, $[v_\eta]_B$ of the vortex (κ) at B $(\xi_0, -\eta_0)$ are given by

$$
[v_\xi]_B=[v_\xi]_A, \qquad [v_\eta]_B=-[v_\eta]_A. \tag{3.3}
$$

For later use the rectangular components of velocities of the vortices will also be calculated. It can readily be seen that the rectangular components of velocity u_A, v_A of the vortex $(-\kappa)$ at A are connected with $[v_\xi]_A, [v_\eta]_A$ as:

$$
\left.\begin{aligned}
u_A &= \frac{c}{h_0}\cosh\xi_0\cos\eta_0[v_\xi]_A-\frac{c}{h_0}\sinh\xi_0\sin\eta_0[v_\eta]_A, \\
v_A &= \frac{c}{h_0}\sinh\xi_0\sin\eta_0[v_\xi]_A+\frac{c}{h_0}\cosh\xi_0\cos\eta_0[v_\eta]_A,
\end{aligned}\right\} \tag{3.4}
$$

where $h_0=c\sqrt{\cosh^2\xi_0-\sin^2\eta_0}$. Or, remembering the obvious relations that

$$
[v_\xi]_A=h_0\frac{d\xi_0}{dt}, \qquad [v_\eta]_A=h_0\frac{d\eta_0}{dt}, \tag{3.5}
$$

the expressions for u_A, v_A can be put in the forms:

$$
\left.\begin{aligned}
u_A &= \frac{d}{dt}(c\sinh\xi_0\cos\eta_0), \\
v_A &= \frac{d}{dt}(c\cosh\xi_0\sin\eta_0).
\end{aligned}\right\} \tag{3.6}
$$

Substituting the values of $[v_\xi]_A, [v_\eta]_A$ as given by (3.2) into the right-hand sides of (3.4), we have, after several calculations,

$$
\left.\begin{aligned}
u_A &= \frac{1}{\cosh 2\xi_0+\cos 2\eta_0}\Big[Ue^{\xi_1}\{\sinh(2\xi_0-\xi_1)-\sinh\xi_1\cos 2\eta_0\} \\
&\quad+\frac{\kappa}{\pi c}\Big\{\frac{\cosh(2\xi_0-\xi_1)\cosh(\xi_0-\xi_1)}{\cosh 2(\xi_0-\xi_1)-\cos 2\eta_0}\sin\eta_0-\frac{\cosh\xi_0}{2\sin\eta_0} \\
&\quad-\frac{\sin\eta_0}{\sinh(\xi_0-\xi_1)}\frac{\sinh(2\xi_0-\xi_1)\sinh^2\xi_0+\sinh\xi_1\cos^2\eta_0}{\cosh 2\xi_0+\cos 2\eta_0}\Big\}\Big], \\
v_A &= \frac{\cos\eta_0}{\cosh 2\xi_0+\cos 2\eta_0}\Big[-2Ue^{\xi_1}\cosh\xi_1\sin\eta_0 \\
&\quad+\frac{2\kappa}{\pi c}\sin^2\eta_0\Big\{\frac{1}{\cosh 2(\xi_0-\xi_1)-\cos 2\eta_0}\frac{\cosh(2\xi_0-\xi_1)}{2\sinh(\xi_0-\xi_1)}+\frac{\sinh\xi_0}{\cosh 2\xi_0+\cos 2\eta_0}\Big\}\Big].
\end{aligned}\right\} \tag{3.7}
$$

On account of the symmetry, the rectangular components of velocity u_B, v_B of the vortex (κ) at B are given by

$$u_B = u_A, \qquad v_B = -v_A. \tag{3.8}$$

4. Calculation of the force acting on the cylinder

We next proceed to the calculation of the drag experienced by the elliptic cylinder ($\xi = \xi_1$) under consideration by directly summing up the fluid pressures acting on the cylinder. The pressure distribution over the surface of the cylinder can be calculated by the well-known pressure equation, namely:

$$p = F(t) - \frac{1}{2}\rho q^2 - \rho\frac{\partial \phi}{\partial t}. \tag{4.1}$$

If we denote the x- and y-components of the force acting on the cylinder by X and Y respectively, we have (**7**)

$$\begin{aligned} X - iY &= -i\oint p\, d\bar{z} \\ &= \frac{1}{2} i\rho \oint \left(\frac{dw}{dz}\right)^2 dz + i\rho \frac{d}{dt}\oint \bar{w}\, d\bar{z}, \end{aligned} \tag{4.2}$$

where $\bar{w}$ denotes the conjugate complex of w, and both the two integrals are taken, in the counter-clockwise sense, once round the circumference of the cylinder.

After some calculations, the first term on the right-hand side of (4.2), which we denote simply by F_q, can be evaluated as:

$$\begin{aligned} F_q &= \frac{1}{2} i\rho \oint \left(\frac{dw}{dz}\right)^2 dz \\ &= 2\kappa\rho \frac{\cos \eta_0}{\cosh 2\xi_0 + \cos 2\eta_0}\Bigg[-2Ue^{\xi_1} \cosh \xi_1 \sin \eta_0 \\ &\quad + \frac{2\kappa}{\pi c} \sin^2 \eta_0 \left\{ \frac{1}{\cosh 2(\xi_0 - \xi_1) - \cos 2\eta_0} \frac{\cosh (2\xi_0 - \xi_1)}{2 \sinh (\xi_0 - \xi_1)} + \frac{\sinh \xi_0}{\cosh 2\xi_0 + \cos 2\eta_0} \right\} \Bigg]. \end{aligned} \tag{4.3}$$

Comparing this with the expression for v_A as given by (3.7), we have

$$F_q = 2\kappa\rho\, v_A, \tag{4.4}$$

which, with the help of (3.6), may also be written as:

$$F_q = 2\kappa\rho c \frac{d}{dt}(\cosh \xi_0 \sin \eta_0). \tag{4.5}$$

Next, the second term on the right-hand side of (4.2), which we denote simply by F_ϕ, can be evaluated as:

$$\begin{aligned} F_\phi &= i\rho \frac{d}{dt}\oint \bar{w} d\bar{z} = i\rho \frac{d}{dt}\oint \bar{w}_2 d\bar{z} \\ &= -2\kappa\rho c \frac{d}{dt}(e^{\xi_1 - \xi_0} \cosh \xi_1 \sin \eta_0), \end{aligned} \tag{4.6}$$

where $\bar{w}_2$ is the conjugate complex of w_2 which is given by (2.4) and denotes the complex velocity potential for the vortex motion. In terms of the velocity components u_A, v_A of the vortex $(-\kappa)$ at A, the value of F_ϕ can also be expressed in the form:

$$F_\phi=\frac{2\kappa\rho e^{\xi_1}\cosh\xi_1}{\cosh 2\xi_0+\cos 2\eta_0}\{(u_A\sin 2\eta_0-v_A\cos 2\eta_0)-v_A e^{-2\xi_0}\}\,. \tag{4.7}$$

Thus, making use of the values of F_q and F_ϕ as given by (4.5) and (4.6) respectively, we have, by (4.2),

$$\left.\begin{aligned} X&=2\kappa\rho c e^{\xi_1}\frac{d}{dt}\{\sinh(\xi_0-\xi_1)\sin\eta_0\}\,,\\ Y&=0\,. \end{aligned}\right\} \tag{4.8}$$

Further, if we use the values of F_q and F_ϕ as given by (4.4) and (4.7) respectively, the drag X can also be expressed in the form:

$$X=\frac{2\kappa\rho e^{\xi_1}}{\cosh 2\xi_0+\cos 2\eta_0}[u_A\cosh\xi_1\sin 2\eta_0+v_A\{\sinh(2\xi_0-\xi_1)-\sinh\xi_1\cos 2\eta_0\}]\,, \tag{4.9}$$

and when the values of u_A and v_A as given by (3.7) are substituted, this becomes ultimately

$$X=\frac{4\kappa^2\rho}{\pi c}e^{\xi_1}\cosh\xi_1\cos\eta_0\frac{\cosh(3\xi_0-2\xi_1)\sin^2\eta_0-\cosh\xi_0\sinh^2(\xi_0-\xi_1)}{\{\cosh 2(\xi_0-\xi_1)-\cos 2\eta_0\}(\cosh 2\xi_0+\cos 2\eta_0)^2}\,. \tag{4.10}$$

It will be seen that in case when the vortices lie on a curve* defined by

$$\sin\eta_0=\sqrt{\frac{\cosh\xi_0\sinh^2(\xi_0-\xi_1)}{\cosh(3\xi_0-2\xi_1)}}\,, \tag{4.11}$$

the cylinder does not experience any drag.

II. Application of the Theorem of Momentum to the Calculation of the Drag

5. The forces acting on the cylinder

We next proceed to the calculation of the drag experienced by the elliptic cylinder ($\xi=\xi_1$) under consideration, by applying this time the theorem of momentum to an infinite mass of fluid surrounding the cylinder as in the papers by Föppl (**1**) and by Sanuki and Arakawa (**4**).

We take the coordinate-axes (x, y) as shown in Fig. 2 and we assume that the cylinder is moving with a constant velocity U in an unlimited perfect fluid in the

* This is the equation for the locus of equilibrium positions of the vortices (**5**), and is easily obtained by eliminating κ from the following two equations:

$$[v_\xi]_A=0\,,\quad [v_\eta]_A=0\,.$$

negative direction of the x-axis. Then, with the same notation as before, the complex velocity potential w for the flow around the elliptic cylinder ($\xi=\xi_1$) under consideration is given by

$$w=w_1+w_2\,, \tag{5.1}$$

where

$$w_1=\frac{1}{2}\,Uc(e^{2\xi_1-\zeta}+e^{-\zeta})\,, \tag{5.2}$$

$$w_2=\frac{\kappa}{2\pi i}\log\frac{(e^{\zeta}-e^{\bar{\zeta}_0})(e^{\zeta}-e^{2\xi_1-\bar{\zeta}_0})}{(e^{\zeta}-e^{\zeta_0})(e^{\zeta}-e^{2\xi_1-\bar{\zeta}_0})}\,. \tag{5.3}$$

Now, as shown in Fig. 3, we take an elliptic contour C_1 just round the elliptic cylinder under consideration, a contour C_2 round the cut connecting the two points A, B and a large circular contour C_3 enclosing the whole system, and we assume that these three contours are connected by some straight lines as shown in the figure.

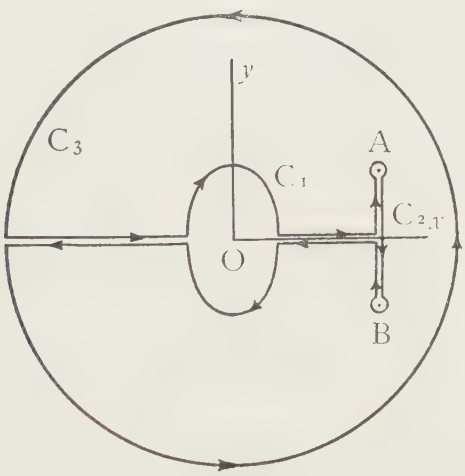

Fig. 3.

If, as before, we denote the x- and y-components of the resultant force acting on the cylinder by X and Y respectively, then by applying the theorem of momentum to the fluid in the region S enclosed by the three contours C_1, C_2, C_3, we have

$$X=-\frac{d}{dt}\iint_S \rho u\,dx\,dy-\oint_{C_3}\rho u v_n\,ds-\oint_{C_3}p\cos(n,x)\,ds\,, \tag{5.4}$$

$$Y=-\frac{d}{dt}\iint_S \rho v\,dx\,dy-\oint_{C_3}\rho v v_n\,ds-\oint_{C_3}p\cos(n,y)\,ds\,, \tag{5.5}$$

where n denotes the outward normal to the contour C_3, ds is the line-element along the contour C_3 reckoned positive in the counter-clockwise sense, and v_n is the velocity component normal to the element ds.

Since, however, it is obvious on account of the symmetry that $Y=0$, it suffices to consider the drag X only.

Remembering that $u=\partial\phi/\partial x$ and applying Green's theorem, we can transform the surface integral $\iint_S \rho u\,dx\,dy$ into a line integral taken, in the counter-clockwise sense, along the closed contour enclosing the region S, which consists of the three contours C_1, C_2, C_3 and some straight lines connecting them (Fig. 3). We then have

$$\iint_S \rho u\,dx\,dy=\iint_S \rho\frac{\partial\phi}{\partial x}dx\,dy=\left(\oint_{C_1}+\oint_{C_2}+\oint_{C_3}\right)\rho\phi\cos(n,x)ds\,. \tag{5.6}$$

Thus, making use of the pressure equation (4.1), the drag X is expressed as:

$$\begin{aligned} X \quad & -\frac{d}{dt}\left\{\left(\oint_{C_1}+\oint_{C_2}\right)\rho\phi\cos(n,x)ds\right\} \\ & -F(t)\oint_{C_3}\cos(n,x)ds+\frac{1}{2}\rho\oint_{C_3}q^2\cos(n,x)\,ds-\rho\oint_{C_3}uw_n ds\,. \end{aligned} \tag{5.7}$$

However, the integral $\oint_{C_3}\cos(n,x)ds$ evidently vanishes, and it can easily be shown that both the last two integrals tend to zero as the large circular contour C_3 recedes away to infinity. Also, it is found that the velocity potential $\phi_1=\Re(w_1)$ contributes nothing to the first two integrals in the brackets. Thus, we finally obtain

$$X=\frac{dI}{dt}\,, \tag{5.8}$$

where

$$I=-\left\{\left(\oint_{C_1}+\oint_{C_2}\right)\rho\phi_2\cos(n,x)ds\right\}, \tag{5.9}$$

where ϕ_2 denotes the velocity potential for the vortex motion alone.

6. Evaluation of the drag

Our next problem is to evaluate the two line integrals in (5.9). After simple calculations the first integral becomes

$$\oint_{C_1}\rho\phi_2\cos(n,x)ds=-\rho c\cosh\xi_1\int_{-\pi}^{\pi}[\phi_2]_{\xi_1}\cos\eta\,d\eta\,, \tag{6.1}$$

where $[\phi_2]_{\xi_1}$ denotes the value of the function ϕ_2 on the surface of the elliptic cylinder $\xi=\xi_1$.

After various calculations we find however that

$$\int_{-\pi}^{\pi}[\phi_2]_{\xi_1}\cos\eta\,d\eta=\Re\int_{-\pi}^{\pi}[w_2]_{\xi_1}\cos\eta\,d\eta=-2\kappa e^{\xi_1-\xi_0}\sin\eta_0\,. \tag{6.2}$$

Therefore we have

$$\oint_{C_1}\rho\phi_2\cos(n,x)ds=2\kappa\rho c e^{\xi_1-\xi_0}\cosh\xi_1\sin\eta_0\,. \tag{6.3}$$

On the other hand, the remaining second integral can easily be evaluated by noticing that the value of ϕ_2 on the right-hand side of the cut AB exceeds the value of ϕ_2 on the left-hand side by the cyclic constant κ. Thus, denoting the y-coordinate of the point A by y_A, we have

$$\oint_{C_2} \rho\phi_2 \cos(n, x)ds = -2\kappa\rho y_A$$
$$= -2\kappa\rho c \cosh\xi_0 \sin\eta_0. \tag{6.4}$$

Hence, we get finally

$$I - 2\kappa\rho c e^{\xi_1} \sinh(\xi_0 - \xi_1) \sin\eta_0, \tag{6.5}$$

and the expression for the drag X experienced by the elliptic cylinder ($\xi = \xi_1$) under consideration becomes

$$X = 2\kappa\rho c e^{\xi_1} \frac{d}{dt}\{\sinh(\xi_0 - \xi_1) \sin\eta_0\}. \tag{6.6}$$

It will be seen that, as we should have expected, this formula is in perfect agreement with the previous one which has been obtained by directly summing up the fluid pressures acting on the elliptic cylinder ($\xi = \xi_1$).

III. A Limiting Case

7. The drag on a circular cylinder

As an addendum, we shall lastly derive from the preceding result the expression for the drag on a circular cylinder accompanied by two symmetrically disposed vortices in its wake. We denote the radius of the circular cylinder by a and the distance of the vortices from the axis of the cylinder by r_0. Then, making, in (4.8) or (6.6), c to tend to zero and both ξ_0, ξ_1 to infinity at the same time in such a manner that ce^{ξ_0} and ce^{ξ_1} become equal to $2r_0$ and $2a$ respectively, we obtain the expression for the drag on the circular cylinder. Thus, we have

$$X = 2\kappa\rho \frac{d}{dt}\left\{\left(r_0 - \frac{a^2}{r_0}\right)\sin\eta_0\right\}.$$

It is readily found that except for the difference in notation, this is in perfect agreement with the correct formula (1.5) for the drag on a circular cylinder.

Appendix

Note on the Influence of Vortices upon the Drag of a Circular Cylinder moving through a Fluid

In a paper (3) published as early as 1938, Sugawara and the senior writer calculated the drag experienced by a circular cylinder moving, with a constant velocity, through an incompressible perfect fluid, assuming the existence of two symmetrically disposed vortices in its wake. Two different methods of calculating the drag were employed. In one method the drag was obtained by summing up the pressures exerted by the fluid upon the surface of the circular cylinder, while in the other it was calculated by applying the theorem of momentum to an infinite mass of fluid surrounding the cylinder.

Recently Dr. K. Tamada has kindly drawn our attention to some errors in our paper cited above which are found in the course of analysis developed on the basis of the theorem of momentum, though fortunately the final result there given needs no alteration. The correct analysis will now be given.

1. We assume that a circular cylinder of radius a is moving with constant velocity U through an incompressible inviscid fluid in the negative direction of the x-axis, and we also assume that the cylinder is accompanied by two symmetrically disposed vortices with strength κ in its wake.

Referring to Fig. 1 in our 1938 paper, the complex velocity potential w for the flow outside the cylinder is given by*

$$w = U\frac{a^2}{z} + \frac{\kappa}{2\pi i}\log\frac{(z-z_C)(z-z_B)}{(z-z_A)(z-z_D)}, \tag{1}$$

where $z_A(=ce^{i\gamma})$ and $z_B(=ce^{-i\gamma})$ are the complex coordinates of the vortices A and B in the fluid, while z_C and z_D are the complex coordinates of the corresponding image vortices C and D in the circular cylinder, i. e. $z_C=(a^2/c)e^{i\gamma}$ and $z_D=(a^2/c)e^{-i\gamma}$.

We take a closed contour similar to that as shown in Fig. 3 in the preceding pages, with only one difference that an elliptic contour C_1 there is now replaced by a circular contour C_1 of radius a. Thus, we take a closed contour Σ which consists of a circular contour C_1 of radius a coinciding with the circular cylinder under consideration, a contour C_2 round the cut connecting the two points A, B and a large circular contour C_3 of radius R enclosing the whole system, and some straight lines connecting these three contours.

Then, if we denote the drag experienced by the circular cylinder by X, we

* It will be noted that the velocity potential ϕ is here defined as $\mathbf{v}=\text{grad}\ \phi$, while in our 1938 paper we defined it as $\mathbf{v}=-\text{grad}\ \phi$.

have, by applying the theorem of momentum to the fluid in the region S enclosed by the above-mentioned closed contour Σ,

$$X=-\frac{d}{dt}\iint_S \rho u\,dx\,dy-\oint_{C_3}\rho u v_n ds-\oint_{C_3} p\cos(n,x)ds, \tag{2}$$

where n denotes the outward normal to the contour C_3, ds is the line-element along the contour C_3 reckoned positive in the counter-clockwise sense, and v_n is the velocity component normal to the element ds.

Remembering that $u=\partial\phi/\partial x$ and applying Green's theorem, we can transform the surface integral $\iint_S \rho u\,dx\,dy$ into a line integral taken, in the counter-clockwise sense, along the closed contour Σ. Thus, we have

$$\iint_S \rho u\,dx\,dy=\iint_S \rho\frac{\partial\phi}{\partial x}dx\,dy=\left(\oint_{C_1}+\oint_{C_2}+\oint_{C_3}\right)\rho\phi\cos(n,x)ds. \tag{3}$$

Therefore

$$X=-\frac{d}{dt}\left\{\left(\oint_{C_1}+\oint_{C_2}+\oint_{C_3}\right)\rho\phi\cos(n,x)ds\right\}-\oint_{C_3}\rho u v_n ds-\oint_{C_3} p\cos(n,x)ds. \tag{4}$$

It can easily be shown that the integral $\oint_{C_3}\rho u v_n ds$ tends to zero as the large circular contour C_3 recedes away to infinity. Also, since U is assumed to be constant, it is found that the velocity potential $\phi_1=\Re(Ua^2/z)$ contributes nothing to the three integrals in the brackets as well as to the last integral. Thus, making use of the pressure equation (4.1) and remembering that $\oint_{C_3}\cos(n,x)ds=0$ and that the integral $\oint_{C_3} q^2\cos(n,x)ds$ vanishes as C_3 recedes away to infinity, we obtain

$$X=-\frac{d}{dt}\left\{\left(\oint_{C_1}+\oint_{C_2}+\oint_{C_3}\right)\rho\phi_2\cos(n,x)ds\right\}+\rho\int_{-\pi}^{\pi}\frac{\partial\phi_2}{\partial t}\cos\theta\cdot Rd\theta, \tag{5}$$

where

$$\phi_2=\Re\left[\frac{\kappa}{2\pi i}\log\frac{(z-z_C)(z-z_B)}{(z-z_A)(z-z_D)}\right]=\frac{\kappa}{2\pi}\Im\left[\log\frac{(z-z_C)(z-z_B)}{(z-z_A)(z-z_D)}\right]. \tag{6}$$

We shall now evaluate the four integrals in (5). First, from our 1938 paper, we find that

$$\left(\oint_{C_1}+\oint_{C_2}\right)\rho\phi_2\cos(n,x)ds=-2\kappa\rho\left(c-\frac{a^2}{c}\right)\sin\gamma. \tag{7}$$

The remaining two integrals can be evaluated as follows. On the circular contour C_3 we have $z=Re^{i\theta}$ and therefore remembering that $z_A=ce^{i\gamma}$, $z_B=ce^{-i\gamma}$, $z_C=(a^2)e^{i\gamma}$, and $z_D=(a^2/c)e^{-i\gamma}$ we have

$$\log(z-z_A)=\log R+i\theta-\frac{c}{R}e^{i(\gamma-\theta)}+O\left(\frac{1}{R^2}\right),$$

$$\log(z-z_B)=\log R+i\theta-\frac{c}{R}e^{-i(\gamma+\theta)}+O\left(\frac{1}{R^2}\right),$$

$$\log(z-z_C)=\log R+i\theta-\frac{a^2}{cR}e^{i(\gamma-\theta)}+O\left(\frac{1}{R^2}\right),$$

$$\log(z-z_D)=\log R+i\theta-\frac{a^2}{cR}e^{-i(\gamma+\theta)}+O\left(\frac{1}{R^2}\right).$$

Thus, we have

$$\phi_2=\frac{\kappa}{2\pi}\left(c-\frac{a^2}{c}\right)\frac{1}{R}\{\sin(\gamma+\theta)+\sin(\gamma-\theta)\}+O\left(\frac{1}{R^2}\right)$$
$$=\frac{\kappa}{\pi}\left(c-\frac{a^2}{c}\right)\frac{1}{R}\sin\gamma\cos\theta+O\left(\frac{1}{R^2}\right), \tag{8}$$

and hence we have,* when $R\to\infty$,

$$\int_{-\pi}^{\pi}\phi_2\cos\theta\cdot Rd\theta=\kappa\left(c-\frac{a^2}{c}\right)\sin\gamma. \tag{9}$$

This gives immediately

$$\rho\int_{-\pi}^{\pi}\frac{\partial\phi_2}{\partial t}\cos\theta\cdot R\,d\theta=\kappa\rho\frac{d}{dt}\left\{\left(c-\frac{a^2}{c}\right)\sin\gamma\right\}. \tag{10}$$

Also, we have

$$\oint_{C_3}\rho\phi_2\cos(n,x)ds=\int_{-\pi}^{\pi}\rho\phi_2\cos\theta\cdot R\,d\theta$$
$$=\kappa\rho\left(c-\frac{a^2}{c}\right)\sin\gamma. \tag{11}$$

Thus, we get finally

$$X=2\kappa\rho\frac{d}{dt}\left\{\left(c-\frac{a^2}{c}\right)\sin\gamma\right\}. \tag{12}$$

2. The drag X can also be evaluated in an alternative manner as follows. If use is made of the pressure equation (4.1) in (4), we have

$$X=-\frac{d}{dt}\left\{\left(\oint_{C_1}+\oint_{C_2}\right)\rho\phi\cos(n,x)ds\right\}$$
$$-F(t)\oint_{C_3}\cos(n,x)ds+\frac{1}{2}\rho\oint_{C_3}q^2\cos(n,x)ds-\rho\oint_{C_3}uw_n ds. \tag{13}$$

The integral $\oint_{C_3}\cos(n,x)ds$ evidently vanishes, and it can easily be shown that both the last two integrals tend to zero as the large circular contour C_3 recedes away to infinity. Thus, since, as mentioned before, the velocity potential ϕ_1 contributes nothing to the first two integrals in the brackets, we obtain

$$X=-\frac{d}{dt}\left\{\left(\oint_{C_1}+\oint_{C_2}\right)\rho\phi_2\cos(n,x)ds\right\}, \tag{14}$$

* In our 1938 paper we have erroneously mentioned that $\int_{-\pi}^{\pi}\phi_2\cos\theta\cdot Rd\theta$ evidently vanishes when $R\to\infty$.

and therefore, by (7), we get ultimately

$$X=2\kappa\rho\frac{d}{dt}\left\{\left(c-\frac{a^2}{c}\right)\sin\gamma\right\}. \tag{15}$$

REFERENCES

1. L. Föppl, 'Wirbelbewegung hinter einem Kreiszylinder'. Sitzungsber. d. Bayr. Akad. d. Wiss., math.-phys. Klasse, (1913), 1.
2. W. G. Bickley, 'The influence of vortices upon the resistance experienced by solids moving through a liquid'. Proc. Roy. Soc. A, **119** (1928), 146.
3. S. Tomotika and N. Sugawara, 'Note on the influence of vortices upon the resistance of a circular cylinder moving through a fluid'. Proc. Phys.-Math. Soc. Japan [3] **20** (1938), 467.
4. M. Sanuki and H. Arakawa, 'Mechanism of the vortex motion behind an elliptic cylinder'. Proc. Phys.-Math. Soc. Japan [3] **13** (1931), 201.
5. S. Tomotika, 'On the vortex motion behind an elliptic cylinder in a stream and some allied problems'. Proc. Phys.-Math. Soc. Japan [3] **13** (1931), 191.
6. A. B. Basset, *A Treatise on Hydrodynamics*, Vol. 2 (1888), pp. 50–51.
7. L. M. Milne-Thomson, *Theoretical Hydrodynamics* (1949), pp. 163–164.

MEMOIRS OF THE COLLEGE OF SCIENCE, University of Kyoto, Series A,
Vol. XXVII, No. 3, Article 2, 1955

SEISMOMETRIC INVESTIGATION OF THE EARTH'S INTERIOR
PART II. ON THE STRUCTURE OF THE EARTH'S CRUST

BY
Yoshimichi KISHIMOTO

(Received March 2, 1955)

ABSTRACT

The structure of the earth's crust was determined by an analysis of the refracted seismic waves of shallow earthquakes propagated along the discontinuous surfaces in the earth's crust. The presumed structure was ascertained, on the other hand, mainly by the study of the transformed waves in earthquakes of deep focus. The structure of the earth's crust thus obtained around Kyoto was found to be composed of four distinct layers of different property whose thickness and propagation velocity of *P*- and *S*-waves are respectively, listing from the earth's surface to the deeper layers, 1.5 km and 3.8, 2.2 km/sec for the sedimentary layer; 6 km and 5.4, 3.1 km/sec for the granitic layer; 14 km and 5.8, 3.4 km/sec for the granodioritic layer; 10 km and 7.0, 4.0 km/sec for the basaltic layer. The velocities of *P*- and *S*-waves of the layer underlying the basaltic layer were estimated to be nearly 8.1 km/sec and 4.7 km/sec, respectively.

Also in this article the regional differences in the crustal structure, especially the local character of the thickness of the basaltic layer, were discussed in some detail, and moreover the correlation between the regional differences of the crustal structure and the focal depths of shallow earthquakes in their respective area is mentioned.

1. Introduction

The seismometric investigation of the structure of the earth's crust was begun early by A. Mohorovičić in his pioneering study of the Kulpa Valley Earthquake of October 8, 1909 (**1**). He confirmed the existence of a sharp discontinuous boundary named the Mohorovičić discontinuity which seismometrically separates the earth's crust from the underlying mantle. Since the discovery of the Mohorovičić discontinuity the crustal structure has been investigated more and more in detail by many researchers such as, for example, B. Gutenberg (**2**), H. Jeffreys (**3**), V. Conrad (**4**) and others who made great contributions to the development of our knowledge in the many-layered structure of the earth's crust.

On the other hand the seismometric investigation of the crustal structure by artificial explosions, which was commenced by O. Hecker on the Oppau Explosion of September 21, 1921 (**5**, **6**, **7**), has become greatly active parallel with that of natural

earthquakes. And after the Second World War the seismometric investigations of the crust with artificial explosions have had a wonderful development in recent years in succession of the great artificial explosion on April 18, 1948 at Heligoland.

In reflection upon the forty years' progress of the seismometric investigation of the crust through natural earthquakes and artificial explosions, the many important facts on the structure and property of the earth's crust have certainly been made clear, but, on the other hand, many more essential and attractive problems on the nature of the crust have been presented in the course of research, and they remain, for the most part, unsolved and are awaiting future development in research. Needless to say, such problems are never completely solved by the seismometric method only, and therefore synthetic investigations are strongly recommended combining the seismometric method with those of gravimetry, structural geology, laboratory experiment of rock under high pressure and temperature, theoretical treatment of physical state and property of rock at deep underground as well as other effective types of research.

In the following, a short review will be made of some interesting problems concerning the crustal structure proposed and discussed in comparatively recent times. In U.S.A. especially in the Eastern District (New England and others) and the Western District (California), the crustal structure has been studied in detail by means of natural earthquakes and artificial cxplosions, and two different values were assigned by some researchers for the velocity of P-wave in the granitic layer such as 5.6 km/sec from the analysis of natural earthquakes and 6.1 km/sec from those of artificial explosions. But P. Byerly (8, **9**) contends that the velocity is determined in California as nearly same value of 5.6 km/sec from both natural and artificial shocks. Also L. Don Leet (**10**, **11**, **12**) proposed a consistent value of about 6 km/sec for the P-velocity in the granitic layer derived from both methods and attributed the inconsistency formerly discussed mainly to the personal misinterpretation of seismic waves. On the other hand, B. Gutenberg, in his early investigation, had an opinion (**13**) on this problem of inconsistency between the velocity values derived from the natural earthquakes and artificial explosions that there exists a sedimentary layer of high velocity ($V_p > 6$ km/sec) overlying the granitic layer of velocity ($V_p \approx 5.6$ km/sec), but recently he proposed an entirely different crustal structure from the former conception (**14**, **15**, **16**, **17**, **18**). Namely he assumed the existence of comparatively low velocity layers at depths 15 km and 80 km below the ground surface, and by such crustal structures explained not only the inconsistency of velocity values derived from both natural and artificial shocks but also gave a different interpretation to the seismic waves which were formerly considered as refracted waves (forerunners) propagated along the crustal discontinuity. Although his theory of low velocity layers is in itself a very attractive and suggestive postulation, it yet contains too many question-

able points to be generally approved. The difficulties are considered to exist in such points as, for example, an unpractical assumption that earthquakes concerned should occur mainly in the low velocity layer, a complex mode of seismic wave-propagation which is somewhat unreasonable in the point of curvature of trajectory of seismic wave, especially at the small epicentral distance, and some other matters. But this theory of low velocity layer in the earth's crust is certainly an interesting and promising idea which relates to the original formation and secular change of the earth's crust, and may be applicable to, though invalid in the case of a problem affecting the whole earth, any particular region such as, for example, a volcanically and seismically active area, the magmatic reservoir and other allied structures being reasonably considered to exist underneath their ground surfaces. This theory should be earnestly examined, in near future, from various standpoints of research. On the problem of inconsistency of obtained values of seismic velocity from natural and artificial shocks, A. Kubotera (**19**) explained it from the standpoint of the rheological property of the crust, and D. S. Hughes and J. H. Cross (**20**) discussed the difference between the velocity values of rocks determined by laboratory experiments and those obtained by natural earthquakes.

In Japan the systematic and detailed observations of seismic waves aroused by five artificial explosions successively fired in 1950–1953 in Northern Honshû (at Isibuti and Kamaisi) (**21**, **22**, **23**, **24**, **25**) should be highly appreciated and their obtained velocities are listed in the last of this paragraph, the velocity of the upper layer being somewhat more highly estimated compared with that of other districts in our country. The seismometric investigation of the earth crust made by T. Matuzawa (**26**, **27**, **28**, **29**) from the analysis of natural earthquakes has been the most comprehensive and detailed in Japan, the obtained results being also listed in the last. And the crustal structure determined by E. A. Hodgson (**30**, **31**) using the data of the Tango Earthquake, in Japan, March 7, 1927 are considerably different from that of Matuzawa. All these results and others suggest implicitly the complexity of the crustal structure in our country.

The problems of the number of layers in the crust and the thickness of the crust have become a more and more attractive object of research in proportion to the recent trend towards accurateness of observation and analysis. H. E. Tatel, M. A. Tuve and others (**32**, **33**) studied the crustal structure in U. S. A. by the analysis of data of 250 artificial explosions, and obtained nearly 6.1 km/sec as the P–velocity of the upper layer, and they could not find any definite intermediate discontinuity between the ground surface and the Mohorovičić discontinuity. On this problem L. Mintrop (**34**) H. Reich and others (**35**) ascertained the existence of two layers in the crust of the granitic ($V_p \approx 5.5$ km/sec) and the gabbroic ($V_p \approx 6.2 \sim 6.6$ km/sec) layers by

the Heligoland Explosion in 1948, but P. L. Willmore (**36**) and J. P. Rothé (**37**) expressed the opinion that the existence of the gabbroic layer above mentioned is highly problematical. In this case the existence of the intermediate discontinuity would certainly be influenced by the locality of the crustal structure, but moreover the uncertainty of its existence is reasonably explained from the fact that the determination of intermediate discontinuity is quite difficult compared with that of the Mohorovičić discontinuity, especially in the analysis of travel time-distance curve, because the degree of discontinuity in the intermediate layer is considered to be less distinct than that in the Mohorovičić discontinuity. Therefore, in the detailed investigation of the crustal structure, the analysis of travel time-distance curves should be appropriately supplemented by other methods such as the analysis of the reflected waves at the discontinuity, the duration of refracted waves (forerunners) along the discontinuity or the transformed waves (*Wechselwellen*) changed at the discontinuity and other available phases of seismic waves.

Regarding the methods of analysing the reflected waves, the transformed waves and the duration of refracted waves at any crustal discontinuity for the study of the crustal structure, their practical applications are considerably few, especially in case of taking into consideration the amplitudes of their respective seismic waves, compared with those of the analyses of only the travel time-distance curves. M. A. Tuve, H. E. Tatel and others (**32**, **33**) had observed the very distinct phases of the reflected wave at the Mohorovičić discontinuity in some areas of North America and discussed the regional differences in the crustal structure. They obtained the same strong reflection under some areas such as, the Atlantic coast, the Tennessee mountains and the pre-Cambrian shield in Minnesota and the Appalachians, the Canadian Shield, and the Colorado Plateau, but in some regions these strong reflections were never observed, no matter how carefully they might search. Under the Colorado Plateau where the elevation is over 2 km, a Mohorovičić discontinuity was found at a depth of some 35 km contrary to the expected depth of 70～80 km from the isostatic compensation. B. Gutenberg (**17**, **38**) observed the reflected waves at a surface a little above the Mohorovičić discontinuity and moreover H. Reich (**39**) discussed the same problem. L. Mintrop (**34**) obtained and discussed not only the crustal reflection but also the reflected waves at the discontinuity in the mantle. On the analysis of the transformed waves T. Matuzawa and others (**40**, **41**) had early in 1928 discussed in detail the transformed waves changed at the interface of the sedimentary layer named the Kantô loam and the underlying granitic layer, and P. Byerly (**42**) also treated various transformed waves in the observation of the Nevada Earthquake in America.

Reviewing generally the development of our knowledge on the crustal structure

Table 1.

No. of Reference	Author (Date)	Locality	Structure (V_p km/sec, V_s km/sec (Thickness km))				
			Sedimentary layer	First layer	Second layer	Third layer	Mantle surface
(1)	Mohorovičić (1910)	Jugo-Slavia		5.6～ 3.2～ 5.7, 3.6 (0—50)			7.8, 4.2 (50—)
(2)	Gutenberg (1915)	Germany		5.6, 3.2 (0—30)	6.2, — (30—44)		8.2, 4.4 (44—)
(3)	Jeffreys (1926)	England		5.4, 3.3 (0—12)	6.3, 3.7 (12—30)		7.8, 4.4 (30—)
(4)	Conrad (1928)	Austria		5.6, — (0—12)	(12—37)	6.5, — (37—45)	8.1, — (45—)
(5)	Hecker (1922)	Germany (Oppau)		5.73, 3.0 (—)			
(6)	Wrinch Jeffreys (1923)	"		5.4, 3.15 (0—15)			
(7)	Gutenberg (1926)	Germany	2～4, — (0—2)	5.5～ 5.6, — (2—)			
(8)	Byerly Wilson (1935)	North California		5.6, — (1—13)	6.6, — (13—25)	7.3, — (25—31)	8.0, — (31—)
(9)	Byerly (1939)	North California		5.61, 3.26 (0—9)	6.72, — (9—)	7.24, — (—32)	8.02, — (32—)
(11)	Leet (1941)	New England		6.13, 3.45 (0—16)	6.77, 3.93 (16—29)	7.17, 4.27 (29—36)	8.43, 4.62 (36—)
(15)	Gutenberg (1951)	South California		5.7～ — 6.0, (0—6)	6.5, 3¾ (6—10)	(10—40)	8.1～ — 8.2, (40—)
(18)	Gutenberg (1954)	South California		5.9～ 3.2～ 6¾, 4± (1—10)	6¾～ 4±～ 6±, 3¼ (10—15)	6±～ 7±, 3¼ (15—40)	8.15, 4.55 (40—)
(21)～(25)	R. G. E. S. (1954)	Northeastern Japan	2.51, — (0—2)	5.75～ — 5.85, (2—)	6.10～ — 6.20, (—)		7.5～ — 8.0, (20～25 —)
(26)～(29) (41)	Matuzawa (1929)	Japan	1.94, 1.14 (1—4)	5.0, 3.15 (4—20)	6.2, 3.7 (20—50)		7.5, 4.5 (50—)
(30) (31)	Hodgson (1932)	Central Japan		6.3, — (0—16)			7.75 — (16—)
(32)	Tatel & others (1953)	U. S. A.		6.2, — (0—30～50)			8.0, — (30～50 —)
(34)	Mintrop (1949)	Germany	3.5, 2 (0—4)	5.2, 2.9 (4—13)	6.5, 3.6 (13—28)		8.1, 4.5 (28—)
(35)	Reich & others (1951)	Germany	3.6, — (0—6)	5.4, — (6—10)	6.18～ — 6.6, (10 -27)		8.19～ — 8.32, (27—)
(36)	Willmore (1947)	Germany	(0—7)	5.95, — (7—27)			8.18, — (27—)
"	"	"	4.4, — (0—6)	5.5, — (6—14)	6.5, — (14—29)		8.18, — (29—)
(37)	Rothé (1947)	Germany		5.5, — (0—30)			8.1, — (30—)
	Kishimoto (1955)	Central Japan	3.8, 2.2 (0—1.5)	5.4, 3.1 (1.5—7.5)	5.8, 3.4 (7.5 -21.5)	7.0, 4.0 (21.5—31.5)	8.1, 4.7 (31.5—)

Table 2. List of the earthquakes used in the present investigation. Latitude and longitude of epicenter and focal depth are those reported by the Central Meteorological Observatory of Japan. Observatories K, A, Aso and B denote the Kamigamo Geophysical Observatory, the Abuyama Seismological Observatory, the Aso Volcanological Laboratory and the Beppu Balneological Laboratory respectively. k denotes the Omori's constant ($k=\Delta$(km), $P\sim S$(sec)).

No.	Date					Latitude and longitude of epicenter		Epicentral region	$P\sim S$	Focal depth	Duration of forerunner		Δ	k	Observatory
			$d.$	$h.$	$m.$	N	E		s	km	s	s	km		
a-Group															
1	1945	Jan.	12	—	—	—	—	near Okazaki City	16.0	—	1.4,	2.3	132	8.2	K
2	1949	June	17	23	14	34.7,	137.6	Lake Hamana	22.0	10	1.5,	3.7	171	7.8	K
3	1947	Feb.	21	15	—	34.8,	138.0	Shizuoka Pref.	23.0	20		3.4	205	8.7	K
4	1945	June	24	—	—	—		"	23.2	—		2.8	—	—	K
5	1936	Oct.	20	23	15	35.0,	138.2	Shizuoka Pref.	25.2	—		3.6	223	8.9	K
9	1949	June	17	23	14	34.7,	137.6	Lake Hamana	23.1	10	1.7,	3.9	187	8.1	A
7	1936	Oct.	20	23	15	35.0,	138.2	Shizuoka Pref.	28.0	—		4.2	243	8.7	A
8	1947	Mar.	11	14	16	34.9,	138.4	"	29.2	20		4.6	242	8.3	K
9	1944	Dec.	9	10	54	34.4,	139.0	Izu Peninsula	36.0	20~40		6.0	306	8.5	K
b-Group															
1	1935	Nov.	19	08	36	33.8,	134.1	Tokushima Pref.	23.2	—		3.1	206	8.9	K
2	1950	Mar.	16	02	40	33.6,	134.6	"	23.2	10		3.0	192	8.3	K
3	1953	May	30	23	37	34.2,	133.2	Central Setoumi	30.1	20		5.1	253	8.4	K
4	1944	Aug.	3	10	42	—		Shimane Pref.	30.7	—		5.8	—	—	K
5	1935	Nov.	19	08	36	33.8,	134.1	Tokushima Pref.	31.3	—		5.1	244	7.8	B
6	1953	July	30	17	25	34.1,	132.8	Western Setoumi	37.3	20		6.9	308	8.2	K
7	1953	May	17	06	20	35.1,	132.6	Shimane Pref.	30.4	40		3.7	288	9.5	K
8	1950	Aug.	22	11	04	35.2,	132.7	"	31.6	30		3.8	280	8.9	K
9	1953	June	8	22	50	35.0,	132.8	Hiroshima Pref.	31.8	10		3.9	270	8.5	K
10	1941	Apr.	6	01	50	34.6,	131.7	Yamaguchi Pref.	44.0	—		5.7	375	8.5	K
c-Group															
1	1941	Mar.	4	—	—	37.5,	138.0	near Naoetsu	32.3	—		6.3	336	10.4	K
2	"	"	7	12	00	—		Nagano Pref.	33.6	<10		6.6	290	8.6	K
3	1937	July	4	00	23	36.9,	138.0	Niigata Pref.	40.0	—		7.4	249	6.2	K

d-Group														
1	1947	May	9	03	32	33.7,	135.3	Tanabe-Bay	18.4	—		3.8	154	8.4	K
2	1947	Jan.	17	02	44	33.8,	134.2	Tokushima Pref.	19.7	10	2.2,	4.7	200	10.1	K
3	1946	May	9	05	17	33.6,	136.0	Katsuura Wakayama Pref.	22.6	0		5.2	162	7.2	K
4	1947	Apr.	29	14	35	33.0,	135.0	off Shionomisaki	24.0	—		5.8	238	9.9	K
5	1949	May	18	07	48	34.0,	133.8	Tokushima Pref.	25.0	20		6.5	214	8.6	K
6	1953	July	31	04	24	33.2,	134.8	Nankaido	27.2	20	4.6,	7.4	224	8.2	K
7	1947	Feb.	16	18	19	33.1,	134.6	"	28.0	—		7.6	242	8.6	K
e-Group															
1	1943	July	1	13	40	36.2,	140.0	Ibaraki Pref.	45.6	50		9.5	410	9.0	K
2	1945	Oct.	24	05	15	36.3,	139.8	Gumma Pref.	45.9	40		9.0	390	8.6	K
3	1954	Feb.	25	02	28	35.9,	139.9	Chiba Pref.	45.9	40~50		8.9	390	8.6	K
4	1950	Sept.	10	10	07	35.3,	140.5	Kujukuri-Hama	46.5	30~40		8.5	440	9.5	K
5	1943	Jan.	20	06	24	36.1,	140.5	Ibaraki Pref.	50.2	40		9.5	448	8.9	K
6	1952	Nov.	2	10	43	36.2,	140.6	Ibaraki Pref.	50.3	45~50		9.1	458	9.1	K
7	1954	July	18	07	36	35.6,	141.0	near Choshi	50.5	40		9.0	485	9.6	K
8	1942	Feb.	19	01	52	35.8,	140.8	"	52.1	—		9.5	470	9.0	K
9	1938	Oct.	29	22	11	35.4,	141.0	Kashima-Nada	55.2	—		9.7	482	8.7	K
10	1953	May	11	04	50	36.2,	141.1	"	59.2	40		10.5	510	8.6	K
11	1953	Apr.	4	14	53	35.8,	141.9	"	61.3	40		11.4	570	9.3	K
12	1946	Apr.	3	22	07	35.9,	141.3	"	61.4	40		10.7	517	8.4	K
13	1927	Oct.	11	10	16		—	"	63.4	—		11.1	—	—	K
f-Group															
1	1929	May	22	01	30	31.8,	131.8	Hyuga-Nada	47.1	—		13.2	514	10.9	K
2	1931	Nov.	2	19	09	32.4,	132.1	"	47.4	—		12.6	448	9.5	K
3	1948	May	9	11	09	32.0,	131.5	"	50.0	—		12.6	520	10.4	K
g-Group															
1	1933	May	24	01	38	31.4,	131.7	Hyuga-Nada	27.7	—		8.0	203	7.3	Aso
2	"	"	"	"	53	31.2,	131.4	"	29.3	—		8.5	225	7.7	Aso

deduced from the seismometric investigation in the past more than forty years, the most important and promising problem concerned is the complexity, the regional difference or, in other words, the local character of the earth crust. On the thickness of the crust, the number of discontinuities in the crust, the velocity of the seismic wave, elasticity and density in the crustal layer, all are diverse from region to region. In the present article the durations of refracted waves (forerunners) propagated along the crustal discontinuities are analysed in detail and the regional differences in the crustal structure in Japan are discussed.

2. Forerunner of long duration

In the previous Part I (**43**), the structure of the earth's upper layer (the sedimentary and granitic layers) was determined by an analysis of the refracted seismic waves (forerunners) of short duration (less than 2 sec) recorded mainly at the Kamigamo Geophysical Observatory with regard to the local and near earthquakes of shallow origin around Kyoto. The structure thus determined around Kyoto was as follows:

Layer	Velocity of *P*-wave km/sec	Velocity of *S*-wave km/sec	Layer-thickness km
Sedimentary layer	3.8	2.1	1.5
Granitic layer	5.4	3.1	6.0
Granodioritic layer	5.8	3.3	?

In the present investigation the forerunners of longer duration (2~13 sec) were analysed from the seismograms recorded with the large Wiechert Seismographs at the Kamigamo Geophysical Observatory (in the main), the Abuyama Seismological Observatory, the Aso Volcanological Laboratory and the Beppu Balneological Labora-

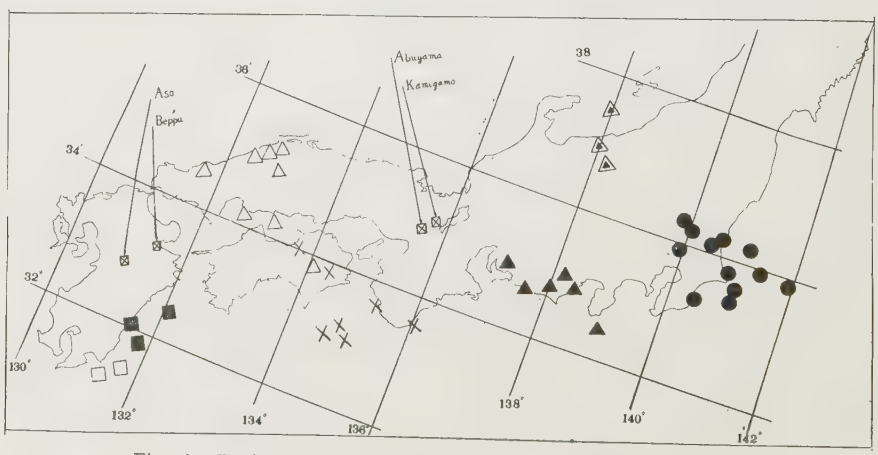

Fig. 1. Positions of the epicenters of earthquakes listed in Table 2 and the Observatories.

tory, all attached to Kyoto University. And from their analyses the structure of the deeper layers of the crust was derived and discussed in some detail.

The observational data of earthquakes used in the present analysis are listed in Table 2, and their epicenters and the referred Observatories are shown in Fig. 1.

Referring to Table 2 and Fig. 1, the duration of each earthquake is plotted, in Fig. 2, with their ($P\sim S$) times as the abscissa in different symbols (▲, △, ◬, ×, ●, ■ and □) according to their respective groups (a, b, c, d, e, f and g). As seen in Fig. 2 it is considered to be convenient to treat them separating in four classes, namely the first class (Group-a, b and c), the second class (Group-d and g), the third class (Groupe-e) and the fourth class (Group-f) respectively.

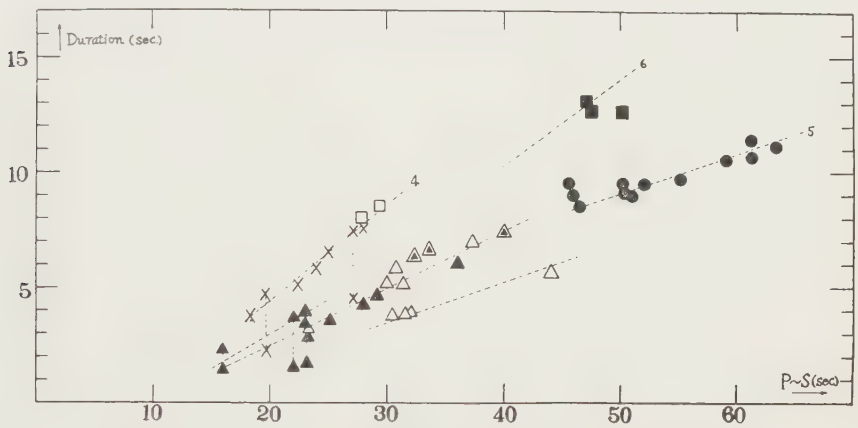

Fig. 2. Relation between the duration of forerunners and the $P\sim S$ time for each Group.

1. On the first class

Group-a, -b and -c contain shallow earthquakes whose epicenters were in the region of Tôkai District (East from Kyoto), Chugoku-Setoumi District (West from Kyoto), and Hokuriku District (North from Kyoto) as shown in Fig. 1. And concerning forerunner duration they are considered to be attributable, roughly speaking, to the same class as seen in Fig. 2. Especially they ought to be clearly distinguished from those of the second class of Group-d. But, treating on the forerunners of the first class in detail, it is convenient to subdivide them into three sub-classes of *X*, *Y* and *Z*, as in Fig. 3, according to their focal depths. Namely, the sub-class *X* contains three earthquakes of comparatively long forerunner duration and their focal depths are roughly estimated to be within 10 km by the Central Meteorological Observatory (C.M.O.) in Japan. And the sub-class *Y* contains the major part of earthquakes in the first class, their focal depths being estimated by C.M.O. to be some 20 km. The sub-class *Z* contains four earthquakes of comparatively

short duration and their focal depths are estimated by C.M.O. to be more than 30 km. In this place it is appropriate to mention briefly the problem on the estimation of the focal depth of an earthquake. Generally speaking, it is a very difficult task to determine an accurate value for the focal depth of an earthquake, and especially in Japan it is not too much to say that it is impossible for the following three reasons. First, for the purpose of accurately determining the focal depth, it is necessary to determine accurately the position of the epicenter and the arrival time of the *P*- and *S*-waves at the epicenter. Nevertheless the accurate determination of the epicenter is generally very difficult in Japan because the epicenters of most of the earthquakes occurring in Japan are situated at the open sea or near the sea coast, and therefore there is no way but to estimate roughly the epicenter position from the data obtained at some observatories which are considerably remote from the epicenter and moreover situated in some limited azimuths seen from the epicenter. Secondly, the focal depth calculated from the arrival time of *P*- and *S*-waves at the epicenter depend, needless to say, upon the crustal structure of the epicentral region. That the calculated value of the focal depth depends on the crustal structure and that the crustal structure is determined by the analysis of seismic wave of known focal depth is an endless circular argument, and unfortunately in the case of our country the situation becomes more and more unfavourable because of the local character of the crustal structure. And as the third trouble, the hypocenter of an earthquake is never a point in a geometrical sense but has some extent, and it is reasonably considered that its extention is proportional to the scale of earthquake. And really the order of magnitude of several kilometers is presumably assigned to the extent of hypocenter in case of a large earthquake. From these three and other reasons it may safely be said, except for a favourable case of inland earthquake in the region of simple crustal structure observed by many observatories of dense and uniform distribution near the epicenter, that regarding the value of the focal depth determined from a shallow earthquake, an inevitable error of several kilometers should be borne in mind. And in the present investigation the values of focal depth determined by the Central Meteorological Observatory in Japan were tentatively adopted except a case of special mention, allowing an inaccuracy of several kilometers.

But to return to the main problem, the forerunners of sub-class *X*, *Y* and *Z* should be individually investigated. On the sub-class *X* it is characteristic that three earthquakes belonging to this sub-class showed two prominent forerunners. Namely, the first forerunner (*Pb*) has, as seen in Figure A (a), a comparatively long period of oscillation and small amplitude, and the second forerunner (Pg_2) shows a short period of oscillation and small amplitude which is succeeded by the clear arrival of direct wave of large amplitude (Pg_1). As seen in Fig. 3 the duration of the second

forerunner is just on the line of duration of the forerunner treated in the previous Part I, therefore the second forerunner is naturally interpreted as the refracted wave transmitted along the discontinuous surface between the granitic layer and the granodioritic layer which will hereafter be designated as 'the *g–g* discontinuity'. And the first forerunner in this case is considered to be the refracted wave transmitted along the discontinuous surface between the granodioritic layer and the basaltic layer which will hereafter be called 'the *g–b* discontinuity'. Therefore the foci of these three earthquakes of very shallow origin are considered to lie in the granitic layer, and the first and second forerunners are interpreted as the refracted waves through the *g–b* discontinuity and *g–g* discontinuity which preceded the direct wave through the granitic layer. Hence, as a natural consequence, the forerunners of sub-class *X* will serve the purpose of determining the thickness of granodioritic layer and the velocity of basaltic layer, but the numbers of earthquakes in the *X*-class are too scanty to calculate accurately the required quantities. And this problem will reasonably be transferred from the scanty *X*-class to the abundant *Y*-class.

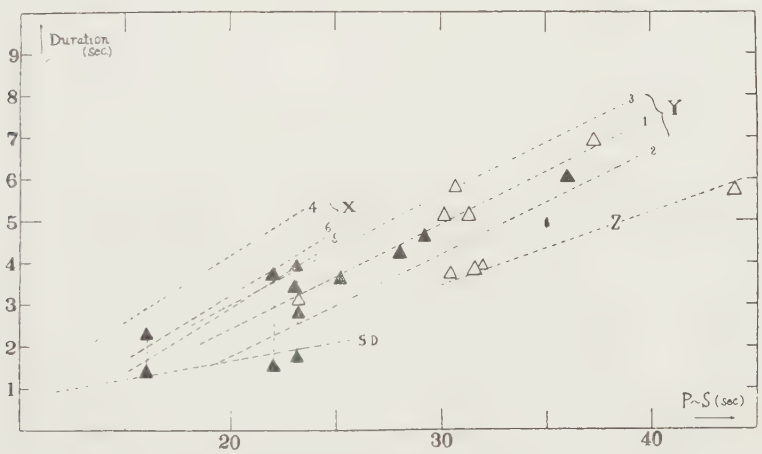

Fig. 3. Relation between the duration of forerunners and the $P\sim S$ time for the first class.
S. D. denotes the duration curve obtained in Part I.

As seen in Figure A (b), each earthquake grouped in the sub-class *Y* is preceded by only one forerunner of long duration (3∼7 sec in the range of epicentral distance from 180 km to 300 km). From these points it is deduced that the foci of earthquakes of *Y*-class lie in the granodioritic layer and the forerunner observed is interpreted as the refracted wave transmitted along the surface of the *g–b* discontinuity. It ought to be mentioned here that, as will be described in a later paragraph, the refracted wave transmitted along the discontinuous surface between the basaltic layer and the upper part of the mantle which will be called 'the Mohorovičić discontinuity'

or simply '*M*-discontinuity', shall clearly precede the above-mentioned forerunner of *Y*-class at the larger epicentral distance beyond some 300 km. For the purpose of determining the seismic velocity in the basaltic layer a similar method to that applied in the previous Part I was used here. Namely, of the earthquakes in *Y*-class the diagram of the forerunner's duration-($P\sim S$) time in Fig. 3 was transformed into an ordinary travel time-distance curve shown as Fig. 4. In this transformation the travel time of the direct wave was calculated under the supposition that the seismic focus lay in the granodioritic layer and at a point 10 km below the *g*-*g* discontinuity. And it was already discussed in Part I that the difference in the tentatively assumed value of focal depth has little influence upon the calculation of the travel time of a direct wave at a station of considerable distance from the epicenter. Then the velocity of the *P*-wave in the basaltic layer is deduced as 6.8~7.2 km/sec from the inclination of the travel time curve of the refracted wave in Fig. 4. And this sort

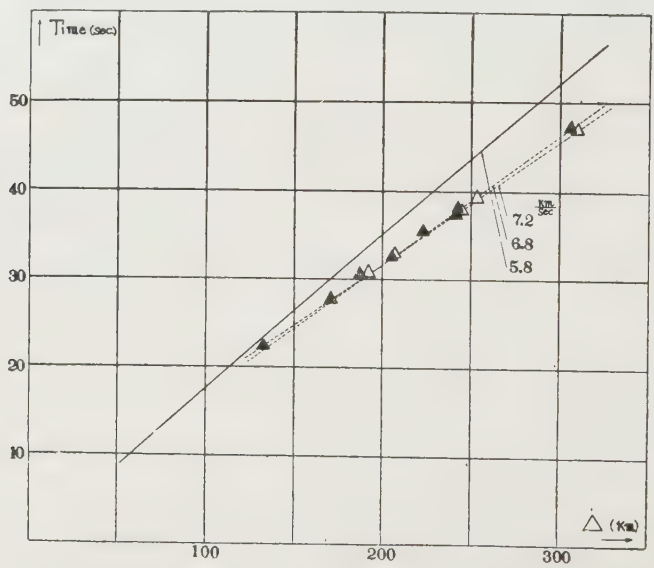

Fig. 4. Travel time-distance curves for Pg_2 (full line) and *Pb* (broken lines).

of inaccuracy in the value of velocity determined is considered to be inevitable because the foci of earthquakes in the *Y*-class may be at various depths in the granodioritic layer and the number of earthquakes used in calculation is not large enough to smooth the individual effect caused by the difference of focal depth. As an example the travel time-distance curve of an earthquake which occurred on May 30, 1953 at the central part of Setoumi is plotted in Fig. 5. This earthquake belongs to the *Y*-class and its focal depth was estimated to be 20 km, and the velocity of

refracted wave is roughly calculated, as seen in Fig. 5, to be 7.0 km/sec. From these factors, the value of the *P*-wave in the basaltic layer (logically speaking, the layer name of 'basaltic' should be designated after determination of velocity of its layer) was tentatively estimated to be 7.0±0.2 km/sec and the velocity of *S*-wave may reasonably be assumed to be 4.0 km/sec under the assumption on the value of Poisson's ratio as 0.26.

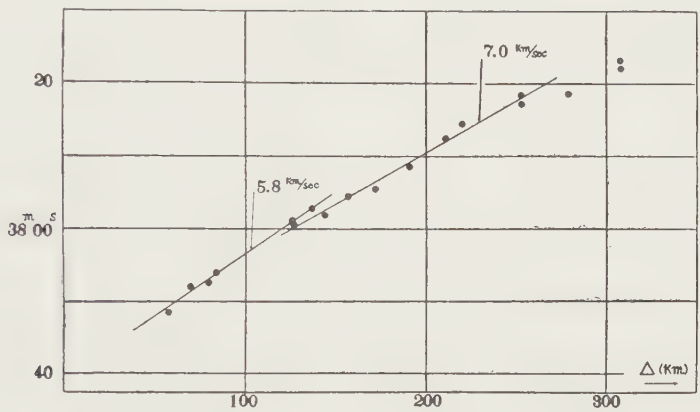

Fig. 5. Time-distance curve (*P*-wave) of the earthquake on May 30, 1953.

Concerning the thickness of the granodioritic layer the following procedure was applied to the forerunners belonging to the sub-class *Y*. Under the assumption that the granodioritic layer is approximately a horizontal layer around Kyoto, the most plausible value of thickness determined to fit the durations of all forerunners of the sub-class *Y* in Fig. 3 was estimated to be nearly 14 km, and the calculated curve for the duration in case of 14 km-thickness of the granodioritic layer and placing the focus at the middle point in the granodioritic layer is shown as curve 1 in Fig. 3. And every point which deviates more or less from the curve 1 is all included in a narrow zone between the curves of 2 and 3 calculated in case of a 14 km-thickness of the granodioritic layer and placing the focus at the uppermost and lowest positions in the granodioritic layer. From these considerations the value of 14 km for the thickness of the granodioritic layer is considered to be the most favourable for the available data of the sub-class *Y*.

Returning again to the sub-class *X* the durations of three forerunners in sub-class *X* are included in a zone of the curves of 4 and 5 in Fig. 3 which are calculated under the assumption that the focus is at the lowest point in the granitic layer and the thicknesses of the granodioritic layer are 10 km and 15 km respectively. Also in this case the value of the granodioritic layer of 14 km is estimated as the most

plausible mean value which is expressed as curve 6.

On the last sub-class *Z* their durations are, as seen in Fig. 3, and Figure A (c), considerably short compared with the other sub-classes of *X* and *Y*. And from the fact that their focal depths were estimated to be some 30～40 km, their foci being considered to be in the basaltic layer, and then their forerunners are interpreted as the refracted waves transmitted along the Mohorovičić discontinuity. As will be discussed in detail in a later paragraph, the thickness of the basaltic layer is supposed to vary widely from region to region in Japan. Therefore the individual crustal structure in each region could not be determined from the present method of forerunner analysis, and should be examined by the analysis of the reflected waves of near earthquakes having their epicenters in the respective regions. From the analysis of forerunners only the *mean* crustal structure is determined under the assumption of horizontally parallel structure of layers.

As already discussed or will be further discussed in a later paragraph, the velocities of the basaltic layer and the surface layer of the mantle are approximately estimated as 6.8～7.2 km/sec and 8.0～8.2 km/sec respectively. And the thickness of the basaltic layer derived from the analysis of forerunner duration under the assumption of horizontally parallel structure depends on the value of velocity of basaltic layer and the mantle surface and moreover the position of focus in the basaltic layer in the present case of sub-class Z. Taking the circumstances into consideration, some values for the thickness of the basaltic layer were calculated to fit the observed durations of forerunners in sub-class *Z* under various plausible assumptions on the layer velocity and the focal depth. The mean value of thickness of the basaltic layer thus obtained is estimated as nearly 14±3 km in the present case of sub-class *Z*.

In concluding the section *1* on the forerunner of the first class the following structures were determined. The thickness of the granodioritic layer is considered to be uniform, as a first approximation, around Kyoto whose value is estimated about 14 km. The velocities of the *P*- and *S*-waves of the basaltic layer underlying the granodioritic layer around Kyoto were calculated as 7.0±0.2 km/sec and 4.0±0.1 km/sec respectively. But on the thickness of the basaltic layer it is appropriate to presume the regional difference which will be discussed in detail in the next section *2*.

2. On the second class

The forerunners of earthquakes belonging to the Group-d are those observed at the Kamigamo Geophysical Observatory, whose epicenters are in the district of the southern part of Kii Peninsula, the south-eastern part of Shikoku and the neighbouring open sea, all being included, roughly speaking, in the district of Nankaido. (The

forerunners belonging to the Group-g are those observed at the Aso Volcanological Laboratory and whose epicenters are in the district of the southern part of Hyuga-Nada as shown in Fig. 1.) Those forerunners have considerably longer durations compared with those of the first class and should be separately treated with the forerunner of the first class.

As a first step the forerunners of Group-d will be treated. The seismograms obtained of the earthquakes in the Group-d show, as seen in Figure A(d), two distinct forerunners. And the durations of the second forerunners are plotted just on the mean curve in case of the sub-class *Y* in the first class as seen in Fig. 2. Moreover the foci of earthquakes in Group-d are estimated as some 10～20 km deep, therefore the second forerunners observed of Group-d are interpreted as the refracted wave transmitted along the *g-b* discontinuity when the focus is in the granodioritic layer. Here another proof on the uniform structure of the granodioritic layer around Kyoto was obtained from the above consideration. Then as what sort of forerunner should the first forerunner of the Group-d be interpreted? Why isn't the forerunner corresponding to the first forerunner of Group-d observed in case of sub-class *Y* in the first class? The problem could not be solved unless the regional difference of the thickness of the basaltic layer is postulated. In the following the problem will be treated from the standpoint that the thickness of the basaltic layer or, more generally speaking, the depth of the Mohorovičić discontinuity or, in other words, the thickness of the earth's crust may be widely different from place to place.

In the first class the velocity of the layer underlying the *M*-discontinuity was tentatively assumed to be about 8.0～8.2 km/sec for the *P*-wave, and in the present paragraph it will be determined for the Nankaido District by an analysis of the earthquake of October 16, 1951. The earthquake in question occurred at open sea off Muroto-Misaki, in the Nankaido District and its focal depth was estimated to be about 40 km. The fact that the seismogram obtained of this earthquake at the Kamigamo Geophysical Observatory was not preceded by any forerunner, as shown in Figure B(a), tells us that its focus was at the point under the *M*-discontinuity and moreover depth of the *M*-discontinuity around this district was estimated as less than 40 km from the ground surface of the sea bottom. On such a method of locating the focal depth of the earthquake by the examination of forerunner some detailed discussion will be made in a later paragraph. From the analysis of the above-mentioned earthquake the apparent velocity of the layer under the *M*-discontinuity in this district was estimated to be about 8.0～8.2 km/sec as seen in the travel time-distance curve of Fig. 6. From this value it was concluded that the velocity of the layer underlying the *M*-discontinuity or, in other words, the surface velocity of the mantle is nearly 8.0～8.2 km/sec all for the District of Tôkaido, Hokurikudo, Chugoku and Nankaido.

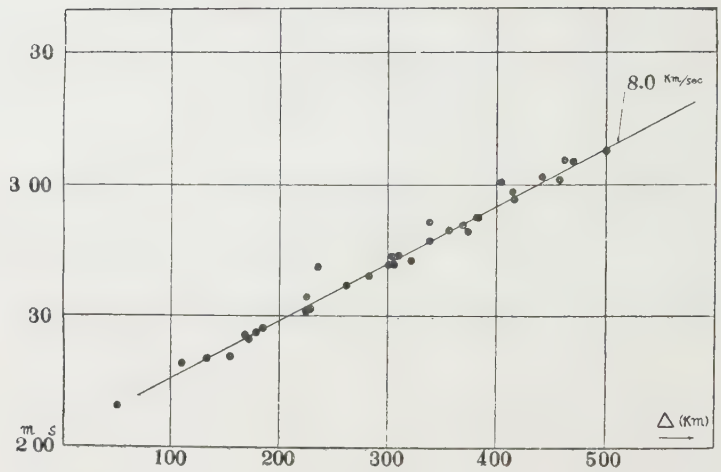

Fig. 6. Time-distance curve (P-wave) of the earthquake on Oct. 16, 1951.

Under the circumstances that the thickness of granodioritic layer is 14 km both for the Nankaido and Kyoto, and moreover the P-velocity in the layer underlying the basaltic layer is of the same value of about 8.0 km/sec for both regions, what value should be attributed to the mean thickness of the basaltic layer under the region between Nankaido and Kyoto? As already stated, the thickness of the basaltic layer under any region is not uniquely determined only from the analysis of an observed forerunner. It depends certainly on the crustal structures of the hypocenter, the observation point and the propagation path of seismic waves. And, moreover, it is generally affected by the assumed value of the propagation velocity of seismic waves in the layers concerned and considerably associated with the orientation of seismic focus. In the present case the most plausible mean value of the thickness of the basaltic layer has been determined to be 6.5 ± 1.2 km under the assumption of horizontally parallel structure under the region between Nankaido and Kyoto, and, moreover, averaging the various values obtained from the some combinations of the velocities for the P-wave in the basaltic layer (6.8～7.2 km/sec), the mantle surface (8.0～8.2 km/sec) and the focal depth in the granodioritic layer. A calculated duration curve for the case of a horizontally parallel structure of the basaltic layer, placing the focus at the middle in the granodioritic layer, and assuming the propagation velocity of 7.0 km/sec for the basaltic layer and 8.2 km/sec for the mantle surface, is expressed as curve 4 in Fig. 2.

Secondly the Group-g will be discussed. This Group contains the earthquakes which occurred in the southern part of Hyuga-Nada, as seen in Fig. 1, and their forerunners were observed at the Aso Volcanological Laboratory. As shown in Fig. 2

the Group-g may be treated approximately in the same manner as the Group-d, in other words, the structural relation of the crust in the southern Hyuga-Nada District to that of Aso is, roughly speaking, similar to the relation between the Nankaido District and Kyoto. The crustal structure around Aso was approximately ascertained by an analysis of somewhat deep earthquakes near Aso as will be discussed in a succeeding article, and the thickness of the earth's crust around Aso is of the same order of magnitude as that around Kyoto. From these it is tentatively stated that the thickness of the basaltic layer in the southern part of Hyuga-Nada is considered to be of the same order of magnitude as in the Nankaido District, namely some several kilometers, which is considerably thin as compared with the other Districts. On this problem the earthquakes having occurred at Hyuga-Nada will be again treated in the Group-f of the fourth class.

In concluding section *2* on the second class it is convenient to mention that the distinct regional difference of the thickness of the basaltic layer was ascertained in this section by analysing the forerunners of earthquakes having occurred in the Nankaido District, and on the other hand, no distinct regional difference was found in the thickness of the granodioritic layer overlying the basaltic layer in the region within some 300 km distance from Kyoto. The thicknesses of the basaltic layer thus determined under the assumption of horizontally parallel structure (which is contrary to the real structure) are roughly estimated to be 6.5 km and 14.0 km for the region of Nankaido-Kyoto and Shimane-Kyoto respectively.

3. On some destructive earthquakes

As discussed in the preceding section *2* the existence of a regional difference in the crustal structure was ascertained from the analysis of the duration of the forerunners of weak or medium earthquakes observed at one station, mainly at the Kamigamo Geophysical Observatory in Kyoto. Too large or destructive near earthquakes are unsuitable for the analysis of forerunners in case of observation with the large Wiechert Seismograph, but for the purpose of accurate determination of the crustal structure the concurrent use of the forerunner with the time-distance curve constructed with the data observed at many stations of a destructive earthquake is the most desirable. In this case the same type of seismograph is recommended for all observatories and their magnifications should be adequately controlled to be able to record ground oscillations of large amplitude at stations near the epicenter and to catch the minute ground oscillations at the distant station. And the accurate time determination for any phase is an important task in this case, and moreover, the identification for any phase is, above all, the most difficult and essential problem. In the present state the above-mentioned conditions are not yet perfectly fulfilled in the

seismometric system of our country, but as a great improvement has recently been made in seismometry in Japan, the development of an accurate and detailed seismometric investigation on the regional difference of crustal structure will be expected in the near future. As will be seen in the following treatment of some destructive earthquakes, it is almost impossible, at present, to get a clear picture of the crustal structure from the analysis of the travel time-distance curve only. The difficulty results from the uncertainty of the position of epicenter and hypocenter, the finite extent of seismic focus, the inaccuracy of travel-time determination, the locality of crustal structure around the observatory, the insufficient or excessive magnification of the seismograph, and other artificial or natural sources of errors. Therefore it is recommended that in an accurate seismometric investigation of the structure of the crust or, more generally, the earth's interior, the analysis of travel time-distance curve should be completed by the analysis of forerunner duration, the comparison of observed amplitude of each seismic phase, the analysis of the reflected and the transformed seismic waves, and other available and effective means.

(a) The Fukui Earthquake of June 28, 1948

The Fukui Earthquake of June 28, 1948 was the most severe and destructive in recent years with a damage of twenty thousand casualties and forty thousand ruined buildings. Its epicenter was estimated to be 36° 08′ N and 136° 16.8′ E, and the seismic magnitude was 7¼ in Pasadena Scale. The focal depth was diversely estimated by several investigators, but in our case it is considered to be most plausible to place it in the granodioritic layer as discussed in the succeeding. This earthquake was by far the most completely and precisely investigated compared with other past destructive earthquakes, and its travel time-distance curve is said to be very much trustworthy as it was derived from the accurate location of an inland epicenter, the recent advance of time determination at the seismological observatories and the authority of synthetic investigation by various fields of science (**44**).

In Fig. 7 is shown the travel time-distance curve studied by the writer using the C.M.O.-data, in which the symbols of ● and + denote the arrival time of the first motion of seismic waves observed at the westerly and the easterly observatories from Fukui respectively. And the symbols of ⊙ and ⊕ denote the arrival time of the distinct phases of seismic waves having appeared after the first motion and which were examined by the writer from the available seismograms. From these arrival times three branches of straight lines connecting the points belonging to the same system are tentatively drawn, as seen in the figure, each expressing the apparent velocity of 8.0, 7.0 and 5.9 km/sec respectively. These seismic *P*-waves of 8.0, 7.0 and 5.9 km/sec-velocity are interpreted respectively as the refracted waves transmitted along the *M*-discontinuity, the refracted wave along the *g*–*b* discontinuity,

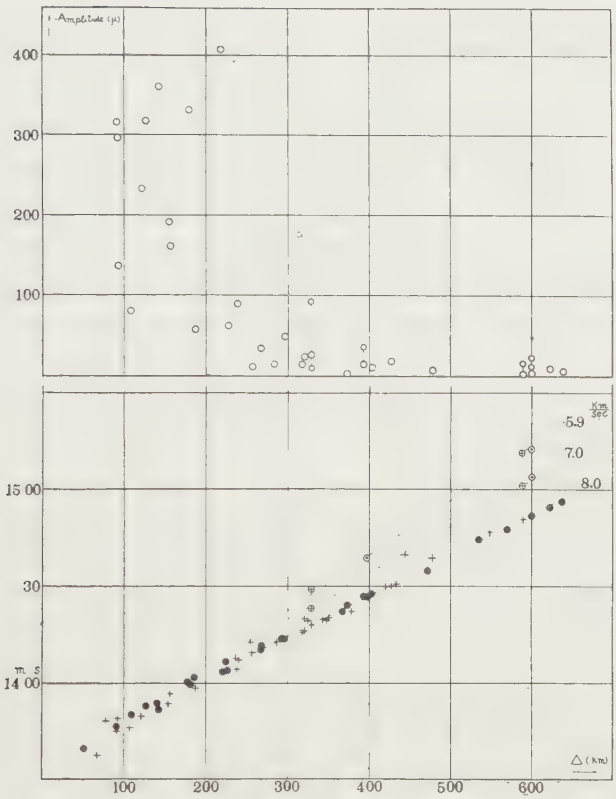

Fig. 7. Time-distance (lower) and amplitude-distance (upper) curves for the P-waves of the Fukui Earthquake on June 28, 1948.

and the direct wave through the granodioritic and granitic layer in case of having the focus in the granodioritic layer. And, moreover, this is ascertained by the observed amplitude relation between three phases mentioned above, namely the observed amplitudes of the seismic waves of first arrival decrease suddenly at the epicentral distance of some 230 km, as expressed in Fig. 7, at the distant places beyond the critical point of 230 km the amplitude of first motion of seismic waves being estimated to be less than one-tenth of those observed at the short distance within the critical point. Beyond the critical point the amplitude relation between the first forerunner, the second forerunner and the direct wave are, as shown also in Fig. 7, in appropriate proportion. It ought to be mentioned here that, in practical cases, the clear separation of three phases can safely be made of the seismograms obtained at places outside the epicentral area of some 300 km. Concerning the problem of placing the focus of the Fukui Earthquake in the granodioritic layer the following examination was also applied. As shown in Fig. 8 the $P\sim S$ times in the ordinate and the epicentral distance in abscissa are expressed of the data observed at the observatories within some 200 km-epicentral distance where the observed seismic

waves of first arrival are considered as the direct wave. The two curves of 1 and 2 in the figure are calculated for the case in which the seismic focus is in the granodioritic layer and the basaltic layer respectively. The structure assumed in this case are (5.4 km/sec, 3.1 km/sec, 6 km) for the granitic layer, (5.8 km/sec, 3.4 km/sec, 14 km) for the granodioritic layer and (7.0 km/sec, 4.0 km/sec, —) for the basaltic layer, the foci being in the granodioritic layer 7 km below the g–g discontinuity for the curve 1 and in the basaltic layer 6 km below the g–b discontinuity for curve 2. Curve 2 is, in this case, not suitable for expressing the plausible curve connecting the data, and we are convinced that the placing of the focus in the granodioritic layer is favourable in the case of the Fukui Earthquake.

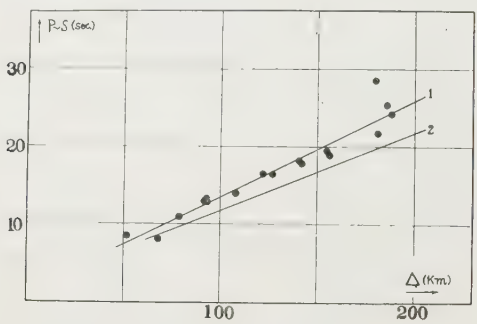

Fig. 8. P~S time-distance curve of the Fukui Farthquake.

Now for the purpose of calculating the thickness of the basaltic layer using the data obtained from the Fukui Earthquake the travel time-distance curve in Fig. 7 will be analysed. But in the present analysis the so-called critical distance (the epicentral distance of the place where the arrival times for both the direct and refracted seismic waves are the same) was not used for the reason that the value of the critical distance could not usually be determined with sufficient accuracy in the analysis of natural earthquakes contrary to that of artificial explosions. In cases of the analysis of natural earthquake including data obtained from such large epicentral distances as several hundreds kilometers, this is due to the fact that the determination of the critical point is greatly disturbed by the local character and regional difference of crustal structure around the respective observatories, and by the inaccurate estimation of the position of seismic focus. Therefore, in the present case, the durations of the first and second forerunners were used to calculate the thickness of the basaltic layer. This method, needless to say, contains also the inaccuracy caused by the same disturbances mentioned above, but it will soon be understood that the loss in this case is very much small compared with that in case of the critical distance. Speaking more in detail, the problem of critical distance concerns the data in a comparatively short distance and that of forerunner mainly the data at far distance, therefore the

local and regional difference of the crustal structure, the instrumental and time errors and other disturbances become more and more prominent, as seen in Fig. 7, and greatly spoil the calculated value of layer-thickness in the former case. But, also in the latter case, the obtained values of apparent velocities of the refracted and the direct seismic waves, and the thencefrom derived values of the layer-thickness could not be free, in some measure, from the above-mentioned disturbances, and therefore the estimated values of the velocity and the layer-thickness in the present investigation are considered to be, roughly speaking, in the degree of accuracy with the mean error of ± 0.2 km/sec for the velocity and ± 5 km for the layer-thickness respectively. Considering these circumstances the most plausible structure derived from the forerunners of the Fukui Earthquake is the basaltic layer of 7.0 km/sec–P velocity and some 20 km–thickness, and the velocity of 8.0 km/sec–P wave for the layer underlying the M–discontinuity when assuming the granodioritic layer of 5.8 km/sec–P velocity and 14 km–thickness, and placing the seismic focus at the middle point of the granodioritic layer. As already discussed in the preceding paragraph the thicknesses of the basaltic layer were estimated to be diverse from place to place, and accordingly the above obtained value of some 20 km–thickness of the basaltic layer is considered as a roughly averaged value for a wide area. Therefore, in order to obtain the accurate structure of the crust around any region, the travel time-distance curve and the forerunner should concurrently be analysed with regard to the data observed at the observatories in any one direction and within some suitable distance from the epicenters of a swarm of earthquakes in the same locality. When the forerunner durations obtained at the observatories in the Kanto district are especially analysed, the averaged value of the horizontally parallel structure of the basaltic layer under the region between Fukui and Kanto is estimated, as in the former case, to be 18.7 ± 1.5 km.

Simply speaking, the crust is considered to be shallow, mediate and deep under the region of Nankaido-Kyoto, Shimane-Kyoto and Kanto-Fukui respectively.

(b) Travel-time distance curves for some other destructive earthquakes

In the above paragraph the travel time-distance curve obtained from the data of the Fukui Earthquake of June 28, 1948 which is considered as the most reliable in recent times in Japan was analysed and it was concluded that even the most trustworthy travel time-distance curve as in case of the Fukui Earthquake gives only a roughly averaged value for the crustal structure. In the present paragraph the travel time-distance curves are presented for some destructive earthquakes having occurred in Japan in past twenty years. In Table 3 the materials obtained by the C.M.O. of these destructive earthquakes are listed and their epicenters are shown in Fig. 9. Their tentatively drawn travel time-distance curves are plotted in Figs. 10～17.

Table 3. List of the destructive earthquakes

No.	Earthquake	Date	Magnitude in Pasadena Scale	Epicenter		Focal depth
				° E	° N	km
1	Kita-Izu	Nov. 26, 1930	7.1	139.0,	35.1	—
2	Sanriku	Mar. 3, 1933	8½	144.7,	39 1	—
3	Hyuga-Nada	Nov. 19, 1941	7.1	132.4,	32.3	—
4	Tottori	Sept. 10, 1943	7½	134.2,	35.5	0
5	Tonankaido	Dec. 7, 1944	8	136.2,	33.7	0~30
6	Mikawa	Jan. 13, 1945	7.1	137.0,	34.7	0
7	Nankaido	Dec. 21, 1946	8.2	135.6,	33.0	0~30
8	Fukui	June 28, 1948	7¼	136 17′,	36 08′	20
9	Tokachi-Oki	Mar. 4, 1952	8¼	143 52,′	42 09′	45

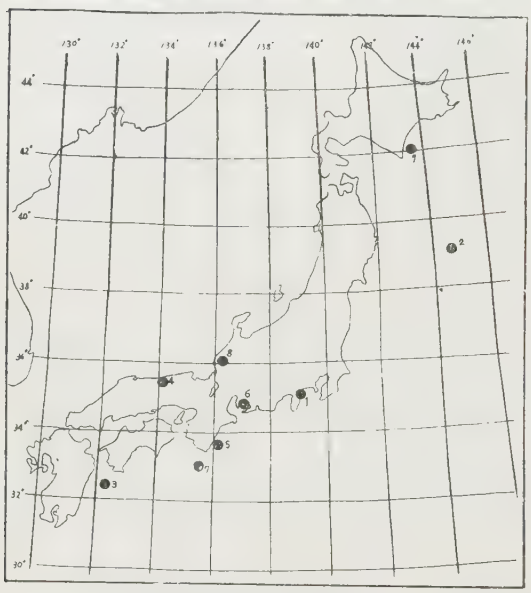

Fig. 9. Positions of nine destructive earthquakes listed in Table 3. The annexed figures are referred to Table 3.

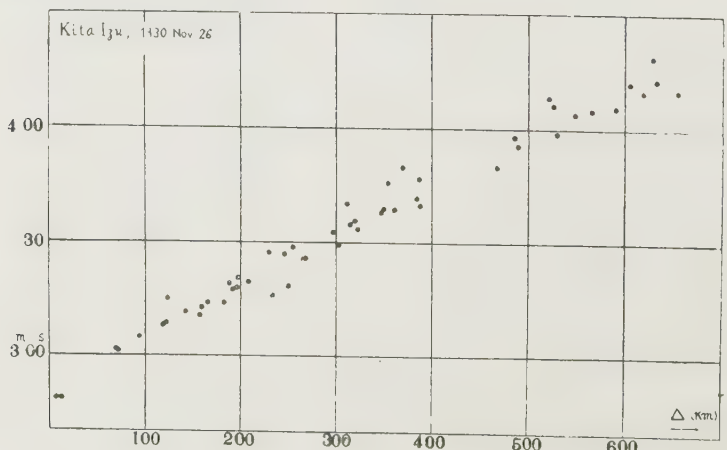

Fig. 10. Time-distance curve (P-wave) of the Kita Izu Farthquake.

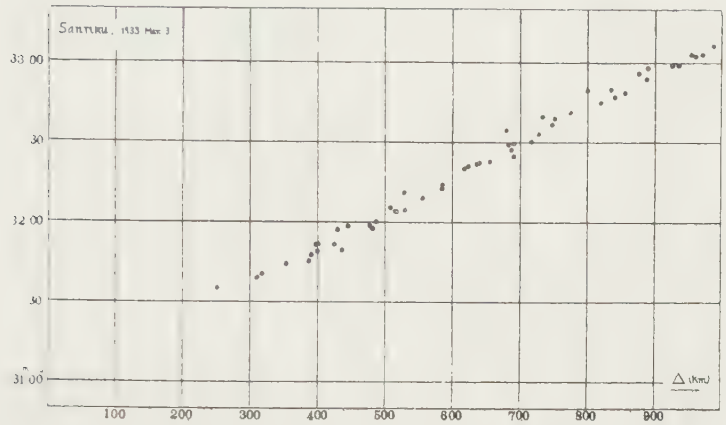

Fig. 11. Time-distance curve (P-wave) of the Sanriku Earthquake.

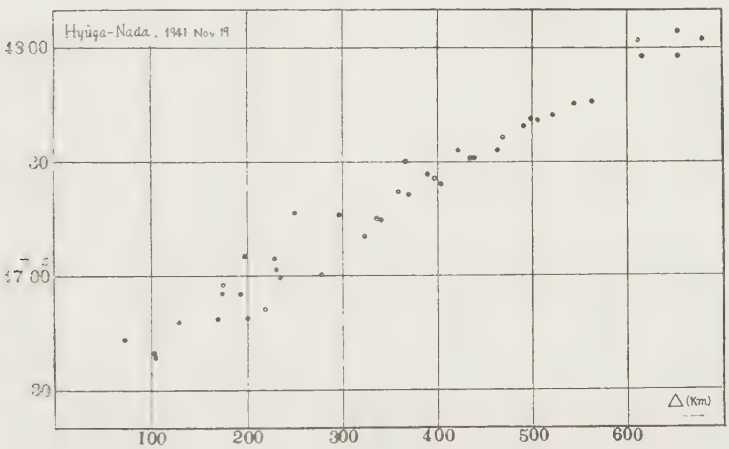

Fig. 12. Time-distance curve (P-wave) of the Hyuga-Nada Earthquake.

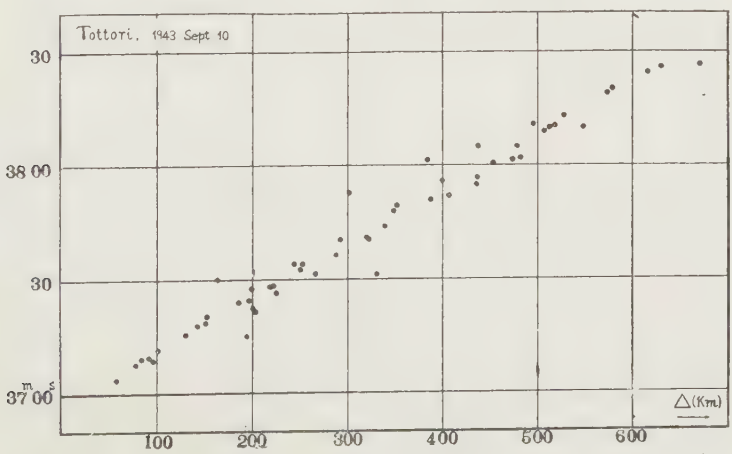

Fig. 13. Time-distance curve (P-wave) of the Tottori Earthquake.

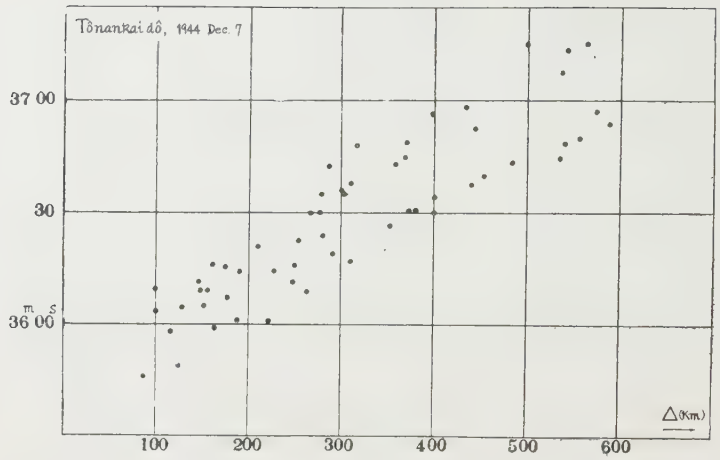

Fig. 14. Time-distance curve (P-wave) of the Tonankaido Earthquake.

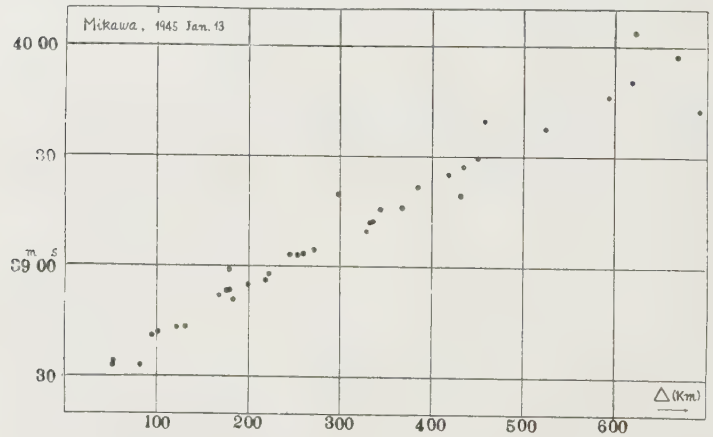

Fig. 15. Time-distance curve (P-wave) of the Mikawa Earthquake.

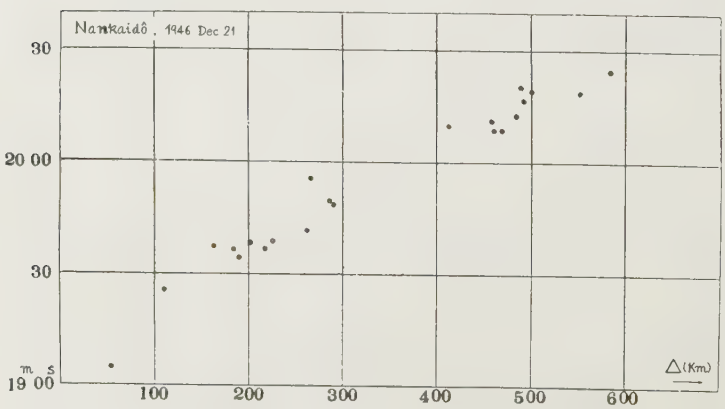

Fig. 16. Time-distance curve (P-wave) of the Nankaido Earthquake.

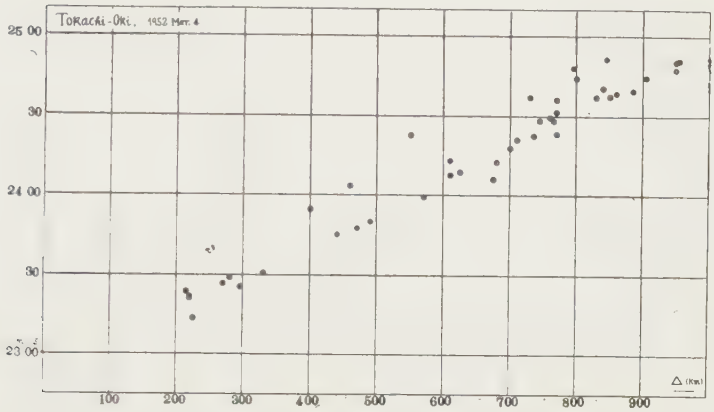

Fig. 17. Time-distance curve (P-wave) of the Tokachi-Oki Earthquake.

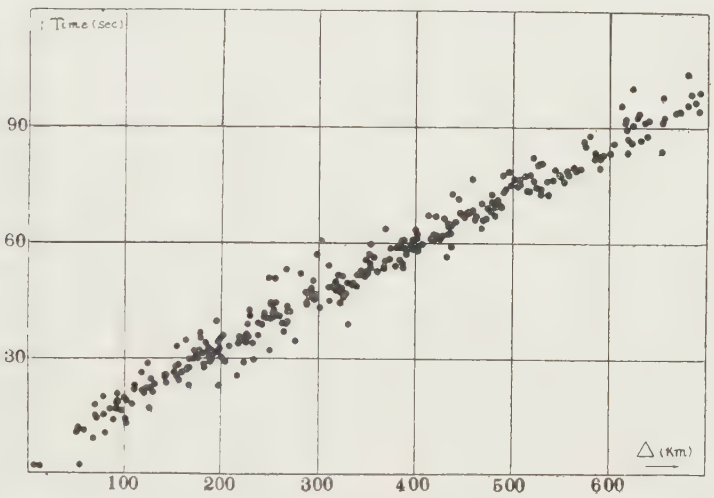

Fig. 18. Superposed time-distance graph (P-wave) of nine destructive earthquakes listed in Table 3.

Comparing these travel time-distance curves derived from nine destructive earthquakes which occurred in the last twenty years in Japan, the difficult circumstances are generally understood for the precise determination of the crustal structure from the analysis of these travel time-distance curves. The difficulties are considered to originate, as already discussed, from the regional differences of the crustal structure, the inaccuracy of time determination, the uncertainty of focal depth and other various disturbances. In a rough treatment all the curves were gathered, as a trial, in a diagram as seen in Fig. 18. In this figure the apparent velocities of the P-wave are roughly estimated as 6.2 km/sec and 8.0 km/sec for the direct and refracted waves respectively, and the critical distance is also tentatively calculated as 150 km. And

these velocities of 6.2 km/sec and 8.0 km/sec are considered to be the mean values of the granodioritic and basaltic layers for the former and that of the mantle surface for the latter respectively. In case of rough calculation of the depth of the *M*-discontinuity under this assumption of one layer structure of the crust, what value of the thickness of the crust will be derived from the above obtained travel time-distance curve superposed with nine destructive earthquakes of various origins? The value of some 40 km is obtained with regard to the depth of the *M*-discontinuity, in other words, the thickness of the crust, under the assumption that the mean focus is at a point 15 km from the ground surface in the 6.2 km/sec-layer. Under various circumstances it is reasonably presumed that the value of some 40 km denotes approximately the averaged thickness of the crust in Japan.

4. On the third class

The third class consists of the earthquakes of the Group-e, and their epicenters are, as seen in Fig. 1, in the eastern part of the Kanto District and its neighbouring open sea. The focal depths of these earthquakes were estimated by C.M.O. as 40～50 km below the ground surface, and deduced from the observed fact of existence of forerunners, shown in Figure B(b), their foci may correctly be placed in the basaltic layer. In this case the precise structure of the upper crust, namely the granitic and granodioritic layers, was not yet determined by the forerunner analysis method in the same sense of our present investigation. But from the crustal structure obtained by T. Matuzawa (**26**, **27**, **28**, **29**) and the velocities of the basaltic layer and the surface layer of the mantle determined from the superposed travel time-distance curve, as shown in Fig. 19, of thirteen remarkable earthquakes of Kashima-Nada's origin in this Group-e, the most plausible curve 5 for connecting the durations of forerunners of the third class is drawn, as in Fig. 2. The curve 5 is calculated under the conditions that the velocity of the *P*-wave in the basaltic layer is 6.8 km/sec, that in the surface layer of the mantle 8.2 km/sec, the thickness of the basaltic layer of horizontal structure between the region of Kanto-Kyoto is 18 km. It ought to be mentioned here that the horizontally parallel structure of the basaltic layer between Kanto and Kyoto assumed above is adopted simply for the sake of convenience, and a conclusive answer to this problem deduced from the detailed investigation on regional differences in the crustal structure of each locality is eagerly awaited, because it is possible to imagine that the mountainous region in the middle of Kanto and Kyoto will show a considerably large anomaly on the depth of the *M*-discontinuity. And moreover a value of some 52 km for the thickness of one layered crust is deduced from the data in Fig. 19, that is 7.3 km/sec, 7.9 km/sec and 300 km for the *P*-velocity in the crust and the mantle, and the critical distance respectively.

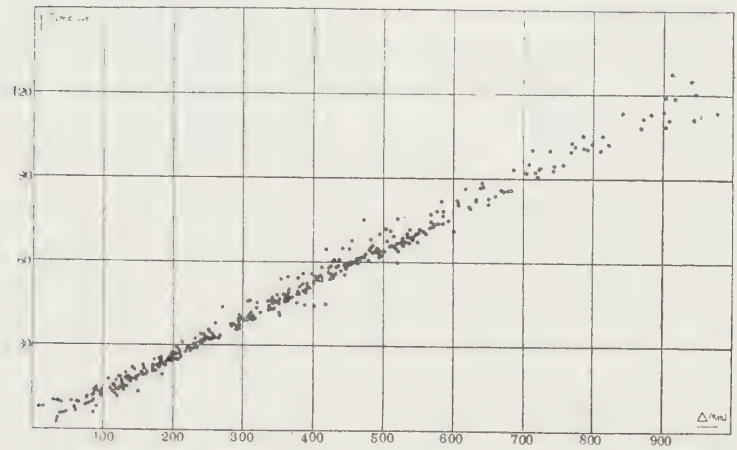

Fig. 19. Superposed time-distance graph (P-wave) of thirteen earthquakes of the third class (e-Group) listed in Table 2.

And it is desirable that a definite conclusion should reasonably be postponed to the day of the accomplishment of a precise and synthetic study on the forerunner and travel time-distance curves of the earthquakes in the Kanto District as deduced from the accurate observed data obtained at some reliable observatories in the same district.

5. On the fourth class

This class contains the earthquakes of Group-f whose epicenters are in the Hyuga-Nada District, as shown in Fig. 1. The epicenters and focal depths of earthquakes belonging to this Group are not accurately determined because their epicenters are generally off in the open sea of Hyuga-Nada and the surrounding observatories are scanty in number and too distant from the origin. But to fit the durations of the forerunners plotted in Fig. 2, it is impossible to place the focus in the basaltic layer no matter what structure the crust might have in a reasonable range. And, as seen in Fig. 20 which is the superposed travel time-distance curve of ten Hyuga-Nada earthquakes, the velocity of the direct wave and the mantle-surface are approximately calculated as 6.0 km/sec and 7.9 km/sec for the P-waves respectively. From these facts the most plausible curve 6 is tentatively drawn, as seen in Fig. 2, under the conditions that the focus is at the middle of the granodioritic layer and the P-velocities of the basaltic layer and the mantle-surface are 7.0 km/sec and 8.1 km/sec respectively. And, moreover, the thickness of the basaltic layer is assumed as horizontally parallel and 15 km for the region between Hyuga-Nada and Kyoto. But this consideration on the crustal structure at Hyuga-Nada, needless to say, should reasonably be postponed till a more precise investigation be made in the future of

the data obtained at the observatories near this Hyuga-Hada District. Also in this case, the averaged value of rough estimation on the crustal thickness referred to the materials in Fig. 20 is calculated as 23 km under the condition that the focus is at the middle of the one layered crust, and the *P*-wave-velocities of the crust and the mantle-surface are 6.0 km/sec and 7.9 km/sec respectively, and the critical distance is 100 km. These considerations referring to the travel time-distance curve are not expected to draw any definite value for the crustal thickness, but it may safely be said that, under the assumption of one layered crust, the value of some 23 km obtained from the superposed travel time-distance curve of the Hyuga-Nada earthquakes is distinctly smaller than that (52 km) of the Kashima-Nada earthquakes as derived from Fig. 19, and thencefrom an essential difference of the crustal thickness can be detected and discussed to a certain degree by the comparison of the materials derived from the superposed travel time-distance curve around any two regions with different crustal structures, considerably distant and diverse from each other.

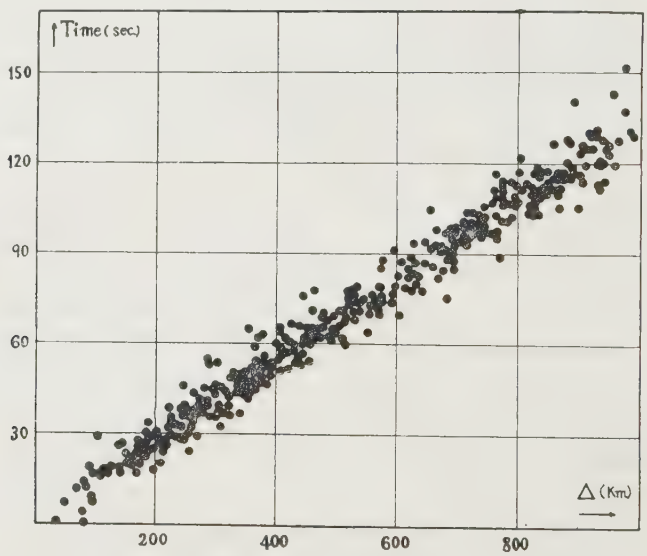

Fig. 20. Superposed time-distance graph (*P*-wave) of ten earthquakes of the fourth class (f-Group).

In concluding the section **2** of "Forerunner of long duration" the following may be summarized: from the analysis of the forerunners supplemented with the materials of travel time-distance curves the crustal structures under various regions in Japan, especially detailed in the Kinki District around Kyoto, were determined and discussed. And from them the existence of large regional differences in the crustal structure in Japan was generally ascertained. In the succeeding section, the problem of these regional differences in crustal structure will be ascertained by other means.

3. Thickness of the basaltic layer

1. Thickness of the basaltic layer under Kyoto

In the preceding paragraphs the existence of regional differences in crustal structure was ascertained by comparing the durations of refracted waves of earthquakes having occurred in various regions. But, in that case, only the mean thickness could be discussed, as already mentioned, under the unpractical assumption of the horizontally parallel structure of the basaltic layer. In order to determine the absolute value of thickness of the basaltic layer under any point, the reflected or transformed seismic waves of near earthquakes to that point should be investigated. On these two methods the detailed treatment will be postponed to a succeeding paper, and in the present place the transformed seismic waves of the earthquakes near Kyoto of somewhat deep focus are tentatively examined for determination of the thickness of the basaltic layer around Kyoto.

In the present treatment the data concerning the various layers around Kyoto are reasonably assumed as follows:

Layer	V_p km/sec	V_s km/sec	Thickness km	Density c.g.s.	Discontinuity
Granitic layer	5.4	3.1	6	2.6	
					..... g–g
Granodioritic layer	5.8	3.4	14	2.7	
					..... g–b
Basaltic layer	7.0	(4.0)	?	3.0	
					..... M
Mantle surface	8.2	(4.7)	—	3.4	

It is to be mentioned here that the values of V_s in parentheses are calculated from the value of V_p taking the value of Poisson's ratio to be 0.26, while the values of density adopted in this table are the most plausible ones obtained by many authors.

The earthquakes used in the present are, as listed in Table 4, those of mediate focal depth (nearly 70 km) whose epicenters were nearly 100 km distant and in the south direction from Kyoto. As shown in Figure C many distinct phases are observed between the arrivals of direct P– and S–waves in their seismograms. As inferred from their focal depths estimated by C.M.O. and the type of their seismograms, namely unaccompanied by forerunners and the lack of predominating surface waves or others which characterize the earthquake of shallow origin, their foci are safely considered to be under the Mohorovičić discontinuity. Taking these conditions into consideration the distinct phases above described may be interpreted as: (a) transformed waves at the discontinuities in the crust, or, (b) reflected waves at the earth surface and again at the discontinuities in the crust, or, (c) transformed or reflected waves in any discontinuities of first order, if exist, in the mantle. In the present

treatment the case of (c) is reasonably excluded, and only two cases of (a) and (b) will be discussed. In our investigation the name of 'transformed wave' is designated for the wave which is transformedly refracted from *P*-wave to *S*-wave or from *S*-wave to *P*-wave at any discontinuous surface, namely 'Wechselwellen'. For the purpose of identification of observed distinct phases the expected amplitude ratio of (a)- and (b)-waves with regard to the earthquakes concerned should be theoretically calculated under the conditions of crustal structure above listed. In this case the propagating seismic wave is assumed to be a plane wave of no damping. And with regard to the *g*-*g* discontinuity, the difference in velocity and density is small compared with the other two *g*-*b* and *M*-discontinuities as seen in the above table, therefore the present calculation concerns mainly the *g*-*b* and *M*-discontinuities. The calculated amplitude ratios are as follows, taking the amplitude of the first incident wave as unit:

	Medium	Transformation	Emergent Angle	*g*-*b* Discontinuity	*M*-Discontinuity	After K & S
(1)	hard → soft	$P \rightarrow S'$	26°	0.151	0.158	0.195
(2)	„	$P \rightarrow P'$	26	—	0.929	0.885
(3)	soft → hard	$P \rightarrow P_1$	54	0.089	—	0.097
(4)	„	$P \rightarrow P_1$	49	—	0.106	0.105
(5)	„	$P \rightarrow S_1$	54	0.093	—	0.105
(6)	„	$P \rightarrow S_1$	49	—	0.19	0.095

Of the above table some remarks should be made. Here 'hard' medium in the first column means that of large velocity and density compared with 'soft' medium. And the 'prime' (′) and 'suffix' ($_1$) denote the refracted and reflected waves at any discontinuity respectively. 'K & S' in the last column is abbreviation of H. Kawasumi and T. Suzuki and the numericals in this column are the amplitude ratio calculated by them (**45**). In 'K & S' case the ratios of hard/soft are 1.1 in density, 1.5 in seismic velocity and 0.25 in Poisson's ratio. As both values obtained by 'K & S' and us are roughly in an agreement, the calculated values after 'K & S' may reasonably be used in our investigation as the amplitude ratios in other various cases. And moreover the calculated values after T. Matuzawa (**46**) are also to be applied as the amplitude ratio of the reflected wave at the free surface of the earth. After these considerations, the transformed and reflected waves worth discussing in the present case are as follows:

$$P \rightarrow S'(M),\quad P \rightarrow S'(g\text{-}b),\quad S \rightarrow P'(M),\quad S \rightarrow P'(g\text{-}b),\quad P \rightarrow P_1 \rightarrow P_1(FS,\ M),$$
$$P \rightarrow P_1 \rightarrow P(FS,\ g\text{-}b)$$

The other waves except the above may safely be excluded in the present discussion by reason of their too small amplitudes and relations of arrival time. In the

Table 4. List of the earthquakes used for the investigation of the transformed waves

Date	Epicenter and focal depth	Epicentral region	$P \sim S$	Incident phases							
				Observational				Calculated			
d. *h.* *m.*			*s*	No.	Duration	(Component,	amplitude ratios)	Phase identification	Duration	(component,	amplitude ratios)
1953 Sept. 1 23 15	34, 0°N 135, 7°E 70km	Southern part of Nara Pref.	13.2	1	*s* 4.0	(*H*,	0.3)	$P \rightarrow S'$ (M)	*s* 4.3	(*H*,	0.31)
				2	6.1	(*H*,	0.29)	$S \rightarrow P'$ (M)	6.2	(*H*,	0.27)
					6.3	(*V*,	0.2)			(*V*,	0.17)
				3	7.7	(*H*,	0.24)	$P \rightarrow P_1 \rightarrow P_1$ (FS, M)	7.6	(*H*,	0.07)
				4	9.2	(*H*,	0.37)	$S \rightarrow P'$ $(g-b)$	8.8	(*H*,	0.46)
					9.1	(*V*,	0.26)			(*V*,	0.25)
1952 Aug. 8 21 41	34, 5°N 135, 8°E 65km	Central part of Nara Pref.	10.2	1	5.2	(*V*,	0.25)	$S \rightarrow P'$ (M)	5.3	(*V*,	0.21)
				2	6.2	(*H*,	0.38)	$P \rightarrow P_1 \rightarrow P_1$ $(FS, g-b)$	6.2	(*H*,	0.06)
						(*V*,	0.11)			(*V*,	0.07)
				3	6.9	(*H*,	0.37)	$S \rightarrow P'$ $(g-b)$	7.0	(*H*,	0.53)

above described waves the figures M, g–b and FS in the parentheses denote the refraction and reflection at the M–, g–b discontinuity and the free surface of the earth respectively. It is a very interesting and essential problem to discuss in detail the individual waves mentioned above for investigating the crustal structure around Kyoto or other regions, but its treatment will be reserved for another occasion. And here the $P \rightarrow S'(M)$ and $S \rightarrow P'(M)$ will mainly be discussed. The thickness of the basaltic layer around Kyoto was roughly estimated to be in the range of 5~15 km after the above described investigation of forerunners, therefore the travel time-distance curves for individual phases are calculated and shown in Figs. 21, 22 and 23 under the assumed thicknesses of the basaltic layer as 5 km, 10 km and 15 km respectively. Comparing these three figures it is natural to conclude that the value of 10 km is the most plausible for the thickness of the basaltic layer under Kyoto. Detailed comparison of the thickness of the basaltic layer under various regions or more general study for the regional difference of the crustal structure by the analysis of the transformed or reflected waves will be postponed to a succeeding investigation.

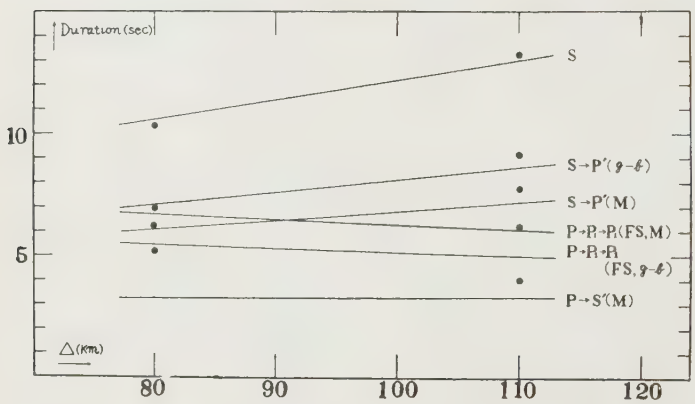

Fig. 21. Durations calculated from the first arrival of P-wave of the transformed and reflected waves in case of 5 km thickness of the basaltic layer.

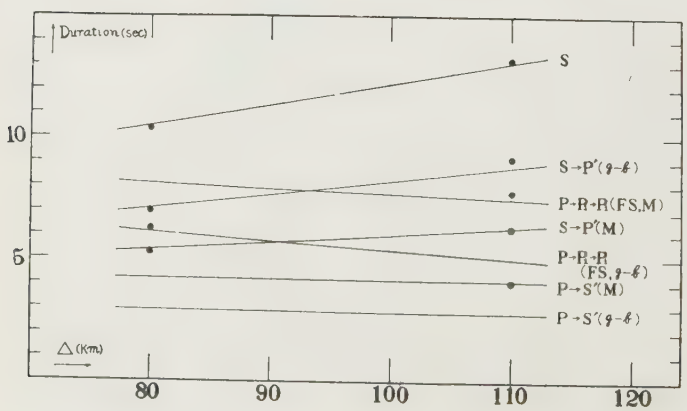

Fig. 22. Durations calculated from the first arrival of P-wave of the transformed and reflected waves in case of 10 km thickness of the basaltic layer.

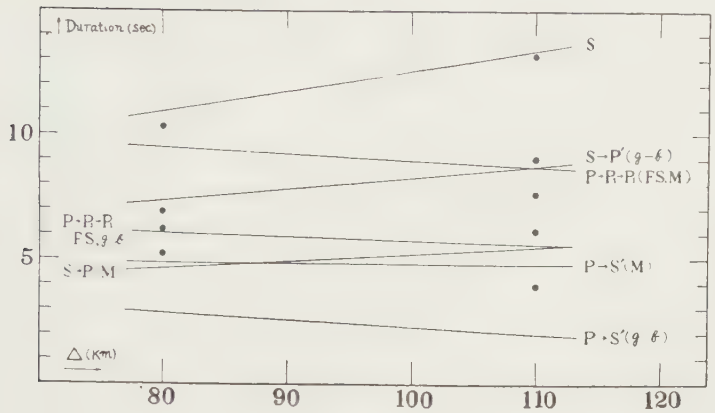

Fig. 23. Durations calculated from the first arrival of *P*-wave of the transformed and reflected waves in case of 15 km thickness of the basaltic layer.

2. Some examples of locating the depth of M-discontinuity

In case of seismometric observations of an earthquake at some proper distance the non-appearance of forerunners can safely be interpreted as a positive proof for the fact that the focus of the concerned earthquake is situated under the *M*-discontinuity, unless an absurdly anomalous crustal structure is assigned to the area concerned. Under this consideration the depth of *M*-discontinuity might roughly be located by comparing two earthquakes, one accompanied and one unaccompanied by forerunners with their epicenters in the same area. As examples, two cases will be reported, namely the earthquakes with their epicenters in Nankaido District and Kanto District. As shown in Figure D on the seismograms obtained with the large Wiechert Seismographs at the Kamigamo Geophysical Observatory, the earthquakes on March 9, 1950(a) and on May 8, 1952(c) were not accompanied by forerunners, and the earthquakes on July 31, 1953(b) and on July 1, 1943(d) inserted for comparison were clearly preceded by forerunners. The epicenters of earthquake (a) and earthquake (b) are close in less than 140 km distance in the open sea of Nankaido ($\varphi=33.2°$ N, $\lambda=136.3°$ E for (a) and $\varphi=33.2°$ N, $\lambda=134.8°$ E for (b)) and the focal depth was estimated by the C.M.O. as 40 km for (a) and 20 km for (b) respectively. From these examples, if the value of focal depth determined by C.M.O. is provisionally confirmed, the depth of the *M*-discontinuity in this area is roughly located as 30～40 km or less than 30 km from the other examples. And this depth value for the *M*-discontinuity is well consistent with that derived from the analysis of forerunners of earthquakes in the Nankaido District. On the other hand, the epicenters of earthquakes (c) and (d) are close in less than 80 km distance in Chiba and Ibaraki Prefectures ($\varphi=35.5°$ N, $\lambda=140.2°$ E for (c) and $\varphi=36.2°$ N, $\lambda=140.0°$ E for (d)) and the focal depth is estimated by C.M.O. as 50～60 km for (c) and 50 km for (d). From the same consideration as the former example, the depth of the *M*-discontinuity

in this area is roughly located as 50 km after the numerical value ascribed by C.M.O., and this figure of 50 km also corresponds to the mean depth of the *M*-discontinuity roughly obtained by the analysis of superposed travel time-distance curves of thirteen Kashima-Nada earthquakes. This method of locating the depth of the *M*-discontinuity has certainly a weak point in the uncertainty of focal depth value, but a wide application and fruitful study might be expected in near future by applying this method of location for suitable earthquakes of accurately determined foci.

3. Focal depths in relation to crustal thickness

It has early been noticed that a swarm of earthquakes occurring in any fixed area has nearly the same focal depths, and in this section a problem will be examined as to whether or not there is any relation between the focal depths of frequent occurrence in any fixed area and the crustal thickness under that area. Before entering the treatment the problem of value of focal depth determined by seismometric observation should again be discussed. The accurate determination of focal depth is, as already mentioned, a very difficult task, especially for earthquakes in Japan. But putting the problem of difficulty aside for a while, the difference in values calculated from the crustal structure obtained by C.M.O. and the present investigation will be treated in this section under the assumption that the travel-time of the *P*-wave or the *S*-wave were accurately determined at the epicenter or its neighbouring points. The crustal structures adopted by C.M.O. for the calculation of focal depth and others are those by K. Wadati and others (**47**, **48**), and the crustal structure adopted in the present investigation for comparison is as shown in Fig. 24. In this figure the travel-times of the *P*-wave and the *P*~*S*-wave at the epicenter are also plotted for comparison under the crustal structure by C.M.O. and the present investigation. As seen in the figure, the relation between the values of focal depth determined by the same travel time of the *P*-wave at the epicenter of the crustal structure with C.M.O. and the present paper is as follows:

C.M.O.	10 km	20	30	40
The present structure	12	23	34	46

And in Fig. 25 the travel time-distance curves by both structures are plotted under the conditions of various positions of focus. In this figure the full lines of 1~4 refer to the present structure in cases of the focus at 1) the middle point in the granitic layer (Ca. 5 km-depth), 2) the middle point in the granodioritic layer (Ca. 15 km-depth), 3) the middle point in the basaltic layer (Ca. 27 km-depth) and 4) the bottom of the basaltic layer (Ca. 32 km-depth), and the broken lines of 5~7 are calculated by C.M.O.-structure under the conditions of focal depth of 5) 0 km, 6)

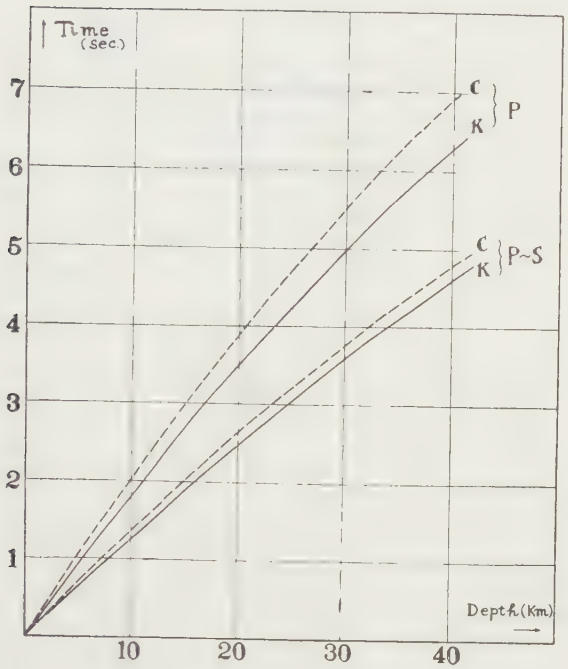

Fig. 24. Travel times of P– and $(P\sim S)$–waves at the epicenter for various focal depths. The full lines (K) and the broken lines (C) represent those calculated by Kishimoto and C.M.O. respectively.

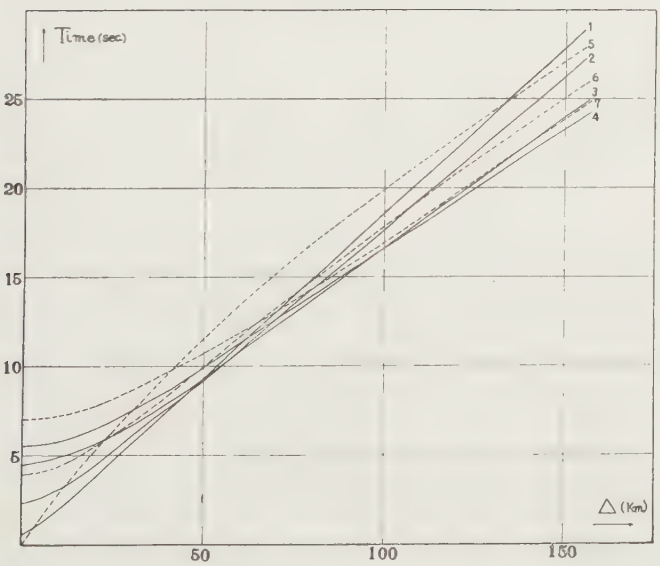

Fig. 25. Comparison of travel time-distance curves between those calculated under the structure of Kishimoto (full lines) and C.M.O. (broken lines) for various focal depths.

20 km and 7) 40 km respectively. From the above described discussion, it is generally understood that the determination of focal depth contains many difficult problems in itself, but in case of permitting errors of some several kilometers the values of focal depth could certainly become an object of discussion, especially in a procedure for

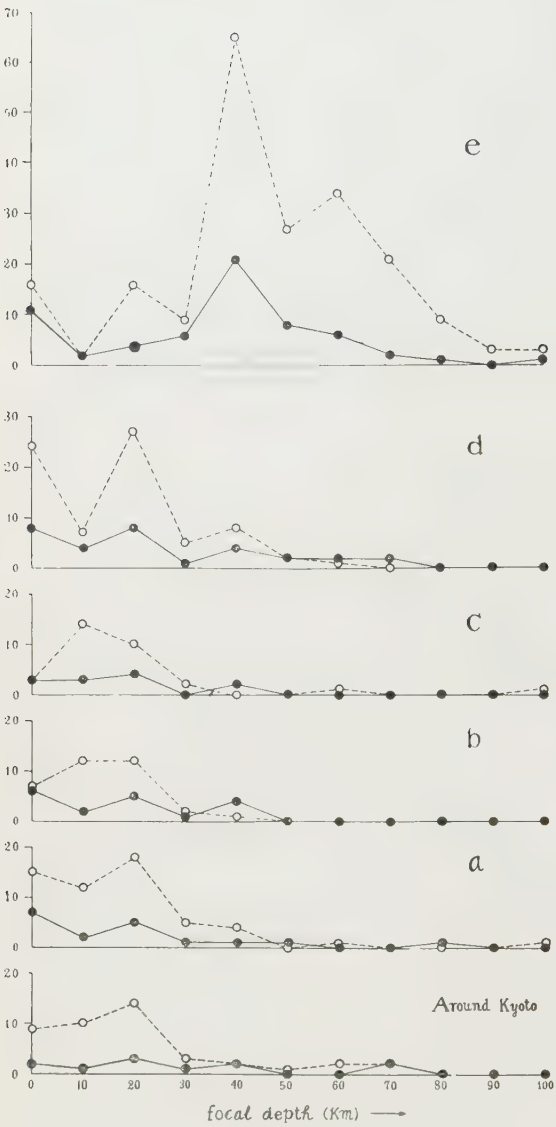

Fig. 26. Relation between frequency of earthquake occurrence and their focal depths classified in the various districts.
The dots and circles denote 'small' and 'moderate and remarkable' earthquakes respectively.

comparing two considerably different values of focal depth.

Remembering the circumstances mentioned above the curves for frequency of occurrence against the focal depth of the earthquakes of 1943 to 1953 at various districts of a～e already denoted in Fig. 1 are plotted in Fig. 26, according as three seismic grades of 'remarkable' (sensible by human feeling at $\Delta > 300$ km), 'moderate' (sensible at $300\text{ km} > \Delta > 200$ km) and 'small' (sensible at $200\text{ km} > \Delta > 100$ km). In this case the focal depths adopted are determined by C.M.O. In the figure the difference of the peak value of focal depth with two regions of (d) and (e) is very remarkable, and these peak values of 20 km and 40 km for the earthquakes of the Nankaido Group and Kashima-Nada show a well consistent correspondency with the crustal thickness of 52 km and 24 km obtained by the analysis of travel time-distance curves and the duration of forerunner for their respective regions. In allowance for a speculative argument the earthquakes are considered to have tendency to occur frequently at the bottom of the crust.

4. Summary

In the present investigation the analysis of seismic refracted wave (forerunner) was made in detail of the seismograms of natural near and mediate distant earthquakes obtained mainly at the Kamigamo Geophysical Observatory in Kyoto. For the purpose of investigating the crustal structure the method of analysing the travel time-distance curve is usually applied, but it contains many inevitable defects as, for example, inaccuracies in determination of seismic focal depth, arrival time, apparent seismic velocity, critical distance and others, in addition to local effects in the area of the hypocenter and observatory. But the concurrent use of analysis of the forerunner duration, the reflected wave and the transformed wave with the travel time-distance curve may greatly improve the research procedure and raise the reliability of the obtained numerical values. In the present treatment some discontinuous layers in the earth crust were successively investigated from the uppermost layer to the lowest layer by separately analysing the durations of seismic wave forerunners according to their direction and the distance of the epicenter from Kyoto, the study being appropriately supplemented by the analysis of travel time-distance curves and transformed waves. From the present treatment the crustal structure under Kyoto was tentatively determined as follows:

	V_p km/sec	V_s km/sec	Thickness km	Depth of the bottom km
Sedimentary layer	3.8	2.1	1.5	1.5
Granitic layer	5.4	3.1	6	7.5
Granodioritic layer	5.8	3.4	14	21.5
Basaltic layer	7.0	4.0	10	31.5
Mantle surface	8.1	4.7	—	—

A remarkable fact deduced from the present treatment is that of the regional differences of the thickness of the earth's crust which is considered to be intimately related to the distribution of gravity anomaly (**49**) and, moreover, the distribution of seismic focal depths of frequent occurrence. The depth of the Mohorovičić discontinuity or, in other words, the thickness of the crust as deduced from the present investigation is schematically shown in Fig. 27. In case of a monotonous inclination, instead of the horizontally parallel structure above mentioned, of the basaltic layer under the assumption of the value of crustal thickness of 30 km at Kyoto, the crustal thickness at various regions around Kyoto are tentatively calculated as shown in the figure. In the present case, the data observed only at the Kamigamo Geophysical Observatory were used, but the same method is recommended to many observatories at various places for the development of our knowledge on the micro-structure of the earth's crust.

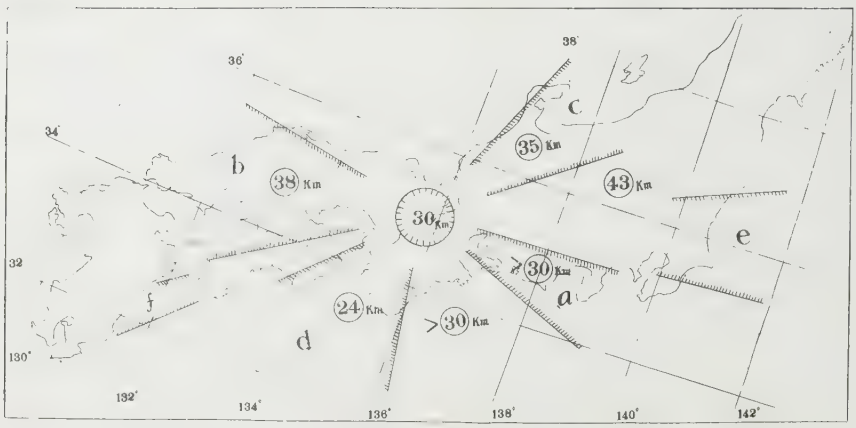

Fig. 27. Schematical representation of the crustal thickness in the various districts.

Acknowledgment

The writer wishes to express his heartfelt thanks to Prof. E. Nishimura for his kind guidance throughout the present study and also to Prof. K. Sassa for his generous permission to analyse seismograms obtained at the Kamigamo Geophysical Observatory and the Abuyama Seismological Observatory during the past so many years. The writer is also greatly indebted to the directors and members of the Central and Provincial Meteorological Observatories in Japan for their kind permission for copying seismograms obtained at their observatories. The cost for the study was partly covered by a grant-in-aid for Scientific Research of the Ministry of Education.

REFERENCES

1. Mohorovičić, A., Das Beben vom 8, Oktober 1909, Jahr. Meteorol. Obs. Zagreb, für das Jahr 1909, 9. T., A. 1. Zagreb, (1910).
2. Gutenberg, B., Die Mitteleuropaischen Beben vom 16, November, 1911 und vom 20, Juli, 1913, Strassburg, Veröff. Zentralbureaus der Internationalen Seismologischen Assoziation, (1915).
3. Jeffreys, H., On near earthquakes, Mon. Not. Roy. Astr. Soc., Geophys. Suppl., **1**, (1926) 385-402.
4. Conrad, V., Das Schwadorfer Beben, Gerl. Beitr. z. Geophys., **20** (1928), 240-277.
5. Hecker, O., Die Explosionskatastrophe von Oppau, Veröff. der Hauptstation für Erdbebenforschung, Jena, **2** (1922), 1-18.
6. Wrinch, D. and Jeffreys, H., On the seismic waves from the Oppau explosion, Mon. Not. Roy. Astr. Soc., Geophys. Suppl., **1** (1923), 15-22.
7. Gutenberg, B., Die Geschwindigkeit der Erdbebenwellen in der obersten Erdschichten und ihr Einfluss auf die Ergebnisse einiger Probleme der Seismometrie, Gerl. Beitr. z. Geophys. **15** (1926), 51-63.
8. Byerly, P. and Wilson, J. T., The central California Earthquakes of May 16, 1933 and June 7, 1934, Bull. Seism. Soc. Amer., **25** (1935), 223-246.

9. Byerly, P., Near Earthquakes in Central California, Bull. Seism. Soc. Amer., **29** (1939), 427–462.
10. Leet, L. Don, Travel times for New England, Bull. Seism. Soc. Amer., **28** (1938), 45–48.
11. ———, Trial travel times for Northeastern America, Bull. Seism. Soc. Amer., **31** (1941), 325–334.
12. ———, The velocity of P in the granitic layer, Trans. Amer., Geophys. Union, **27** (1946), 631–635.
13. Gutenberg, B., Seismological evidence for the roots of mountains, Bull. Geol. Soc. Amer., **54** (1943), 473–492.
14. ———, Crustal layers of the continents and oceans, Bull. Geol. Soc. Amer., **62** (1951), 427–440.
15. ———, Trave times from blasts in Southern California, Bull. Seism. Soc. Amer., **41** (1951), 5–12.
16. ———, Revised travel times in Southern California, Bull. Seism. Soc. Amer., **41** (1951), 143–163.
17. ———, Waves from blast recorded in Southern California, Trans. Amer. Geophys. Union, **33** (1952), 427–431.
18. ———, Low-velocity layers in the earth's mantle, Bull. Geol. Soc. Amer., **65** (1954), 337–348.
19. Kubotera, A., Rheological properties of the earth's crust and alluvial layers in relation to propagation of seismic waves, J. Phys. Earth, **1** (1952), 25–34.
20. Hughes, D. S. and Cross, J. H., Elastic wave velocities at high pressures and temperatures, Geophysics, **16** (1951), 577–593.
21. The Research Group for Explosion Seismology, Tokyo, The first explosion seismic observations in North-Eastern Japan, Bull. Earthq. Res. Inst., **29** (1951), 27–106.
22. ———, The second explosion seismic observations in North-Eastern Japan, Bull. Earthq. Res. Inst., **30** (1952), 279–292.
23. ———, The third explosion seismic observations in North-Eastern Japan, Bull. Earthq. Res. Inst., **31** (1953), 281–289.
24. ———, The fourth explosion seismic observations in North-Eastern Japan, Bull. Earthq. Res. Inst., **32** (1954), 79–86.
25. ———, Bulletin of the Group, No. 10, published by the Group, 1954.
26. Matuzawa, T., Observation of some of recent earthquakes and their time-distance curves (Part I), Bull. Earthq. Res. Inst., **5** (1928), 1–28.
27. ———, ——— (Part II) Bull. Earthq. Res. Inst., **6** (1929), 177–204.
28. ———, ——— (Part III) Bull. Earthq. Res. Inst., **6** (1929), 205–212.
29. ———, ——— (Part IV) Bull. Earthq. Res. Inst., **6** (1929), 213–229.
30. Hodgson, E. A., The P-curve and the S-curve resulting from a study of the Tango Earthquake, Japan, March 7, 1927, Bull. Seism. Soc. Amer., **22** (1932), 38–49.
31. ———, Epicentral time and surface structure determined for the Tango Earthquake, Japan, March 7, 1927, Bull. Seism. Soc. Amer., **22** (1932) 270–287.
32. Tatel, H. E., Adams, L. H. and Tuve, M. A., Studies of the Earth's crust using waves from explosions, Proc. Amer. Philos. Soc., **97** (1953), 658–669.
33. Tuve, M. A., Tatel, H. E. and Hart, P. J., Crustal structure from seismic explosion, Journ. Geophys. Res., **59** (1954), 415–422.
34. Mintrop, L., On the stratification of the earth's crust according to seismic studies of a large explosion and of earthquakes, Geophysics, **14** (1949), 321–336.

35. Reich, H., Foertsch, O. and Schulze, G. A., Results of seismic observations in Germany on the Heligoland Explosion of April 18, 1947, Journ. Geophys. Res. **56** (1951), 147–156.
36. Willmore, P. J., Seismic experiments on the North German Explosions 1946 to 1947, Phil. Trans. Roy. Soc. London, Ser. A, **242** (1947), 123–151.
37. Rothé, J. P., L'enrégistrement dans les stations françaises des ondes séismiques de l'explosion d'Heligoland, Comptes Rendus de l'Académie des Sciences, Paris, **224** (1947), 1572-1574.
38. Gutenberg, B., Reflected and minor phases in records of near-by earthquakes in Southern California, Bull. Seism. Soc. Amer., **34** (1944), 137–160.
39. Reich, H., Ueber seismische Beobachtungen des PRAKLA von Reflexionen aus grossen Steinbruchsprengungen in Blaubeuren am 4 März und am 10 Mai, 1952, Geol. Jahrbuch, **68** (1953), 225–240.
40. Matuzawa, T., Hasegawa, K. and Haeno, S., On the forerunners of earthquake-motions of certain earthquakes, Bull. Earthq. Res. Inst., **4** (1928), 85–106.
41. Matuzawa, T., Yamada, K. and Suzuki, T., On the forerunners of earthquake-motions (The second paper), Bull. Earthq. Res. Inst., **7** (1929), 241–260.
42. Byerly, P., The first preliminary waves of the Nevada Earthquake of December 20, 1932, Bull. Seism. Soc. Amer., **25** (1935), 62–80.
43. Kishimoto, Y., Seismometric investigation of the earth's interior, Part I. On the structure of the earth's upper layer, Mem. Coll. Science, Kyoto Univ., A, **27** (1954), 125-143.
44. Tsuya, H. (Chairman), The Fukui Earthquake of June 28, 1948, Report of the Special Committee of the study of the Fukui Earthquake, Published by the Committee, Tokyo, (1950).
45. Kawasumi, H. and Suzuki, T., On reflections and refractions of the earthquake waves at the crustal discontinuities (in Japanese), Zisin, **4** (1932), 277–307.
46. Matuzawa, T., An example of the reflection of plain waves at the Earth's surface (in Japanese), Zisin, **4** (1932), 125–139.
47. Wadtai, K., Sagisaka, K. and Masuda, K., On the travel time of earthquake waves (Part I), Geophys. Mag., **7** (1933), 87–99.
48. Sagisaka, K. and Takehana, M., Tables of the travel times of S-waves and the preliminary tremors in case of the near earthquakes (in Japanese), Kenshin-Ziho, **8** (1935), 149–161.
49. Tsuboi, C., Gravity survey along the lines of precise levels throughout Japan by means of a Worden Gravimeter, Part 4 Map of Bouguer anomaly distribution in Japan based on approximately 4,500 measurements, Bull. Earthq. Res. Inst., Suppl. Vol. IV, Part III, (1954).

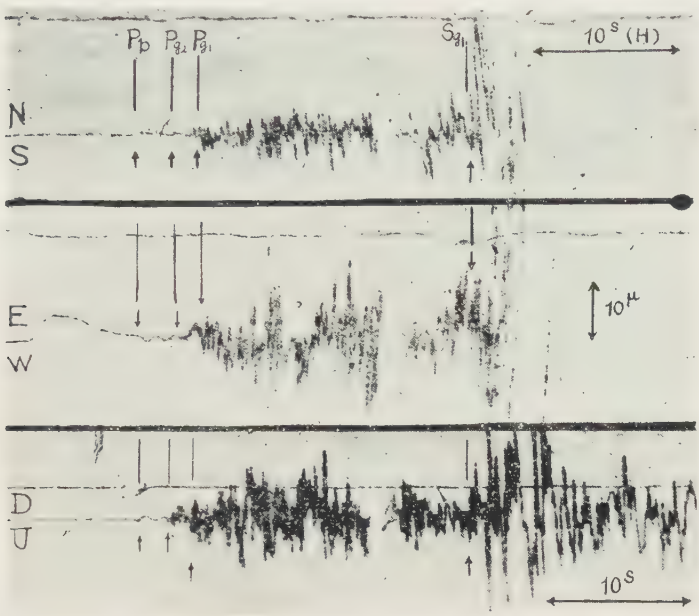

Fig. A a . Wiechert-seismograms, June 17th 23h 14m, 1949, Lake Hamana, $Pg_1 \sim Sg_1 = 22.0$ sec, $Pb \sim Pg_1 = 3.7$ sec, $Pg_2 \sim Pg_1 = 1.5$ sec, focal depth = 10km [sub-class X in the First class; a-No. 2 in Table 2]
Pg_1, Pg_2 and Pb denote the direct wave through the g_1-layer, the refracted wave at the g-g discontinuity and the refracted wave at the g-b discontinuity.

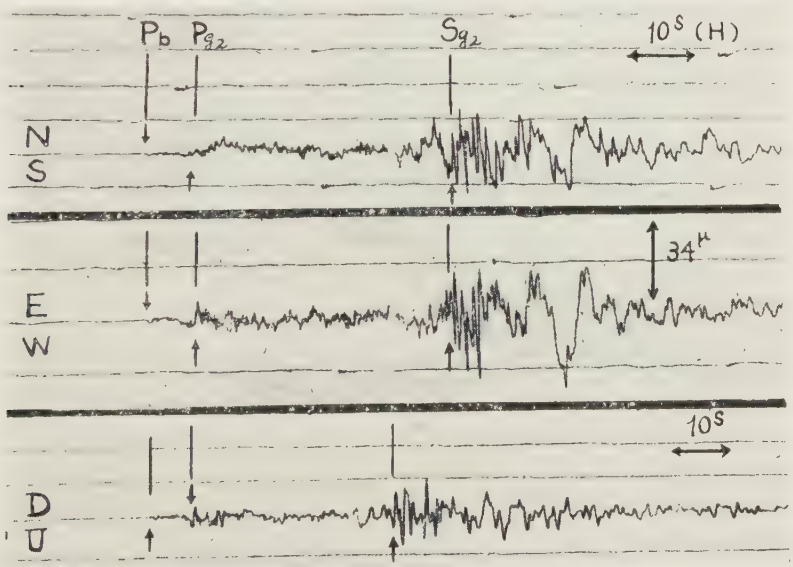

Fig. A (b). Wiechert-Seismograms, May 30th 23h 37m, 1953, Central Setoumi, $Pg_2 \sim Sg_2 = 30.1$ sec, $Pb \sim Pg_2 = 5.1$ sec, focal depth = 20km [sub-class Y in the First class; b-No. 3 in Table 2]
Pg_2 and Pb are the direct wave through the g_2- and g_1-layers and refracted wave at the g-b discontinuity.

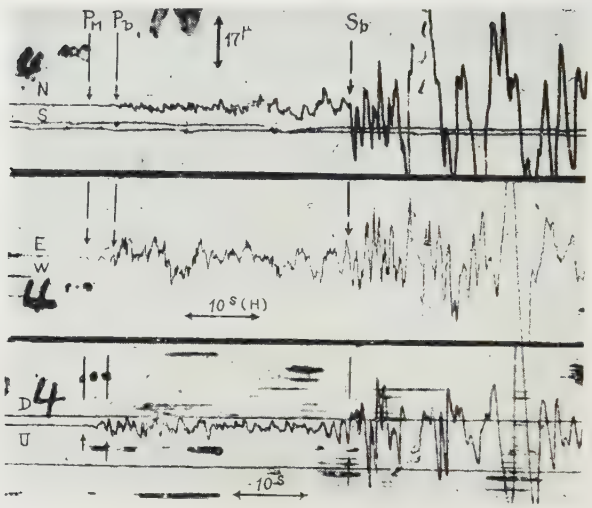

Fig. A (c). Wiechert-Seismograms, Aug. 22nd 11h 04m, 1950, Shimane Pref., Pb~Sb=31.6 sec, P_M~Pb=3.8 sec, focal depth=30 km [sub-class Z in the First class; b-No. 8 in Table 2]
Pb and P_M denote the direct P-wave through the b-, g_2- and g_1-layers, and the refracted wave at M-discontinuity.

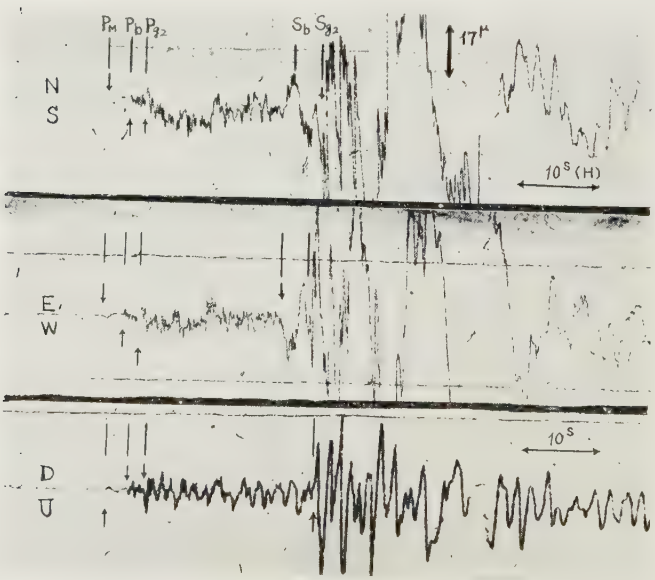

Fig. A (d). Wiechert-Seismograms, Jan. 17th 02h 44m, 1947, Tokushima Pref., Pg_2~Sg_2=19.7 sec, Pb~Pg_2=2.2 sec, P_M~Pg_2=4.7 sec, focal depth=10km [d-Group in the Second class; d-No. 1 in Table 2]
Pg_2, Pb and P_M denote the direct wave through the g_2- and g_1-layers, the refracted wave at the g-b discontinuity and the refracted wave at the M discontinuity.

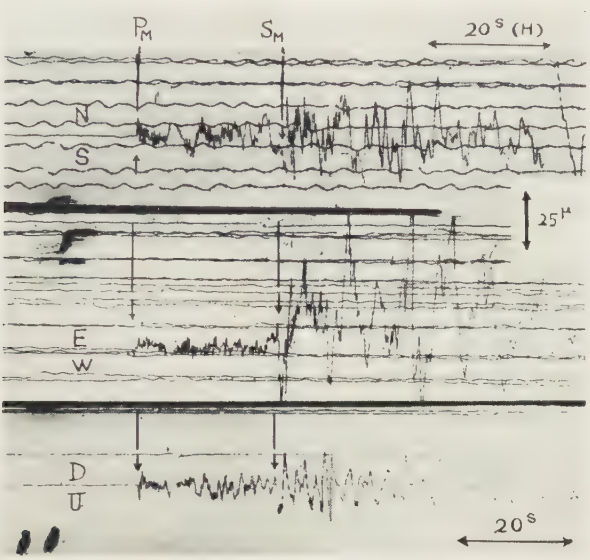

Fig. B (a). Wiechert-Seismograms, Oct. 16th 06h 02m, 1951, off Muroto-Misaki, P_M~S_M=23.7 sec, focal depth=40km
P_M denotes the direct wave through the mantle and crust.

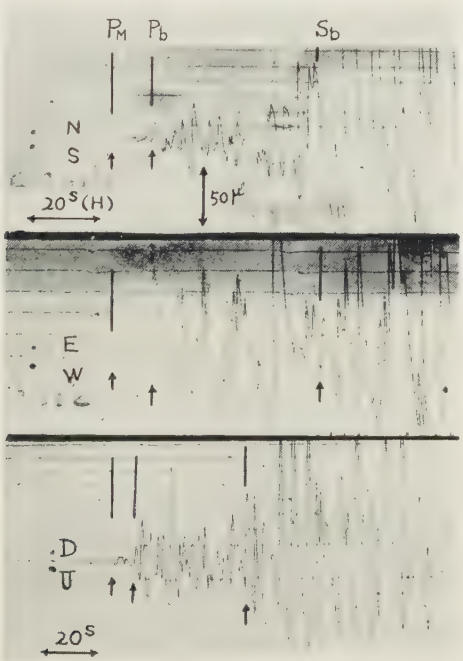

Fig. B (b). Wiechert-Seismograms, July 18th 07h 36m, 1954, near Choshi, Pb~Sb=50.5 sec, P_M~Pb=9.0 sec, focal depth=40km [e-Group : e-No. 7 in Table 2]
Pb and P_M denote the direct wave through the b-, g_2- and g_1-layers and the refracted wave at the M-discontinuity.

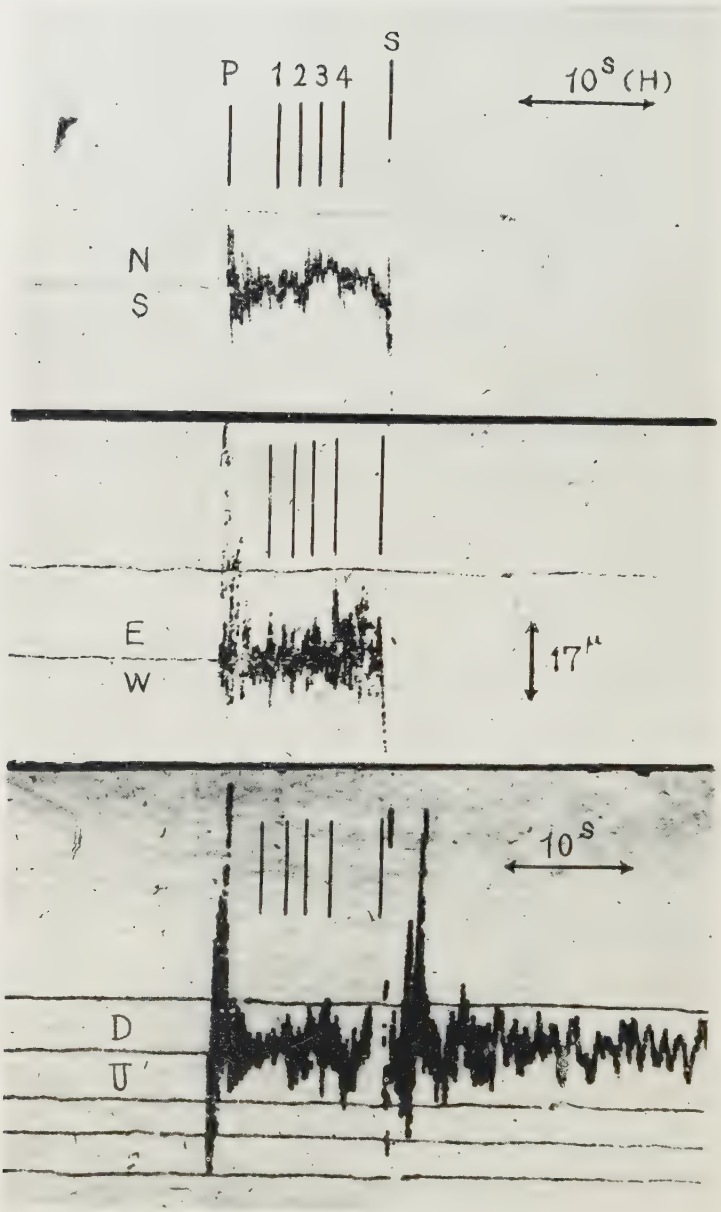

Fig. C. Wiechert-Seismograms of the mediate deep earthquake; Sept. 1st 23h 15m, Nara Pref., $P\sim S=13.2$ sec, focal depth=70 km.
The annexed figures may be referred to Table 4.

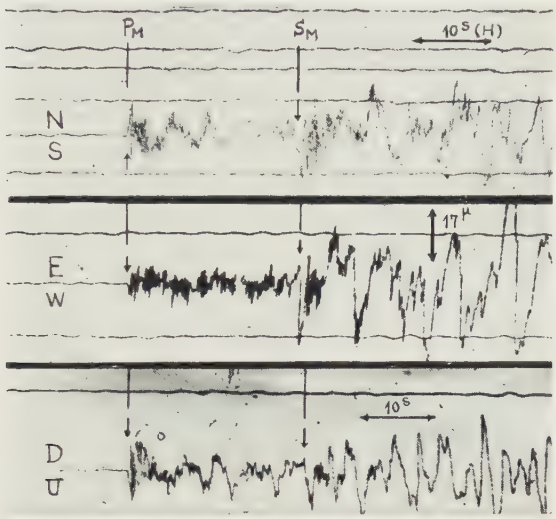

Fig. D(a). Wiechert-Seismograms not accompanied by the forerunner in the d-district; Mar. 9th 17h 59m, 1950, off Shionomisaki, $P_M \sim S_M = 21.9$ sec, focal depth=40km.
P_M denotes the direct wave through the mantle and crust.

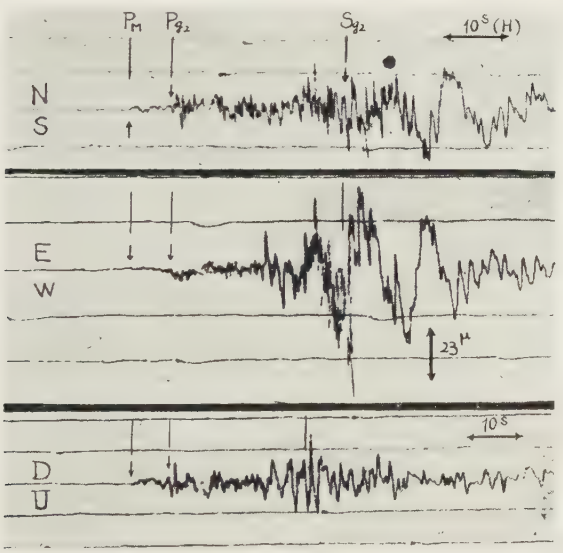

Fig. D(b). Wiechert-Seismograms accompanied by the forerunner in the d-district; July 31st 04h 24m, 1953, Nankaido, $Pg_2 \sim Sg_2 = 27.2$ sec, $P_M \sim Pg_2 = 7.4$ sec, focal depth= 20km [d-Group in the Second class; d-No. 6 in the Table 2]
Pg_2 and P_M are the direct wave through the g_2- and g_1-layers and the refracted wave at the M-discontinuity.

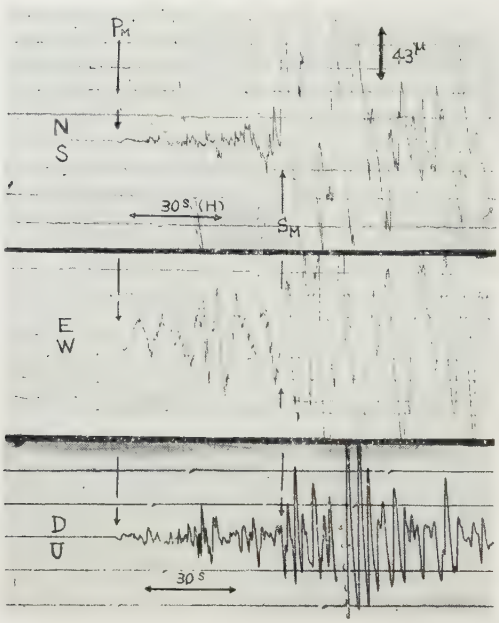

Fig. D (c). Wiechert-Seismograms not accompanied by the forerunner in the e-district; May 8th 09h 58m, 1952, Chiba Pref., P_M~S_M=52.4 sec, focal depth=50~60km
P_M denotes the direct wave through the mantle and crust.

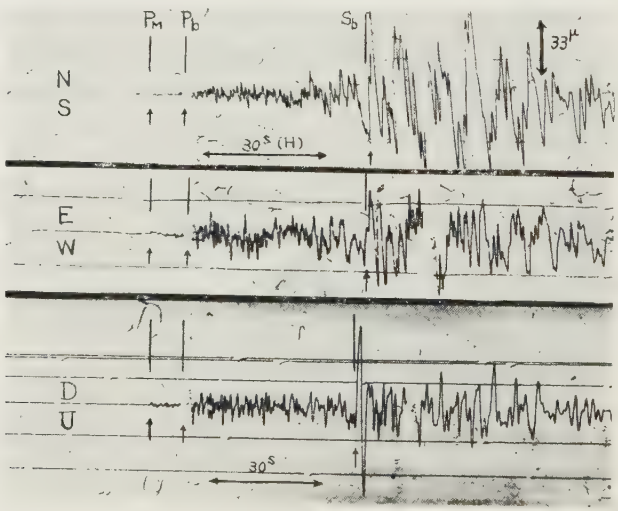

Fig. D (d). Wiechert-Seismograms accompanied by the forerunner in the e-district; July 1st 13h 40m, 1943, Ibaraki Pref., Pb~Sb=45.6 sec, P_M~Pb=9.5 sec, focal depth=50km [e-Group; e-No. 1 in Table 2]
Pb and P_M denote the direct wave through the b-, g_2- and g_1-layers and the refracted wave at M-discontinuity.

Memoirs of the College of Science, University of Kyoto, Series A,
Vol. XXVII, No. 3, Article 3, 1955

STUDY ON CHANGE OF GRAVITY WITH TIME
PART I. ON THE TIDAL VARIATION OF GRAVITY

BY

Tokio ICHINOHE

(*Received May 20, 1955*)

ABSTRACT

In this article, a newly devised gravimeter of the double bifilar suspension type was treated theoretically and experimentally for the purpose of precise and continued observation of tidal and secular variation in gravity. It was proved theoretically and experimentally that the sensitivity of the gravimeter of this type may easily be raised to a degree as high as 10^{-9}g/mm/5m. A test observation with the double bifilar gravimeter has been operated continuously for about three years at the deep-seated observation room of the Ikuno Copper Mine, and the value for the tidal factor of gravity for the M_2-component was tentatively calculated as 1.08. Furthermore, in the present treatment, minimizing the gravimeter drift proved to be a most difficult but important problem for a perfect and precise gravimetric observation.

1. Introduction

The problem of gravitation and of terrestrial gravity in particular has been an essential and everlastingly attractive field of research in geophysics, ever since Newton's time. The mode of surface distribution of gravity on the earth depends on the shape of the earth and the density distribution of the earth's interior. The continuous and serious efforts of many geodesists for the precise and world-wide survey of gravity, even in the ocean areas, has made great contributions to the development of our knowledge on the figure and internal mass distribution of the earth. Under such circumstances as above-mentioned, the mode of gravity distribution on the earth's surface has been investigated more and more in detail, especially with the recent developments of survey technique by use of the static gravimeter of small size and easy manipulation. The gravity anomaly thus obtained informs us of the regional and local complexity of the structure of the earth's crust, and provides us with many interesting problems of a geological and geodetic nature. Contrary to the great progress of our knowledge on the mode of gravity distribution on the earth's surface, the problem of change of gravity with time, shortly expressed as time variation of gravity, may be said to remain an uncultivated field of research. Two ways of change of gravity with time are generally supposed, the one being periodic variation and

the other non-periodic. The periodic variation of gravity caused by the tide-producing forces due to the Sun and Moon is mainly treated by the gravimetric observation of earth tides concurrently with tiltmetric and extensometric observations. The periodic gravity change of this kind is usually referred to as 'tidal variation of gravity' and its investigation gives us important information as to the elastic property of the earth.

As to non-periodic gravity change, however, only little definite knowledge has been ascertained as yet, but the observation on anomalous changes in gravity, if they exist, of short duration (rapid change) or of long duration (secular variation) may greatly serve for the development of our knowledge on the change of state or motion of the deep underground material. In a succeeding series of articles, some problems on the time variation of gravity will be treated from the standpoint of geodesy and seismology. In the present article, some considerations are made on the phenomena of the tidal variation of gravity, especially on a newly designed gravimeter of high sensitivity and its application.

On the problem of earth tides Lord Kelvin first discussed the phenomena in 1863 (**1**) from the theoretical treatment of the earth as an elastic sphere. Since the first successful observation of earth tides with the tiltmeter of the horizontal pendulum type by E. v. Rebeur-Paschwitz in 1892 (**2**), a great many tiltmetric observations of earth tides have been made at various places in the world. And the number of orthodox observations of earth tides with the tiltmeter amounted to nearly twenty five since the day of Rebeur-Paschwitz to the present time. On the contrary, the gravimetric observation of earth tides may correctly be said to have remained untouched, because of the technical difficulty of observation with this instrument. Under such circumstances the problems of intensity variation of gravity vector caused by the tide-producing forces of the Sun and Moon are little solved at the present time, in contrast to the great advance in knowledge on the tidal change of gravity direction by tiltmetric observation, and we are eagerly awaiting future developments in research by the method of gravimetric observation.

After the first but provisional observation of tidal variation in gravity with the gravimeter of the bifilar suspension type by W. Schweydar in 1914 (**3**), a precise and orthodox gravimetric observation was made by R. Tomaschek and W. Schaffernicht in 1932 with a bifilar gravimeter of high sensitivity. And after a long interruption during the Second World War many but provisional gravimetric measurements of tidal variation have been made with portable gravimeters which were largely developed for the purpose of geophysical exploration for oil fields and other subterranean resources. The findings obtained by these gravimetric measurements of tidal variation will be listed in Table 1 at the end of this section.

On the theoretical treatment of earth tides, A. E. H. Love (**4**), in 1909, greatly deve-

loped and generalized the pioneering and brilliant work originated by Lord Kelvin, and recently in 1950, H. Takeuchi (5) fully discussed the problem of earth tides on the compressible earth of variable density and elasticity taking into consideration the density distribution of K. E. Bullen (6). According to this theory the quantity Δg of the tidal variation of gravity at the earth's surface is expressed by the formula:

$$\Delta g \quad G\left(\frac{\partial U_2}{\partial r}\right)_{r=a}, \qquad G \equiv 1-\frac{3}{2}k+h,$$

where U_2 denotes the tide-producing potential expressed by a spherical solid harmonic of the second degree, r the radius vector from the earth's centre, a the mean radius of the earth, and h and k are dimensionless constants called the Love-numbers which are correlated with the elasticity and density distribution of the earth's interior. In case of a perfectly rigid earth, h and k are to become zero and then

$$\Delta g = \left(\frac{\partial U_2}{\partial r}\right)_{r=a}.$$

Therefore, in the case of a real deformable earth, the tidal variation of gravity shall be observed on the earth's surface G times as large as that in case of the hypothetical rigid earth. With such an interpretation the symbol G—the ratio of the observed amplitude of tidal variation of gravity to that of the theoretical force— is conveniently called the 'tidal factor of gravity' or 'gravimetric factor'. Corresponding to G of the tidal factor of gravity in the gravimetric observation of earth tides, the diminishing factor D should be introduced in the tiltmetric observation of earth tides which is also derived as the ratio between observed and theoretical amplitudes. Since D is expressed by the formula $D \equiv 1+k-h$, the values of the Love-numbers h and k will directly be determined by the concurrent gravimetric observation with a tiltmeter at any place on the earth's surface. But the determination of the Love-numbers by the combination of gravimetric and tiltmetric observation is, in practice, troublesome for the following reasons. The tiltmetric observations of earth tides for determining the D-factor are greatly disturbed by the secondary effect of ocean tides at any place, especially near the open sea, and they are also spoiled by the large tilting motion of ground caused by rain fall, sun shine and other meteorological effects at some stations, especially at shallow-seated observation rooms. And with regard to the gravimetric observation, the precise and long continuous observation itself is very troublesome mainly on account of technical difficulty, namely the problem of raising the sensitivity of instrument to a sufficiently high degree, maintaining the instrument in a high sensitive and stable condition during the several years' continuous observation, and above all the most unmanageable problem of the so-called 'drift' or 'zero shift' of the instrument. But in spite of these difficult circumstances it is

certain that the observation of earth tides and general crustal change concurrently with the tiltmeter, gravimeter, and extensometer will greatly increase our knowledge on the nature of earth tides and general crustal deformation. And in the present and succeeding articles some problems on the gravimetric observation on earth tides and rapid or secular changes of gravity will be treated in combination with the tiltmetric and extensometric observation.

Returning to the problem of the tidal factor of gravity, the values obtained by R. Tomaschek and W. Schaffernicht are greatly diverse from those obtained by other researchers, as will be seen in Table 1. The cause of its diversity in spite of their cautious observation with a highly sensitive gravimeter and at a deep and good conditioned room has yet remained uninterpreted. Other observations listed in Table 1 show various numerals from 0.9 to 1.6 as the tidal factor of gravity, and it is an essential and attractive problem on the gravimetric study of earth tides to seek the cause of the diversity of their values. The observation periods in Table 1 are for the most part two or four weeks duration and moreover the observation rooms are on the ground surface. Therefore the error in process of analysis for the data of short period or the instrumental error caused by temperature change and other disturbances might have vitiated the obtained G-value and caused their diversity. Or the effect caused by the difference of surface or subterranean geological structure or the perturbation effect of the ocean tides and other unknown forces should be examined as the source of diversity. Some detailed consideration will be made on these points in a succeeding article. In the present article several points will be treated on 'How to raise the sensitivity of gravimeter to a sufficiently high degree?', 'By applying what kind of material to the instrumental construction can we put the gravimeter in a stable condition?', 'At what sort of observation room should the gravimeter be set up and how should observation be conducted for the purpose of the precise and trustworthy study of earth tides?'. On these points both the theoretical and experimental aspects in our investigation will be described below.

The following list in Table 1 are the data of observation for tidal variation of gravity hitherto obtained by several investigators. In this table 'Total' and 'M_2, S_2, K_1, O_1' refer to the resultant tide and each component tide respectively, and G and κ denote respectively the ratio of the observed amplitude to the theoretical one and the phase lag between the observed and the theoretical phases. The plus sign means that the observed phase is behined the theoretical one, while the minus sign shows that the observed phase is in advance of the theoretical one. The data in this table are mainly taken from the papers of W. D. Lambert (7), P. J. Melchior (8) and other original papers.

Table 1

Author	Year	Period of harmonic analysis	Station	Room depth	Instrument	Value of the tidal factor of gravity									
						M_2		S_2		K_1		O_1		Total	
						G	κ	G	κ	G	κ	G	κ	G	κ
W. Schweyder (**9**)	1913		Potsdam	25 m.	Bifilar	1.20	−2°.8								
R. Tomaschek and W. Schaffernicht (**10**)	1932	3 months	Marburg Berchtesgaden	25 » 140 »	Bifilar	0.55 0.57	41.7 42.0	0.35	97 .0	0.58	16 .2	0.51	14 .4		
R.D. Wyckoff (**11**)	1935		Pittsburg		Galitzin									1.10	50
O.H. Truman (**12**)	1936		Houston		Truman	1.13	4.4								
E.A. Eckhardt (**13**)	1939		Santa Barbara Varde		Gulf Gulf									1.14 1.24	
M.S. Reford (**14**)	1949	29 days	Toronto		North American	1.08	2.6	1.10	8.0	0.97	−2.0	1.03	0.9		
A.J. Hoskinson (**15**)	1949	14 » 15 » 14 » 15 » 15 » 15 » 14 » 29 » 15 » 15 » 15 » 15 » 14 » 15 » 14 » 15 » 15 »	Muna Honolulu Panuco Houston Houston Beaumont Austin Pasadena Albuquerque Tulsa Washington Fort Morgan Salt Lake City Toronto Ottawa Edmonton Edmonton		Mott Smith La Coste Mott Smith La Coste Worden La Coste La Coste La Coste Humble La Coste La Coste North American Worden North American North American North American North American	1.19 1.24 1.14 1.16 1.15 1.17 1.15 1.19 1.23 1.24 1.17 1.25 1.08 1.28 1.01 0.94	5.3 11.2 1.9 1.5 −4.0 −0.6 2.1 7.4 2.9 −2.3 3.9 0.0 3.2 4.8 5.5 −2.4	1.29 1.36 1.17 1.17 1.16 1.32 1.10 1.26 1.54 1.07 1.01 1.07 1.11 1.42 1.37 1.47	10.9 17.0 13.9 −7.6 −8.7 −2.8 6.3 5.1 −11.1 1.7 −4.3 8.9 6.8 5.2 −6.4 4.7	1.78 1.30 1.35 0.89 1.21 1.24 1.16 0.93 1.36 1.18 1.13 1.39 0.97 1.17 1.13 1.06	−0.9 −10.4 −2.4 3.8 −4.5 −7.2 1.1 3.8 −19.3 −6.2 −2.6 8.4 −8.8 2.6 −0.3 −7.1	1.28 1.56 1.16 1.15 1.16 1.26 1.05 1.14 1.11 1.17 1.17 1.06 1.04 1.26 1.15 1.32	−2.9 −0.8 2.9 −1.6 −6.6 0.3 −0.3 0.6 −3.1 0.8 −5.1 −21.2 −1.6 2.9 −7.6 −1.5		
L.H. Tarrant and R. Tomaschek (**16**), (**17**)	1949	14 » 14 »	Peebles Kirklington		Frost Frost	1.09 1.24	352 349	1.09 (1.30)	348 354	1.06 1.08	359 3	1.13 1.11	12 6		
J.T. Pettit, L.B. Slichter and L. La Coste (**18**)	1949	2 » 29 » 90 » 36 »	Attu Pasadena Los Angels Hawaii											1.17 1.32 1.35 1.54	52.5 20 20 45
R. Tomaschek (**19**)	1951	8 »	Winsford	143 »	Frost	1.26	7	1.26	7	1.17	7	1.17	7		

2. Double bifilar gravimeter

(1) Gravimeter of bifilar suspension type

The diversity of G-values hitherto obtained was mentioned in the preceding section, the range of their extreme values having been estimated to be 0.9 to 1.6, which can not simply be attributed to observational and instrumental errors. W. D. Lambert (**20**) has attributed its sources to the following three main causes: (i) secondary effects of oceanic tides, (ii) effects of local geological structure and (iii) departures from statical theory, such as those due to the existence of the liquid core of the earth. In order to remove such disturbing factors and obtain an accurate value for G, we must make our observations (1) at various stations under various conditions, (2) during a sufficiently long period and (3) with the tiltmeter and extensometer concurrently. The gravimeter conforming to these three requirements must be a self-recording apparatus, structurally stout and easily manipulated. Under such circumstances, many portable gravimeters as used in these days for geophysical exploration cannot be regarded as the most suitable ones for these requirements. On the contrary, the 'bifilar gravimeter' or gravimeter of Perrot-Schmidt is considered to be the one that satisfies these requirements, and its structure is schematically shown in Fig. 1. A. Schmidt (**21**) has discussed the sensitivity of a bifilar gravimeter which he has called the 'trifilar gravimeter'; however, it appears that he did not make use of his gravimeter in practice. W. Schweydar first observed with a bifilar gravimeter and discussed the value of G. Long after the pioneering observation by Schweydar, R. Tomaschek and W. Shaffernicht greatly improved the bifilar gravimeter of the Schweyder type and made a precise and long continuous observation at a deep-seated underground room. The main points of the improvements were that 'elinvar' was used for the spring, and electrostatic force was utilized for calibration of sensitivity, along with other minor improvements. And they succeeded for the first time in taking a photographic record of the tidal variation of gravity. This type of gravimeter was also studied in detail by A. Berroth (**22**). Recently, H. Ellenberger (**23**) has fundamentally reanalyzed the bifilar suspension principle and has devised a new type of gravimeter named the 'Doppelbifilargravimeter'. His idea is very interesting, and it is easily supposed that its sensitivity will show a great increase over that of the ordinary bifilar gravimeter, though its adjustment will be considerably more troublesome; and we are awaiting for the observational results of tidal variation with his gravimeter. It ought to be mentioned here that, in the point of name of 'double bifilar gravimeter', the gravimeter designed by the writer and that by Ellenberger are entirely the same, but they are quite different in the principle of construction. According to experiments, it is considerably difficult to raise the sensitivity of the ordinary bifilar gravimeter to a degree sufficiently high to record the tidal

variation of gravity. The source of the difficulty lies in the fact that the sensitive range of the instrument is very narrow, and furthermore, it lies near a labile equilibrium point. The writer has examined the above-mentioned circumstances and devised a new type of highly sensitive gravimeter, which was designated as 'double bifilar gravimeter'. Its principle of construction and some test experiments were reported at the Autumnal Meeting of the Seismological Society of Japan in 1949 and published in Japanese in 1950 (**24**) and in 1951 (**25**).

(2) Theoretical considerations on the sensitivity of an ordinary bifilar gravimeter.

An ordinary bifilar gravimeter is schematically shown in Fig. 1. If the instrument is in a state of equilibrium for the present value of gravity g, the conditions of equilibrium are expressed by

$$\left.\begin{aligned} s(l-l_0)+p\sin\alpha-Mg&=0\,,\\ f(\omega-\varphi)-p\frac{ab\sin\varphi}{m}&=0\,,\end{aligned}\right\} \qquad (1)$$

and geometrically

$$\left.\begin{aligned} l&=h_0+h\,,\\ \sin\alpha&=h/m\,,\\ h^2&=m^2-(a^2+b^2-2ab\cos\varphi)\,,\end{aligned}\right\} \qquad (2)$$

where $\frac{1}{2}p$ is the tension of the string, s and f the elastic constants of the spring with regard to elongation and torsion respectively, ω and φ the turning angle of the spring head and the weight respectively, M the mass of the weight system, and other symbols are as shown in the figure. If φ varies by $d\varphi$ correspondingly to the variation of gravity dg, the sensitivity $\frac{d\varphi}{dg}$ is calculated from (1) and (2) as follows:

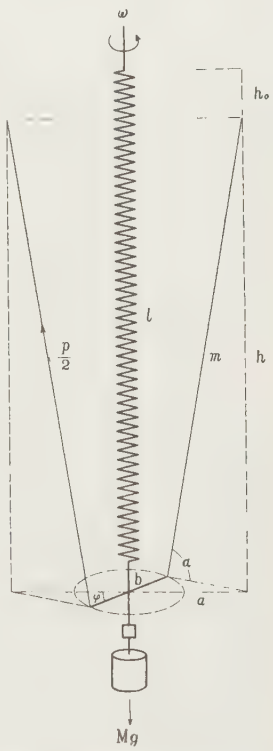

Fig. 1. Schematic figure of an ordinary bifilar gravimeter.

$$\frac{d\varphi}{dg}=-\frac{ab\sin\varphi}{mf+abp\cos\varphi}\cdot\frac{m}{h}\left\{M-\left(s+\frac{p}{m}\right)\frac{dh}{dg}\right\}. \qquad (3)$$

Putting $m\simeq h$, $\frac{dh}{dg}\simeq 0$ in a first approximation, we have

$$\frac{d\varphi}{dg}=-\frac{abM\sin\varphi}{mf+abp\cos\varphi}. \qquad (4)$$

Next, let us calculate the correlation between the free oscillating period of rotation and the sensitivity. Assuming that φ is virtually varied by ε as a result of some

minute disturbing force, then the restoring moment R is as follows:

$$R - f\{\omega - (\varphi + \varepsilon)\} - p\frac{ab \sin(\varphi+\varepsilon)}{m}.$$

Putting $\cos\varepsilon = 1$, $\sin\varepsilon = \varepsilon$ approximately, since ε is small, we have

$$R = \left\{f(\omega-\varphi) - p\frac{ab\sin\varphi}{m}\right\} - \left\{f + p\frac{ab\cos\varphi}{m}\right\}\varepsilon.$$

By (1) the first term on the right-hand side is equal to zero, and therefore the equation of motion becomes

$$I\frac{d^2\varepsilon}{dt^2} = -\left\{f + p\frac{ab\cos\varphi}{m}\right\}\varepsilon, \tag{5}$$

where I is the moment of inertia of the weight. From this equation, the oscillating period P is expressed by

$$P = 2\pi\sqrt{\frac{I}{f + p\dfrac{ab\cos\varphi}{m}}}. \tag{6}$$

Inserting (6) into (4) with the substitution of $I = r^2M$, we obtain

$$\frac{d\varphi}{dg} = -\frac{ab\sin\varphi}{4\pi^2 mr^2}P^2. \tag{7}$$

In this expression, a, b, m and r are constants fixed to the instrument. Therefore, it will be understood that if φ is held constant, the sensitivity is proportional to the square of period. This relation is usually applied, in practice, to estimating the sensitivity of the gravimeter. In the expression (4), $\frac{d\varphi}{dg}$ is a function of p and φ. Fig. 2 shows the relation between p, φ and $\frac{d\varphi}{dg}$, in which the adopted numerical values of the constants are as follows: $a=6$, $b=3$, $m=130$, $f=1000$, $M=50$, $g=980$ c.g.s. units respectively, and $p=\frac{8.5}{50}Mg$ for curve I and $=\frac{15}{50}Mg$ for curve II.

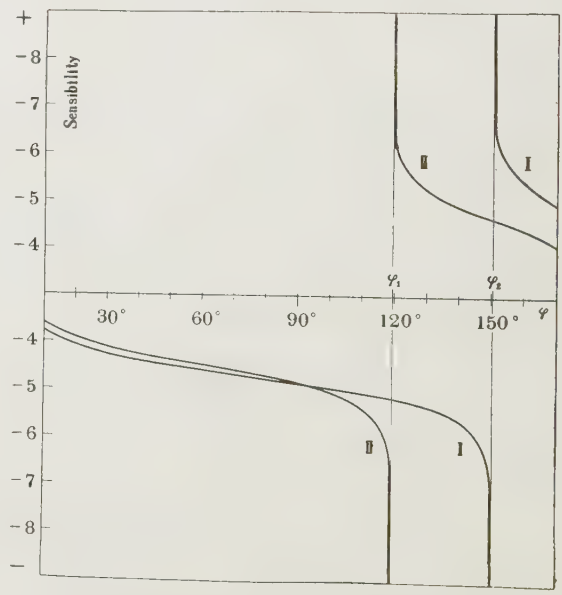

Fig. 2. Sensitivity curve of an ordinary bifilar gravimeter.

The numerals on the sensitivity-axis indicate the common logarithms of $\frac{dg}{g}$ corresponding to 1 mm. displacement of the optical image on the recording paper of which optical distance is 5 meters.

As clearly seen in Fig. 2, $\frac{d\varphi}{dg}$ suddenly varies from minus infinity to plus infinity at φ_1 or φ_2, and a sensitive domain is limited within the very narrow neighbourhood of φ_1 or φ_2. And furthermore, on account of the sensitivity curve being very abrupt at that point, the sensitivity is very labile, consequently the gravimeter itself is liable to become unstable. This is the cause of the difficulty of raising the sensitivity of the ordinary bifilar gravimeter to such a high degree.

For the purpose of removing the source of the difficulty and raising the sensitivity, let us again examine the expression (4). We learn from the expression (4) that in order to increase the absolute value of $\frac{d\varphi}{dg}$ over the whole range of φ, the first term mf in the denominator of the right-hand side may need to be minimized because p and φ in the second term are at our option. While, in the case of shortening the length of the string m, $\frac{dh}{dg}$ becomes large and is not neglected as above treated in a first approximation. From the relation (3), it is understood that the increase of $\frac{dh}{dg}$ results in a way to decrease the absolute value of $\frac{d\varphi}{dg}$. Therefore we must abandon this manner of shortening the length of string m but endeavour to reduce the value of the torsional elastic constant f.

The most direct method of reducing the torsional constant f is to use a feeble spring. While, the use of a feeble spring implies the decrease of the mass M of the weight for which the spring is endurable. According to the expression (4), the decrease of M results in the decrease of the absolute value of $\frac{d\varphi}{dg}$. Therefore, after all, the problem of raising the sensitivity of the bifilar gravimeter to a sufficiently hign degree comes to a point as to whether or not there exists a spring which would tolerate a considerably heavy load and yet have a low-enough torsional elastic constant. For the purpose of investing the spring with such quality as above required, the writer has devised the following construction of the instrument. The construction is simply to connect the lower end of the main spiral spring and the weight with a fine string as shown in Fig. 3. The finer the string is, the more favourable the condition, as long as it endures a considerably heavy load. Such a combination of a fine string with the main spring of a bifilar gravimeter makes it possible to gain a single spring with a small torsional constant and a large tenacity for load.

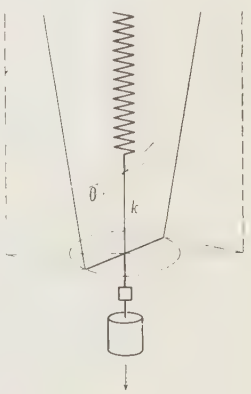

Fig. 3.

Now, let the torsional constant of string τ be equal to one-hundredth of that of spring f, then the sensitivity of the bifilar gravimeter equipped with such a string and spring is as follows:

$$\frac{d\varphi}{dg}=-\frac{ab\sin\varphi}{m\frac{\tau f}{\tau+f}+abp\cos\varphi}\cdot\frac{m}{h}\left\{M-\left(s+\frac{p}{m}\right)\frac{dh}{dg}\right\}. \tag{8}$$

Putting $m\simeq h$, $\frac{dh}{dg}\sim 0$ as in the previously assumed approximation, and since $\tau \ll f$, we have approximately

$$\frac{d\varphi}{dg}=-\frac{abM\sin\varphi}{m\tau+abp\cos\varphi}. \tag{9}$$

The last expression is indentical with that in which f is replaced by τ in the expression (4). And it indicates that if only we appropriately control the tension of the bifilar strings p, the absolute value of $\frac{d\varphi}{dg}$ increases to the extent of a hundred times as large as that of the ordinary bifilar gravimeter over the whole range of φ. Namely, we can easily raise the sensitivity of a gravimeter a hundred times as high as that of the ordinary bifilar gravimeter by such a simple modification as the string connection. The writer has experimentally ascertained that the above condition is practically satisfied. Thus it may safely be said that this method of connecting a string might to some extent serve as one solution for the problem of raising the sensitivity of the bifilar gravimeter. However, it was experimentally proved that the gravimeter thus modified also has many points of inconvenience which should be examined for the purpose of precise and long continuous observation of tidal variation of gravity. Namely, the drift of the zero position of the gravimeter caused by the inevitable flow of the spring and the undesirable effect of temperature change upon the function of the instrument are generally the most troublesome problem for every gravimetric observation, and the case of present gravimeter cannot be an exception. Since the string connecting the spring and the weight yields to torsional force, the above-mentioned manner is disadvantageous for the drift and the temperature change. For the purpose of avoiding the foresaid inconvenience, the writer has further devised the following construction. It is the construction of connecting the spring and the weight with two strings so fine that the torsional moment is negligible, in place of one elastic string, as seen in Fig. 4. The writer has given a name of 'double bifilar gravimeter' to the bifilar gravimeter improved in this way. In the next, the function of a double bifilar gravimeter will be discussed in some detail.

(3) Function of the double bifilar gravimeter

If a double bifilar gravimeter is in a state of equilibrium for the present value

of gravity g, neglecting the torsional moment of strings, the conditions of equilibrium are as follows: dynamically, in the vertical direction

$$T\sin\beta+t\sin\alpha-Mg=0 \tag{10-1}$$

$$s(l-l_0)-T\sin\beta=0\,, \tag{10-2}$$

in the rotational direction

$$T\frac{ce\sin\theta}{n}-t\frac{ab\sin\varphi}{m}=0 \tag{10-3}$$

$$f(\omega-\theta-\varphi)-T\frac{ce\sin\theta}{n}=0\,; \tag{10-4}$$

and geometrically

$$l+k=h_0+h \tag{11-1}$$

$$\sin\alpha=\frac{h}{m} \tag{11-2}$$

$$\sin\beta=\frac{k}{n} \tag{11-3}$$

$$h^2=m^2-(a^2+b^2-2ab\cos\varphi) \tag{11-4}$$

$$k^2=n^2-(c^2+e^2-2ce\cos\theta)\,, \tag{11-5}$$

where t and T are the tensions of the outer and inner bifilar strings respectively; s and f the elastic constants of the spring with regard to elongation and torsion respectively; ω, θ and φ the turning angle of the spring head, the angle between the lower end of the spring and the weight, and the turning angle of the weight; M the mass of the weight system; and other symbols are as shown in Fig. 4.

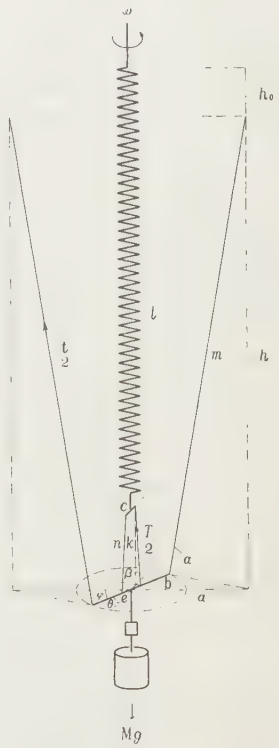

Fig. 4. Schematic figure of a double bifilar gravimeter.

Introducing a new quantity q by the relation:

$$t=qT\,, \tag{12}$$

we can obtain the sensitivity formula from these conditions in the following way. From (10-1), (11-2), (11-3) and (12)

$$T=\frac{Mg}{\frac{k}{n}+q\frac{h}{m}}\,. \tag{13}$$

Inserting (13) into (10-4) and differentiating we get

$$-f(d\theta+d\varphi)=\frac{ceM}{n}\left[\frac{\left(\frac{k}{n}+q\frac{h}{m}\right)(\sin\theta dg+g\cos\theta d\theta)-g\sin\theta\left(\frac{dk}{n}+\frac{h}{m}dq+\frac{q}{m}dh\right)}{\left(\frac{k}{n}+q\frac{h}{m}\right)^2}\right]. \tag{14}$$

On the other hand, from (10-3) and (12)

$$\left.\begin{aligned} \sin\theta &= q\frac{abn}{cem}\sin\varphi \\ \cos\theta d\theta &= \frac{abn}{cem}\sin\varphi dq + \frac{abn}{cem}q\cos\varphi d\varphi \\ d\theta &= \pm\frac{\sin\varphi dq + q\cos\varphi d\varphi}{\sqrt{\left(\frac{cem}{abn}\right)^2 - (q\sin\varphi)^2}}, \end{aligned}\right\} \tag{15}$$

where the plus sign corresponds to the case $0 \leqq \theta \leqq \frac{\pi}{2}$, and the minus sign corresponds to the case $\frac{\pi}{2} < \theta \leqq \pi$.

Inserting (15) into (14) gives

$$-f\left\{d\varphi \pm \frac{\sin\varphi dq + q\cos\varphi d\varphi}{\sqrt{\left(\frac{cem}{abn}\right)^2 - (q\sin\varphi)^2}}\right\} - \frac{ceM}{n} \times \frac{1}{\left(\frac{k}{n} + q\frac{h}{m}\right)^2} \times \left[\left(\frac{k}{n} + q\frac{h}{m}\right)\left\{q\frac{abn}{cem}\sin\varphi dg\right.\right.$$

$$\left.\left. + g\left(\frac{abn}{cem}\sin\varphi dq + \frac{abn}{cem}q\cos\varphi d\varphi\right)\right\} - gq\frac{abn}{cem}\sin\varphi\left(\frac{1}{n}dk + \frac{h}{m}dq + \frac{q}{m}dh\right)\right].$$

Taking out $d\varphi$ and regulating, we get

$$-\left[f\left\{1 \pm \frac{q\cos\varphi}{\sqrt{\left(\frac{cem}{abn}\right)^2 - (q\sin\varphi)^2}}\right\} + \frac{abqMg\cos\varphi}{m\left(\frac{k}{n} + q\frac{h}{m}\right)}\right]d\varphi$$

$$\frac{abqMg\sin\varphi}{m\left(\frac{k}{n} + q\frac{h}{m}\right)}dg + \left[\frac{M}{\left(\frac{k}{n} + q\frac{h}{m}\right)^2}\left\{\frac{abg\left(\frac{k}{n} + q\frac{h}{m}\right)}{m} - \frac{abqg}{m}\cdot\frac{h}{m}\right\}\right.$$

$$\left. \pm \frac{f}{\sqrt{\left(\frac{cem}{abn}\right)^2 - (q\sin\varphi)^2}}\right]\sin\varphi dq - \frac{abqMg\sin\varphi}{m\left(\frac{k}{n} + q\frac{h}{n}\right)^2}\left(\frac{1}{n}dk + \frac{q}{m}dh\right). \tag{16}$$

Next, dq in the expression (16) is calculated from the conditions in the following way. From (11-1)

$$dl = dh - dk. \tag{17}$$

Inserting (11-3) and (13) into (10-2) gives

$$s(l - l_0) \quad \frac{Mg}{\frac{k}{n} + q\frac{h}{m}}\cdot\frac{k}{n} \quad 0.$$

Differentiating this and substituting dl in the result with (17), we get

$$s(dh-dk)-\frac{M}{m}\cdot\frac{\left(\frac{k}{n}+q\frac{h}{m}\right)(kdg+gdk)-gk\left(\frac{1}{n}dk+\frac{1}{m}dq+\frac{q}{m}dh\right)}{\left(\frac{k}{n}+q\frac{h}{m}\right)^2}=0\,.$$

After rearrangement, we get

$$dq=-\frac{m}{h}\left[\frac{1}{gk}\left(\frac{k}{n}+q\frac{h}{m}\right)\left\{\frac{ns}{M}\left(\frac{k}{n}+q\frac{h}{m}\right)(dh-dk)-(kdg+gdk)\right\}+\left(\frac{1}{n}dk+\frac{q}{m}dh\right)\right]. \tag{18}$$

If necessary, we can express dh and dk by $d\varphi$ and dg by using the remaining conditions (11-4) and (11-5). However, the process of the calculation is very troublesome in spite of the circumstances that dh and dk are negligible quantities and do not affect the estimation of $\frac{d\varphi}{dg}$. Therefore it is useless to discuss in detail the values of dh and dk in general for the present treatment. Combining (16) with (18), we obtain the final formula for the sensitivity:

$$\left.\begin{aligned}\frac{d\varphi}{dg}=&-\frac{\sin\varphi}{f\left(1\pm\frac{q\cos\varphi}{F}\right)+\frac{abq\,Mg\cos\varphi}{m\left(\frac{k}{n}+q\frac{h}{m}\right)}}\times\left[\left\{\frac{abMg}{\frac{mn}{k}\left(\frac{k}{n}+q\frac{h}{m}\right)^2}\pm\frac{f}{F}\right\}\frac{dq}{dg}\right.\\&\left.+\frac{abqM}{m\left(\frac{k}{n}+q\frac{h}{m}\right)}\left\{1-\frac{g}{\left(\frac{k}{n}+q\frac{h}{m}\right)}\left(\frac{1}{n}\frac{dk}{dg}+\frac{q}{m}\frac{dh}{dg}\right)\right\}\right],\end{aligned}\right\} \tag{19}$$

with

$$\left.\begin{aligned}\frac{dq}{dg}=&-\frac{m}{h}\left[\frac{1}{gk}\left(\frac{k}{n}+q\frac{h}{m}\right)\left\{\frac{ns}{M}\left(\frac{k}{n}+q\frac{h}{m}\right)\left(\frac{dh}{dg}-\frac{dk}{dg}\right)-\left(k-g\frac{dk}{dg}\right)\right\}-\frac{1}{n}\frac{dk}{dg}-\frac{q}{m}\frac{dh}{dg}\right],\\F=&\sqrt{\left(\frac{cem}{abn}\right)^2-(q\sin\varphi)^2}\,.\end{aligned}\right\}$$

We can simplify the formula (19) by putting

$$m\simeq h,\quad n\simeq k\quad\text{and}\quad\frac{dh}{dg}\simeq\frac{dk}{dg}\simeq 0\,. \tag{20}$$

Then, since $q\ll 1$, we get

$$\frac{dq}{dg}=\frac{1}{g} \tag{21}$$

Inserting (20) and (21) into (19), we obtain the approximate sensitivity formula as:

$$\left.\begin{aligned}\frac{d\varphi}{dg}=&-\frac{\left(abM\pm\frac{mf}{gF}\right)\sin\varphi}{mf\left(1\pm\frac{q\cos\varphi}{F}\right)+abqMg\cos\varphi},\\F=&\sqrt{\left(\frac{cem}{abn}\right)^2-(q\sin\varphi)^2}\,.\end{aligned}\right\} \tag{22}$$

with

The formula (22) corresponds to the formula (4) for the sensitivity of the ordinary bifilar gravimeter. Next, let us obtain the correlation between the free oscillating period of rotation and the sensitivity. Consider that φ and θ are virtually varied by ε and δ respectively by some minute disturbing force. Then, according to the condition (10-4), the following relation ought to be established:

$$f\{\omega-(\theta+\delta)-(\varphi+\varepsilon)\}-T\frac{ce\sin(\theta+\delta)}{n}=0,$$

which, after transformation, becomes

$$\left\{f(\omega-\theta-\varphi)-\frac{Tce\sin\theta}{n}\cos\delta\right\}-\left\{f(\delta+\varepsilon)+\frac{Tce\cos\theta}{n}\sin\delta\right\}=0. \tag{23}$$

Since ε and δ are both small angles, we may put $\sin\delta=\delta$ and $\cos\delta=1$. Then, the terms in the first bracket of (23) vanish owing to (10-4), and we have

$$f(\delta+\varepsilon)+\frac{Tce\cos\theta}{n}\delta=0,$$

whence we get

$$\delta=-\frac{f}{f+T\dfrac{ce\cos\theta}{n}}\varepsilon. \tag{24}$$

Therefore, by (10-3) and (12), the restoring moment R caused by the angular variation ε becomes as follows:

$$R=T\left\{\frac{ce}{n}\sin\left(\theta-\frac{f}{f+T\dfrac{ce\cos\theta}{n}}\varepsilon\right)-q\frac{ab}{m}\sin(\varphi+\varepsilon)\right\} \tag{25}$$

As proved by numerical estimation,

$$\left|\frac{Tce}{fn}\cos\theta\right|\ll 1,$$

so that

$$\frac{f}{f+T\dfrac{ce\cos\theta}{n}}\varepsilon=0(\varepsilon).$$

Therefore we may put approximately as follows:

$$\sin\left(\frac{f}{f+T\dfrac{ce\cos\theta}{n}}\varepsilon\right)=\frac{f}{f+T\dfrac{ce\cos\theta}{n}}\varepsilon \quad\text{and}\quad \cos\left(\frac{f}{f+T\dfrac{ce\cos\theta}{n}}\varepsilon\right)=1.$$

Consequently, (25) is reduced to the following formula:

$$R \quad T\left(\frac{ce}{n}\sin\theta \quad q\frac{ab}{m}\sin\varphi\right) \quad T\left(\frac{ce}{n}\cos\theta \quad \frac{f}{f+T\frac{ce\cos\theta}{n}}+q\frac{ab}{m}\cos\varphi\right)\varepsilon .$$

The first term on the right-hand side vanishes according to (10-3). Consequently,

$$R=-T\left(\frac{ce}{n}\cos\theta\frac{f}{f+T\frac{ce\cos\theta}{n}}+q\frac{ab}{m}\cos\varphi\right)\varepsilon . \tag{26}$$

Therefore, the equation of motion for the rotation becomes

$$I\frac{d^2\varepsilon}{dt^2}=-T\left(\frac{ce}{n}\cos\theta\frac{f}{f+T\frac{ce\cos\theta}{n}}+q\frac{ab}{m}\cos\varphi\right)\varepsilon , \tag{27}$$

where I is the moment of inertia of the weight. From (27) we get the oscillating period P as

$$P=2\pi\sqrt{\frac{I}{T\left(\frac{ce}{n}\cos\theta\frac{f}{f+T\frac{ce\cos\theta}{n}}+q\frac{ab}{m}\cos\varphi\right)}} . \tag{28}$$

On the other hand, from (10-3)

$$\left.\begin{aligned}\sin\theta&=\frac{qnab}{mce}\sin\varphi ,\\ \cos\theta&=\pm\sqrt{1-\left(\frac{qnab}{mce}\sin\varphi\right)^2},\end{aligned}\right\} \tag{29}$$

and from (10-1), we have approximately

$$T=Mg . \tag{30}$$

Inserting (29), (30) and $I=r^2M$ into (28), and squaring both sides we have

$$P^2=4\pi^2mr^2\frac{M\pm\frac{mf}{abg}\cdot\frac{1}{\sqrt{\left(\frac{mce}{nab}\right)^2-(q\sin\varphi)^2}}}{mf\left\{1\pm\frac{q\cos\varphi}{\sqrt{\left(\frac{mce}{nab}\right)^2-(q\sin\varphi)^2}}\right\}+abqMg\cos\varphi} , \tag{31}$$

where r is the radius of gyration of the weight. Combining (22) and (31), we obtain the following correlation:

$$\frac{d\varphi}{dg}=-\frac{ab\sin\varphi}{4\pi^2mr^2}P^2 . \tag{32}$$

The expression (32) is indentical with the period-sensitivity relation (7) of ordinary

bifilar gravimeter. Fig. 5 shows the relation between q, φ and $\frac{d\varphi}{dg}$. The numerical values of constructional constants adopted in the calculation are as follows: $a=6$, $b=3$, $c=e=0.1$, $m=130$, $n=10$, $f=1000$, $M=50$, $g=980$ c.g.s. units respectively, and $q=\frac{7.0}{1000}$ for curve I and $=\frac{7.2}{1000}$ for curve II. In Fig. 5, the full-line curves correspond to the plus sign of the formula (22) and the broken-line curves to the minus sign. The numerals on the sensitivity axis, similarly to Fig. 2, indicate the common logarithms of $\frac{dg}{g}$ corresponding to 1 mm. displacement of the optical image on the recording paper of which optical distance is 5 meters. The chain-line curves show the relation between P and $\frac{d\varphi}{dg}$ in the case of $r^2=2$ c.g.s. unit. The sensitivity of the double bifilar gravimeter thus theoretically obtained should be experimentally ascertained, and it will be described in some detail in the next section.

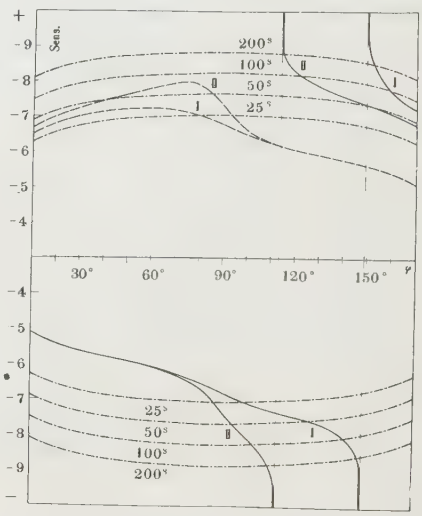

Fig. 5. Sensitivity curve of a double bifilar gravimeter.

(4) Some experiments on the function of the double bifilar gravimeter.

The writer has tentatively constructed a double bifilar gravimeter whose constructional constants are nearly the same as the above-mentioned numerical values. The method of appending a small mass to the gravimeter's weight is adopted for the measurement of the sensitivity. This is the most simple and sure method, but on the other hand, it also has a weak point in that the gravimeter cannot be used in so sensitive state on account of the lower limit of the dimension of the appendant mass. Therefore the experiment for sensitivity calculation had to be carried out in the condition of somewhat low sensitivity.

At first, the experiment on the period-sensitivity correlation will be mentioned. Since $\frac{d\varphi}{dg}$ is proportional to $\sin\varphi$ and the square of P by the expression (32), $\left(\varphi-\frac{d\varphi}{dg}\right)$ correlation ought to be expressed by a sine curve when P is kept constant, and $\left(P-\frac{d\varphi}{dg}\right)$ correlation by a parabola when φ is kept constant. Figs. 6 and 7 show those correlations respectively. The three dots in Fig. 6 and the four dots in Fig. 7 represent the experimental values respectively. These two figures indicate that the experimental results coincide perfectly with the theoretical ones, allowing for some experimental errors. Extraporating the experimental results obtained in the state of low sensitivity to the high sensitivity, we get the results as given in Table 2.

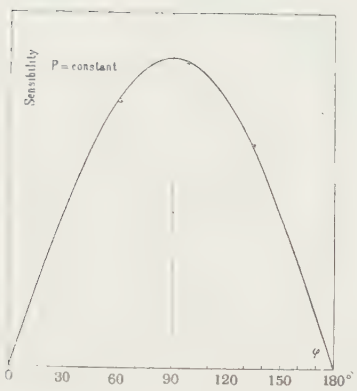

Fig. 6. Correlation between φ and $\frac{d\varphi}{dg}$.

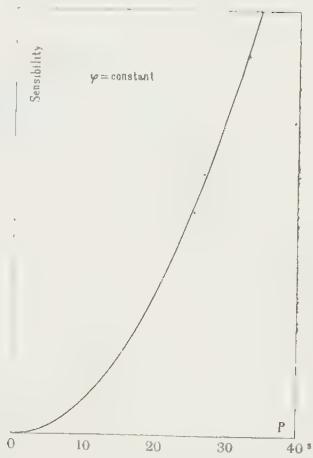

Fig. 7. Correlation between P and $\frac{d\varphi}{dg}$.

Table 2

φ	Optical distance	Period	Sensitivity
120°	5 meters	25 seconds	178.0×10^{-9} g/mm
"	"	50 "	44.4 "
"	"	100 "	11.1 "
"	"	150 "	4.93 "
"	"	200 "	2.78 "

Fig. 8 gives one example of gravitogram obtained by the above-stated double bifilar gravimeter constructed for a trial with a period of 160 seconds at the Abuyama Seismological Observatory of Kyoto University ($\lambda=135°34'$E, $\varphi=34°52'$ N, $h=200$ m). The subsequent restlessness is caused by the microseisms of the ground and the convection current of the air. Therefore, even if we could make the gravimeter more highly sensitive, it would be useless unless some devices were applied to reduce the effect of microseisms to negligibly small degree. Fig. 9 gives also another example of gravitogram obtained during one week by the same gravimeter as that in Fig. 8 with a period of 82 seconds at the same Observatory. The semi-diurnal periodic

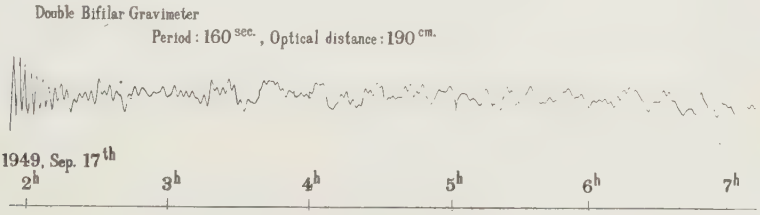

Fig. 8. Gravitogram in rapid recording at Abuyama.

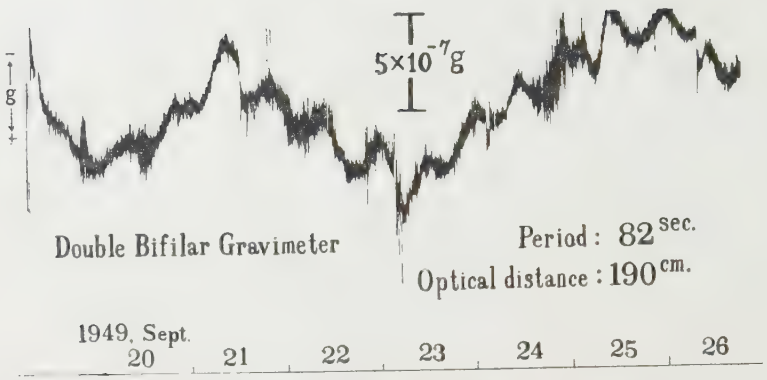

Fig. 9. Gravitogram in slow recording at Abuyama.

variation in the figure was proved to be the tidal variation of gravity, and the large swell was found to be caused by the variation of atmospheric pressure.

In conclusion, the problem of raising the sensitivity of gravimeter may be said to be settled to a certain degree by adopting the principle of double bifilar suspension, but in practical case other undesirable disturbances such as the earth's tremors, the change of meteorological elements and above all the unmanageable plastic flow of the main spring will greatly vitiate the gravimetric observation, and would really impede the aim of our research. In the next section, the experimental treatment on the problem of plastic flow of the gravimeter's main spring will shortly be reported.

3. Some experiments on the plastic flow of the spiral spring

The experiment on the plastic flow of the spiral spring of the bifilar gravimeter was made with the spring materials available in our laboratory. Since the plastic flow of the spring or, in other words, the drift of the gravimeter is the most essential and troublesome problem in all gravimetric observation, a detailed investigation should be made from every possible approach, and it will be discussed at other opportunity. In the present section a short account will be mentioned.

The materials used for the experiment are 'Tungsten', 'Steel', 'Tōhoku-elinvar' (manufactured by the Metal Research Institute, Tōhoku University), 'Sumitomo-elinvar A, B, C' (manufactured by the Sumitomo Metal Corporation), 'Fused silica' (manufactured by the Houston Technical Laboratories, U. S. A.), and 'Isoelastic alloy' (manufactured by the North American Geophysical Co., U. S. A.). These materials except 'Fused silica' and 'Isoelastic alloy' were formed into nineteen spiral springs whose annealing conditions were respectively different. The annealing conditions of these samples are as inserted in Table 3.

These samples were tested by the method shown in Fig. 10. The drift speed obtained from the experiment is shown in Figs. 11, 12, 13 and 14. In these figures,

Table 3

Number of group	Number of spring	Material	Annealing condition			
			Annealing temperature	Heating time	Holding time	Cooling method
	1	Fused silica				
	2	Sumitomo-elinvar				N. C.
I	3	Sumitomo-elinvar				N. C.
	4	Tungsten				N. C.
	5	Steel A				N. C.
	6	Sumitomo-elinvar C	580°C	44 min.	0 min.	N. C.
	7	Sumitomo-elinvar C	580	40	0	Q. O.
II	8	Sumitomo-elinvar C	580	39	0	Q. W.
	9	Sumitomo-elinvar B	580	52	0	N. C.
	10	Sumitomo-elinvar B	580	30	0	Q. O.
	11	Sumitomo-elinvar C	700	62	10	Q. O.
	12	Sumitomo-elinvar C	800	73	10	Q. O.
III	13	Sumitomo-elinvar C	900	58	0	Q. O.
	14	Sumitomo-elinvar C	800	7	0	Q. O.
	15	Sumitomo-elinvar C	580	40	0	Q. O.
	16	Steel B				
	17	Sumitomo-elinvar A				
IV	18	Sumitomo-elinvar A				
	19	Tōhoku-elinvar				
	20	Tōhoku-elinvar				
	21	Isoelastic alloy				

N.C.: Natural cooling, Q.O.: Quenching in cotton-seed oil, Q.W.: Quenching in water

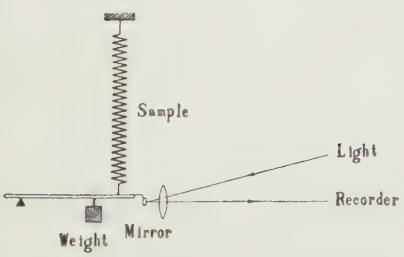

Fig. 10. Schematic diagram of drift experiment.

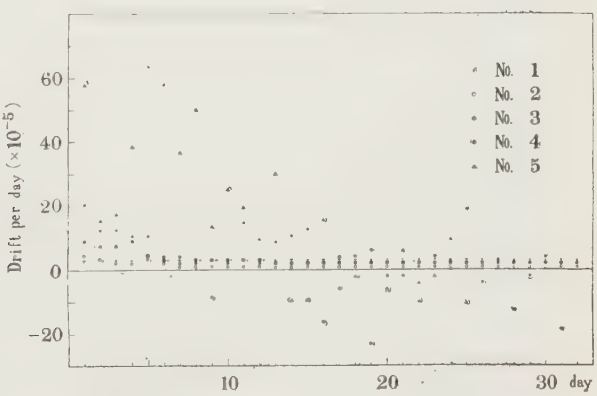

Fig. 11. Change in rate of drift with time.

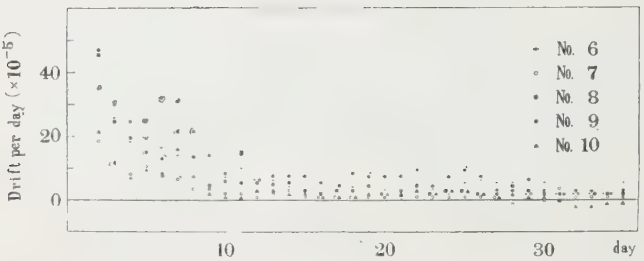

Fig. 12. Change in rate of drift with time.

the numerals on the abscissae denote the number of days from the beginning of the suspension of springs, except for the spring made of 'Fused silica' whose value is that of about fifteen months after suspension.

From these experiments, the following may be concluded:

1. Among them, the spring made of 'Isoelastic alloy' is considered to be the best in the point of drift, and no drift of the spring was observed in a range of the present measurement. Among the other materials except 'Isoelastic alloy', 'Sumitomo-elinvar C' is comparatively excellent.

2. With regard to the cooling methods, qnenching in cotton-seed oil produces a good effect on springs with respect to drift.

3. With regard to the heating conditions, the following case was the best as far as 'Sumitomo-elinvar' was concerned:

a. Heating temperature is about 600°C,

b. Heating time is between from 8 to 10 minutes,

c. Holding time in maximum temperature is about 10 minutes. But it is to be remarked that, in any case, the heating was carried out in air.

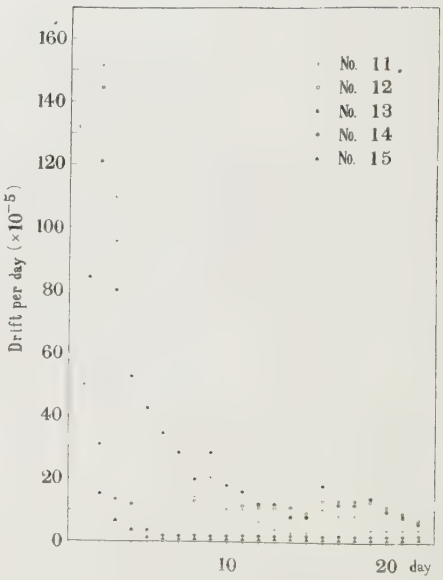

Fig. 13. Change in rate of drift with time.

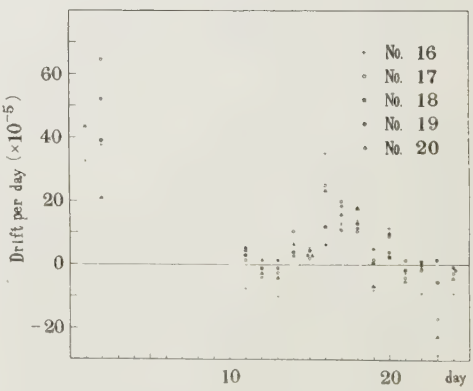

Fig. 14. Change in rate of drift with time.

4. Regarding drift, the putting of 'Carbon' in the furnace for the purpose of preserving the materials from oxidation seems to be effective.

Among the all springs except that of 'Isoelastic alloy', as seen in the figures, the spring of No. 2 has the smallest drift, even which amounts to 0.76×10^{-5}/day. Converting it into gravity change, this value is equivalent to about thirty times as large as the total amplitude of tidal variation. In practice, such an enormously large plastic flow of the gravimeter spring as above described greatly hinders the gravimeter from increasing its sensitivity to exceedingly high degree, and the elimination of secular drift of the gravimeter is the most important as well as the most unmanageable and troublesome matter, the solution of which should necessarily be found in near future for the purpose of precise and continuous secular observation of the gravity change.

4. Observation of tidal variation of gravity with the double bifilar gravimeter

The first long period observation of the tidal variation of gravity by the use of a double bifilar gravimeter was carried out at the adit of the Ikuno Copper Mine. The situation of the observation room in the mine is as follows: $\lambda=134°50'$E, $\varphi=$

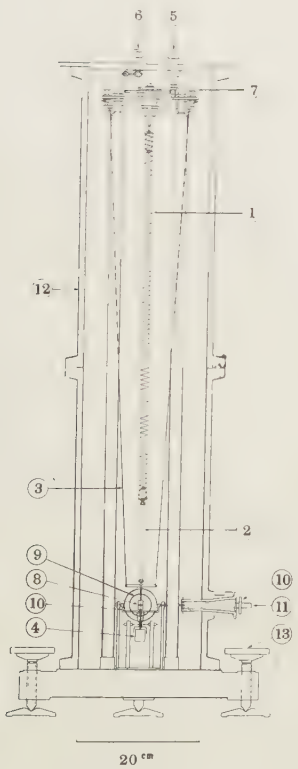

Fig. 15. Plan of the double bifilar gravimeter at Ikuno.

1: Main spiral spring (fused silica)
2: Inner bifilar string (30 microns super invar)
3: Outer bifilar string (30 microns super invar)
4: Weight (brass)
5: Fine torsion adjuster of main spring
6: Fine vertical adjuster of main spring
7: Vertical adjuster of outer bifilar string
8: Reflecting mirror
9: Lens
10: Calibration apparatus
11: Exhaust-opening
12: Cover (glass)
13: Level adjuster

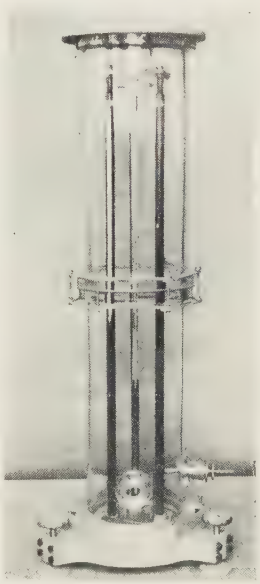

Fig. 16. Photograph of the double bifilar gravimeter at Ikuno.

35°10′ N, h = 440 m above the sea level, and 237 m depth under the ground surface, in which mine the tiltmetric observations had continued since 1943. The temperature of the observation room is 17°C, and it maintains almost the same temperature through the year. The gravimeter had been set on April 3rd, 1952, and the observation was commenced on April 26th, 1952, it being continued to the present. The gravimeter used for the observation at Ikuno is somewhat smaller compared with that described in § 2. The structure of the gravimeter and its exterior view are as illustrated by the plan of Fig. 15 and the photograph of Fig. 16. The main spring was made of 'fused silica' which was No. 1 in Fig. 11 and manufactured by the Houston Technical Laboratories, U. S. A., the maximum durable load and the extension of which are 40 grams and 1.8 cm/gr respectively. The inner and outer bifilar strings are both composed of super-invar wires of 30 microns in diameter. The materials of the other main constructions are as explained in the figures. The gravimeter has no temperature compensater, for temperature variation in the observation room is very small. The gravimeter has an air-evacuating apparatus, but it was not used in the present observation. The rotating speed of the recording paper is 22.0 mm. per day, and the recording cylinder revolves once in two weeks. The optical distance is 398 cm. As mentioned in § 3, the spring has a considerable drift. Therefore, in order to prevent the light image of the gravimeter from getting out of the recording photographic paper, the sensitivity of the gravimeter should be kept at undesirably low degree. This restraint of sensitivity greatly reduced the efficiency of the double bifilar gravimeter and practically vitiated the present observation. Fig. 17 gives one example of gravitogram obtained during present long period observation. The calibration was done by means of the method of appending a small mass to the weight, similar to the method described in § 2. The numerical values of the quantities concerned with the calibration are as inserted in Table 4.

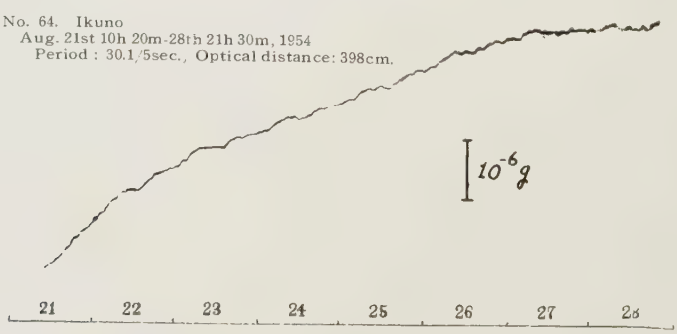

Fig. 17. Gravitogram with the double bifilar gravimeter at Ikuno.

Table 4

φ	120°
Period	6 sec
Optical distance	398 cm
Mass of the weight system	26.690 gr
Weight, containing a mirror and a cross-shaped body	21.789 gr
A half of mass of the main spring	4.901 gr
Mass of the appendage	0.63 mgr
Displacement of the light image on the recording paper	57.5 mm

The motion of the light image when the appendage was put on the weight and removed was as shown in the record of Fig. 18. From the record, we lean that the gravimeter does not leave any hysteresis caused by such a procedure. In consequence of the calculation by Table 4, we obtain the following value as the sensitivity:

$$\text{Sensitivity}: \quad 4.105\times10^{-7}\ g/\text{mm},$$

This is almost twice the sensitivity of Schweydar's gravimeter, but it is too low to be applied for the precise observation of tidal variation of gravity. From these

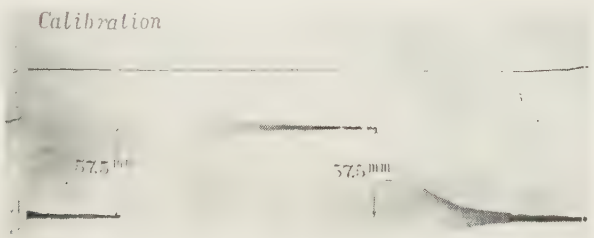

Fig. 18.

circumstances it is naturally understood that the most urgent problem in the precise gravimetric observation is to minimize the drift of the gravimeter as much as possible for the purpose of keeping sufficiently high degree of sensitivity in the gravimeter. The experiments on the effect of ground-tilt for the gravimeter was made by means of the method of really tilting the triangular base on which the gravimeter was set up. According to the results of the experiments, the changes becaused by tilting of 1″ angle are expressed in terms of variation of gravity as follows:

$$\text{In the longitudinal direction}: \quad -2.67\times10^{-8}\ g/\text{second angle},$$

$$\text{In the transversal direction}: \quad +30.05\times10^{-8}\ g/\text{second angle}.$$

According to the tiltmetric studies of E. Nishimura (**26**), the observed tidal variations of tilting of M_2-component at Ikuno are as follows:

In the N–S direction: $0''.00240 \cos(2t - 264°)$,
In the E–W direction: $0''.00458 \cos(2t - 88°)$.

On the other hand, the expected amplitude of the tidal variation of gravity of the M_2–component was about $5 \times 10^{-8} g$. Therefore, we usually did not take any account of the corrections for tilting as far as the present tentative observation was concerned. The duration of the observation was about thirty-one months, but the period which was made subject to harmonic analysis was about three months during July 17th to October 17th, 1953, for various reasons such as interruptions in recording. Since the drift speed was not uniform through the period of analysis, the drift was reduced by subtracting from the corresponding observed values the running averages of the observed values over periods of 25 hours. As a result of a harmonic analysis of the data drift-removed, the following tidal values of gravity were obtained:

M_2(lunar semi-diurnal component): $5.43 \times 10^{-8} g \cos(2t - 145°.03) \pm 0.16 \times 10^{-8} g$
S_2(solar semi-diurnal component): $13.42 \times 10^{-8} g \cos(2t - 17°.24)$
O_1(lunar diurnal component): $8.17 \times 10^{-8} g \cos(t - 193°.38)$

As seen at a glance, these results are very curious, for the amplitudes of the S_2 and O_1–components are larger than the M_2–component, notwithstanding the fact that the former should theoretically be smaller than the latter. Detailed discussions on the cause of this curious result will be made later on. The theoretical value of the tidal variation of gravity, in other words, the tidal variation of gravity in the case that the earth be perfectly rigid is calculated as follows:

$$M_2(\text{theor.}): 5.01 \times 10^{-8} g \cos(2t - 180°).$$

The tidal factor G calculated by dividing the value of observed amplitude by that of theoretical amplitude is

$$G = 1 - \frac{3}{2} k + h = 1.08 \pm 0.03,$$

and the phase lag κ is as follows:

$$\kappa \quad 325°.03 \ (\text{or} \ -34°.97).$$

The value of $G = 1.08$ thus obtained is considered to be right in approximation, but its accuracy is not sufficient to discuss the small difference, if it exists, of the G–value, because the present observation at Ikuno had to be operated with an undesirably low sensitivity in the gravimeter because of the large drift of the instrument. And, on the other hand, the G–value recently obtained by the one-month's precise observation with a portable Worden Gravimeter at Kyoto (**27**) was estimated as $G = 1.18_5$, $\kappa = 1°.96$. The difference between these values at both stations of Ikuno and Kyoto seems to be too large, even if the effects of geological structure, influences of oceanic tide and

others might be different for both stations. The detailed treatment of the problem of the local character of the G-value, if it exists, will be reported in a succeeding article after the accomplishment of precise gravimetric observations at many stations under various conditions. Returning to the present observation at Ikuno the cause of the anomalous fact that the observed amplitude of the S_2-component is larger than M_2-component may be interpreted as follows. The curve of the S_2-component (including the S_1-component) bears a good resemblance to that of the diurnal variation of atmospheric pressure except phase difference of about three hours as seen in Fig. 19. By reason of the similarity between the forms of both curves, it is concluded that

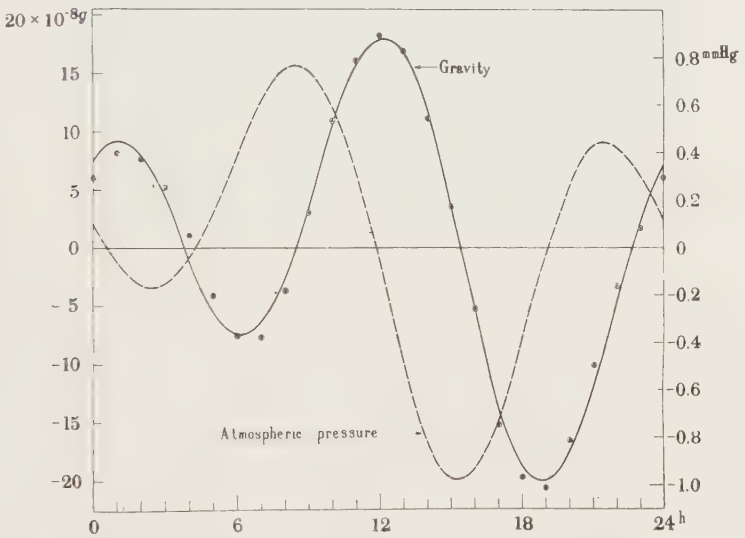

Fig. 19. Solar term in gravity variation and change of atmospheric pressure.

the abnormality of the amplitude of the S_2-component would certainly originate in the variation of atmospheric pressure. The similarity between the gravity-curve and the pressure-curve is also clearly recognized at the time of the passing of a typhoon, as in Fig. 20 which is a typical example among the many which indicate its similarity. In this case, contrary to the case of the S_2-curve, the phase difference is almost undetectable. Two ways as to how the variation of atmospheric pressure has an influence on the gravimeter may be supposed: the one is by way of the variation of buoyancy for the weight, and the other the variation of upperward attraction of air mass. By whichever manner, the decrease of pressure should apparently present itself as the increase of gravity, but the actual state is contradictory to this. In the present time it cannot be interpreted through what mechanism the variation of pressure has an influence as is shown in Figs. 19 and 20 upon the gravimeter. This question must be further examined in the future.

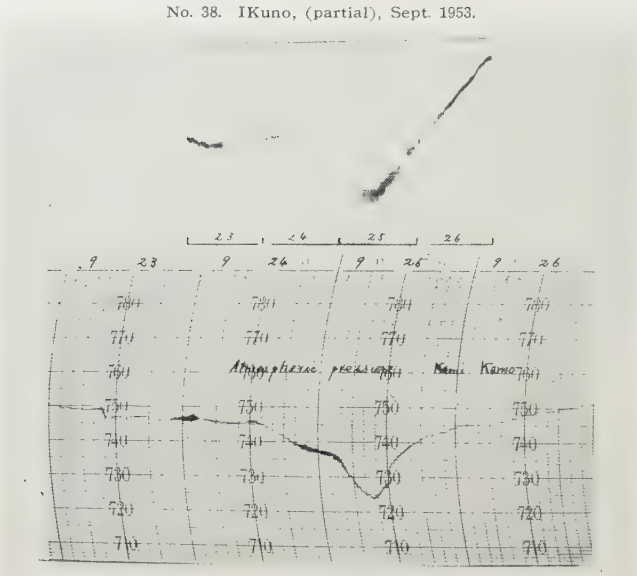

Fig. 20. Anomalous change of gravity at the time of the passing of a typhoon.

In concluding this section it was ascertained from the present observation at Ikuno that the problems of high sensitivity of the gravimeter and the effect of temperature change upon the instrument might, to a certain degree, be solved by the application of a double bifilar suspension and by setting the instrument in a deep underground room. But it is also quite evident that the remaining and most difficult problem for a long continuous and precise observation of tidal and secular variation of gravity is how to minimize gravimeter drift. The problem of drift will persistently be treated in succeeding articles.

Summary and acknowledgement

All the contents described in the present article may be summarized as follows. For the purpose of raising the sensitivity of the gravimeter, a double bifilar gravimeter was devised by the improvement of an ordinary bifilar gravimeter. Also, the function of double bifilar gravimeter was ascertained from both the theoretical and experimental sides. It became very easy to raise the sensitivity of the gravimeter to a sufficiently high degree by the application of a double bifilar suspension, but, to our regret, it was also proved that its efficiency was greatly reduced by the large drift of the gravimeter in the practical observation. A long period observation with the double bifilar gravimeter had been carried out, as a trial, at a deep underground room of the Ikuno Copper Mine, and a value of 1.08 was obtained as the tidal factor of gravity, referred to as the M_2-component. Although the accurate value of the

tidal factor was not obtained by the present observation, it was proved that a gravimeter of the double bifilar suspension type is certainly useful for a long continuous and precise gravimetric observation with the condition of a suitably small instrumental drift.

Finally, it is the writer's pleasure to express his sincere gratitude to Professor E. Nishimura for his consistently kind guidance throughout this study. The writer's hearty thanks are also expressed to Mr. I. Nakagawa who assisted him with all calculations and drawings, and Mrs. I. Yasuda and Y. Tsushima who undertook the manufacture of the instruments. The writer also wishes to acknowledge indebtedness to the members of the Ikuno Copper Mine who have given much assistance on the occasion of the long period observation. The cost of this study was partly defrayed by the grant-in-aid for scientific research of the Ministry of Education.

REFERENCES

1. KELVIN, LORD, 'On the rigidity of the Earth' Phil. Trans. Roy. Soc. London, A **153** (1863)' 573–582; 'Dynamical problems regarding elastic spheroidal shells and spheroids of incompressible liquid', Phil. Trans. Roy. Soc. London, A **153** (1863), 583–616.
2. REBEUR-PASCHWITZ, E. v., 'Horizontalpendel-Beobachtungen auf der Kaiserlichen Universität-Sternwarte zu Strassburg 1892–1894', Gerl. Beit. z. Geophys., **2** (1897).
3. SCHWEYDAR, W., 'Beobachtung der Änderung der Intensität der Schwerkraft durch den Mond', Sitz. d. König. Preuss. Akad. Wiss., **14** (1914), 454–465.
4. LOVE, A. E. H., The yielding of the earth to disturbing forces', Proc. Roy. Soc. London A **82** (1909), 73–88; '*Some Problems of Geodynamics*', Cambridge (1926).
5. TAKEUCHI, H., 'On the Earth Tide of the Compressible Earth of Variable Density', Trans. Amer. Geophys. Union, **31** (1950), 651–689; 'On the Earth Tide', Journ. Faculty of Sci. Tôkyô Univ., II **7** (1951), Part 2.
6. BULLEN, K. E., 'The variation of density and ellipticities of strata of equal density within the Earth', M. N. R. A. S., Geophys. Suppl., **3** (1936), 395–401; 'The problem of Earth's density variation', Bull. Seis. Soc. Amer., **30** (1940), 235–250; 'The density variation of the Earth's central core', Bull. Seis. Soc. Amer., **32** (1942), 19–30.
7. LAMBERT, W. D., *Report on Earth Tides*', I. U. G. G., 9th Gen. Assembly, Brussels, (1951); 10th Gen. Assembly, Rome, (1954).
8. MELCHIOR, P. J., 'Les marées terrestres (3 me partie)', Ciel et Terre, **70** (1954), 191–217.
9. SCHWEYDAR, W., ibid. **3**.
10. TOMASCHEK, R. and SCHAFFERNICHT, W., 'Untersuchungen über zeitlichen Änderungen der Schwerkraft. I, Messungen mit dem Bifilargravimeter', Ann. d. Phys., 5 Folge **15** (1932), 787–824; 'Über die Messung der zeitlichen Schwankungen der Schwerebeschleunigung mit Gravimetern,' Zs. f. Geophys., **9** (1933), 125–136.
11. WYCKOFF, R. D., 'Study of Eerth Tides by Gravitational Measurements', Trans. Amer. Geophys. Union, I (1936), 46–52.
12. TRUMAN, O. H., 'Variation of Gravity at one Place', Astrophys. Journ., **89** (1939), 445–462.
13. ECKHARDT, E. A., 'Diurnal Variations in the Acceleration of Gravity', Trans. Amer. Geophys. Union, **30** (1949), 183–184.
14. REFORD, M. S., 'Tidal Variations of Gravity', Trans. Amer. Geophys. Union, **32** (1951), 151–156.
15. HOSKINSON, A. J., 'Harmonic Analysis of Gravity Observations', Trans Amer. Geophys.

Union, **32** (1951), 163–165.

16. TARRANT, L. H., 'Tidal gravity experiments at Peebles and Kirklington', M. N. R. A. S., Geophys. Suppl., **6** (1951), 278-285.
17. TOMASCHEK, R., 'Harmonic analysis of tidal gravity experiments at Peebles and Kirklington', M. N. R. A. S., Geophys. Suppl., **6** (1951), 286–302.
18. PETTIT, J. T., SLICHTER, L. B. and La COSTE, L., 'Earth Tides', Trans. Amer., Geophys. Union, **34** (1953), 174-184.
19. TOMASCHEK, R., "Tidal gravity observations at Winsford (Cheshire)', M. N. R. A. S., Geophys. Suppl., **6** (1952), 372-382.
20. LAMBERT, W. D., ibid. **7** (1951), 20–21.
21. SCHMIDT, A., 'Das Trifilargravimeter', Beit. z. Geophys., **4** (1900), 109–115.
22. BERROTH, A., 'Theorie einiger gravimetrischer Instrumente nach dem Prinzip der bifilaren Aufhängung', Zs. f. Geophys., **8** (1932), 331–370.
23. ELLENBERGER, H., 'Das bifilare Prinzip und seine Anwendung zum Bau von hochempfindlichen und handlichen Schweremessern (Die Neukonstruktion eines Doppelbifilargravimeters)', Deutsche Geodät. Kommission, Reihe C: Dissert.-Veröff. Nr. 2.
24. ICHINOHE, T., 'On a type of highly sensitive gravimeter', KAGAKU, **20** (1950), 325–326, (in Japanese).
25. ICHINOHE, T., 'Highly Sensitive Double Bifilar Gravimeter', ZISIN (Journ. Seism. Soc. Japan), 2nd series, **3** (1951), 49–56, (in Japanese).
26. NISHIMURA, E., 'On Earth Tides', Trans. Amer. Geophys. Union, **31** (1950), 357–376.
27. ICHINOHE, T. and NAKAGAWA, I., 'Observations of the Tidal Variation of Gravity', Sokuchi Gakkai Shi (Journ. Geodet. Soc. Japan), **1** (1954), 62–66, (in Japanese).

Memoirs of the College of Science, University of Kyoto, Series A,
Vol. XXVII, No. 3, Article 4, 1955

STUDY ON CHANGE OF GRAVITY WITH TIME
PART II. REPEATED GRAVITY SURVEYS IN THE KINKI DISTRICT

BY
Tokio ICHINOHE

(*Received July 20, 1955*)

ABSTRACT

Gravity surveys with a portable gravimeter of the North American type were made repeatedly four times during 1950–1953 at about one hundred and sixty points in the Kinki District as a preliminary study on the problem of probable secular variation in gravity. In this article some important conditions, which are considered to be noteworthy for the future development of the investigation of secular variation of gravity, comprise the main discussion as deduced from the data of the present surveys. It should be mentioned that, in the present surveys, some remarkable secular variations in gravity, though not without some uncertainty, were observed in the western shore region of Lake Biwa and the City of Ōsaka.

1. Introduction

The value of gravity acceleration at any fixed point on the earth is dependent on three factors: attraction by the earth's mass, centrifugal force caused by the rotation of the earth, and attraction by the celestial bodies. The latter has already been dealt with in the first Part of the present investigation as the tidal variation of gravity. In the present article the non-periodic variation of gravity, if it exists, caused by changes in the first two factors will be investigated by repeated gravity surveys at many points within a small area.

The non-periodic variation in gravity of short duration (sudden change) or long duration (secular variation) may be caused by the following changes: upheaval and sinking of the ground, effusion of volcanic lava, change of groundwater level, displacement of oceanic water mass, change of atmospheric state, orogenic movements, epeirogenetic movements, and, generally speaking, a change in the geoidal figure caused by displacement or mass changes on the surface or in the interior of the earth. And, moreover, sudden or secular changes of the earth's rotation speed would theoretically affect the gravity value, though in a minute order of magnitude, and could be detected in the future course of fine observation of gravity changes.

In former times, a comparison was made of the gravity values measured at inter-

vals of some fourty years at four stations in India, and changes in gravity of from 27 mgal to 103 mgal were found. But it is questionable as to whether such changes may have been caused by a real change in gravity or attributable to some observational and instrumental errors (**1**). Absolute measurements of gravity were made at Washington, U. S. A., in 1936, and at Teddington, England, in 1939, and these values were referred to the absolute value determined at Potsdam, Germany, in 1906. B. C. Browne and E. C. Bullard (**2**) discussed the problem of difference in the absolute values of gravity at the three stations of Potsdam, Washington, and Teddington, and concluded that the value at Potsdam should reasonably be corrected to −17 mgal in magnitude. In the treatment by Browne and Bullard it was assumed *a priori* that the gravity value at Potsdam had been invariable during the period of thirty years from 1906 to 1936. It is not unthinkable that a part, if not the whole, of the discrepancy in the absolute values of gravity might be attributable to some secular variation at Potsdam. On this point a re-measurement of the absolute value of gravity at Potsdam is most earnestly hoped for towards the development of the research in the secular variation of gravity.

On the other hand, the recent development of a highly sensitive and portable gravimeter has greatly facilitated the quick and precise relative measurement of gravity over large survey areas. The world-wide surveys of gravity with the Worden Gravimeter made by G. P. Woollard (**3**) is an epochmaking step in the research field of gravity, as evidenced by his precise relative measurement of gravity at thirty-three pendulum stations and one hundred and twenty-five gravity stations connecting all continents of the world in the relatively short period of three months, the measurements hitherto having been made under non-uniformity with different instruments and at different times. But the changes deduced from the results of Woollard's surveys and old values should not be considered as directly attributable to any actual secular variation, because the old values were obtained by different instrumtnts and with varying accuracies from those of Woollard. It is expected that, the problem of the secular variation of gravity on a world-wide basis will be developed by the repetition of such surveys as Woollard's in successive decades.

At the Meeting of the International Gravimetric Comission at Paris in 1953, it was resolved and recommended that the selection of a network of some thirty "first order" international gravity stations be established all over the world, with frequent and efficient connection between the first international stations for each other and between the first international stations and the national reference stations. The completion of such a program would certainly make a great contribution to the advancement of research in geoidal figure and in world-wide secular variation of gravity.

Setting the phenomena of world-wide scope aside, the non-periodic variation of

gravity of local or regional character observed in this country will be mentioned. Previously, the secular change in the rate of speed of the Riefler-clock in the Tokyo Astronomical Observatory was examined by M. Ishimoto and K. Tuzi (**4**) in connection with the occurrence of the Great Earthquake near Tokyo on September, 1, 1923. Assuming that the whole change of rate of the Riefler-clock would be caused only by a gravity change, the gravity value at Tokyo might have change 10 mgal before the earthquake occurrence. But this problem remains undetermined, as indicated by C. Tsuboi's study, for the relation between the clock rate and gravity change is not so simple as above assumed. After the occurrence of the strong earthquake on December 26, 1949, at Imaichi, 7 km distant from Nikkō, in Tochigi Prefecture, it was found by K. Iida, M. Hayakawa, and K. Katayose (**5**) that the gravity value at Imaichi had decreased by the amount of 0.15 mgal compared with that at Nikkō during three months after the earthquake occurrence. The change of gravity at the area of Volcano Mihara in Ōshima of Izu Islands was also observed by the same members above mentioned (**6**) at the time of violent eruption in 1950. This report is reasonably appreciated since an abundant effusion of lava may cause a local deformation in the gravitational field. The results above described are considered to be quite accurate since the gravimeter used in both cases was of the North American type whose sensitivity is enough to detect such a degree of gravity change and instrumental drift is estimated to be exceedingly small. On December 21, 1946, the Great Nankaidō Earthquake occurred at the area 50 km offshore in the open sea southward of the Kii Peninsula. This destructive earthquake of a magnitude of 8.2 (Pas.) brought about great damage by Tsunami along the neighbouring harbours, and, moreover, an upheaval and sinking of the ground exceeding the amount of 1 meter in the region of the southern part of Kii Peninsula and the south-eastern part of Shikoku. Referring to this earthquake the plumb-line deviation was re-surveyed by T. Okuda (**7**) at thirteen points around the epicentral region, and it was ascertained that the large secular change of the plumb-line occurred during several years from the old epoch (1939 –1946) to the new epoch (1947–1950), whose amount reaches nearly 4 seconds angle in the maximum. The above result means, in other words, a local change of geoid in the epicentral region and consequently a local change in gravity intensity. Really the change of gravity at several points in the southern part of Kii Peninsula was observed by N. Kumagai (not yet published) with the Meinesz' gravity pendulum, amounting to several milligals. These observations throw some light upon the little known field of secular variation of gravity and suggest a method of future research. In connection with these phenomena a gravity survey along the lines of precise levels throughout Japan with a Worden Gravimeter has recently been accomplished by C. Tsuboi (**8**). This precise survey of dense net not only revealed the fine subterranean

structure in Japan but also will certainly make a great contribution to the future study on the secular variation of gravity when these values are compared with those which will be observed after one or two decades.

Concerning the problem of crustal deformation, the concurrent observations of self-recording by the highly sensitive gravimeter with the tiltmeter and the extensometer of high quality have been operated under the auspices of our Geophysical Institute, Kyoto University, since 1951 at several points in the Kinki District. As already described in the preceding paper, the highly sensitive station gravimeter is unsuitable for the study of secular variation of gravity owing to its enormously large drift of zero position. But it will certainly promise the possibility of detecting sudden changes in gravity because of its high sensitivity. On the secular variations in gravity at these stations, the precise and frequently repeated relative measurements of gravity with the pendulum will commence early in 1956. Parallel to this series of observations, the frequent repetition of dense net gravimetric surveys in the Kinki District with the highly sensitive (0.09104 mgal/div. with the negligibly small drift of 0.05 mgal/day) portable North American Gravimeter was planned by Profs. K. Sassa and K. Iida for the purpose of determining the fine subterranean structure of the Kinki District and of obtaining profitable data for the study of secular variation of gravity. Four surveys have been made from 1950 to 1953 at 160 points near Kyoto and Ōsaka by the operators, K. Iida, M. Hayakawa, Y. Kotani, T. Sugiyama, and the writer. In the present article the observational data and results of the four surveys will be reported by the writer by permission of the planners and operators, confining the subject mainly to the problem of time variation in gravity.

2. Results of surveys

Present series of gravity surveys were originally planned to investigate the following three points:

(a) To investigate the fine subterranean structure of the Kinki District by applying the precise and dense gravity surveys to a relatively small area, complemented with the knowledge obtained from the analyses of seismic waves in near earthquakes.

(b) To estimate the amount of secular variation in gravity, if any, and to find a fitting method for its investigation by applying the ruled and frequent repeated surveys to one and the same area.

(c) To obtain useful data for investigating the phenomenon of ground-subsidence, in particular, in the area of Ōsaka City from both sides of the distribution mode of gravity anomlies and its time variation.

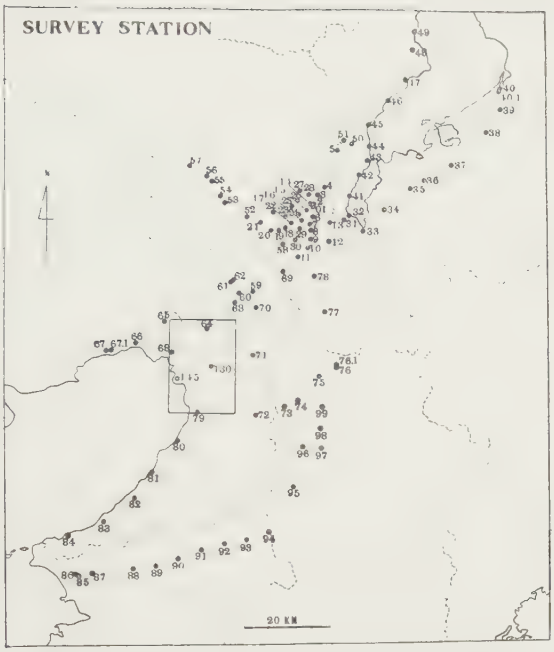

Fig. 1a. Survey stations in the Kinki District (near Kyoto, Ōsaka, Kōbe, Nara, and Wakayama)

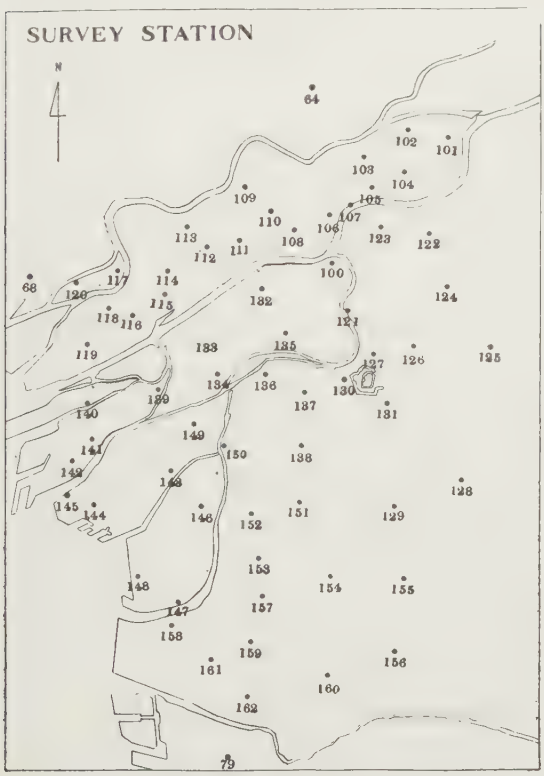

Fig. 1b. Survey stations in Ōsaka City

The survey stations are shown in Fig. 1, and the instrument used is the North American Gravimeter AG–1, 108, belonging to the Geological Survey of Japan, and whose construction and function can be obtained by referring to the article by T. Matsuda (**9**). The four surveys were made in the periods of December, 1950 (I); December, 1951–January, 1952 (II); November–December, 1952 (III); and December, 1953 (IV). The materials obtained in surveys I and II and corrected for both effects of "drift" and "tidal force" have already been published by K. Sassa and K. Iida (**10**). In the present paper the materials of all four surveys are tabulated at the end of the article, and it should be remarked that the gravity values in the table are listed in the figure of 0.1 mgal for the sake of assurance, though the instrument is designed to measure and read in the figure of 0.01 mgal. By the analysis of data obtained in survey I some problems were treated by the writer (**11**), and the Bouguer anomalies calculated in that treatment are again shown in Fig. 2, which well coincides with that derived independently from a different survey made by C. Tsuboi (8). Of the data of survey II some detailed discussions were made on the problem of ground-subsidence in the area of

Ōsaka City referring to the distribution mode of the Bouguer anomalies in that area, and some considerations were applied to the difference of gravity values at the re-measured places in surveys I and II. Two papers on survey III were read at the Annual Meeting of the Seismological Society of Japan at Kanazawa on May, 1953, but they are not yet printed. In the following section the problems on the time variation in gravity and its observational degree of reliability are discussed mainly by analyzing all materials obtained from the present four gravity surveys from 1950 to 1953 in the Kinki Ditrict.

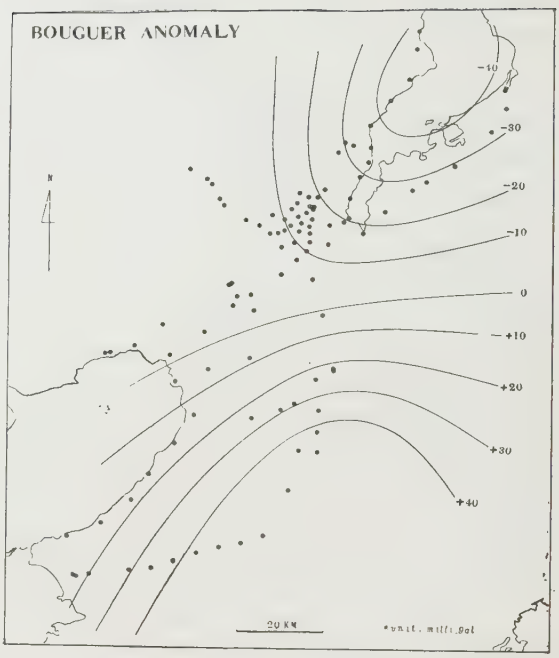

Fig. 2. Bouguer anomaly in the Kinki District

3. Observed secular variation of gravity

The stations surveyed in the present series of four gravity surveys amounted to about one hundred and sixty in all, and among them about sixty stations are situated in the area of Ōsaka City. Consequently, it is convenient to treat the observed materials by separating those of the Ōsaka area from those of the remaining area. As seen in the table at the end, the observed values at any place in each survey differ greatly from each other. An essential problem in the present article is whether these variations may be correctly interpreted as secular change in gravity or whether they were caused by some instrumental or observational error. On this point, for the purpose of examining whether there is any systematic variation of the measured gravity in any region or not, the amounts of change in gravity are graphically shown by the survey route in Fig. 3. As shown in this figure, considerable amount of variation in the measured gravity values are found in some periods, but it is generally difficult to find any route of systematic change throughout all four surveys. Only route B, from Kyoto (station-number, 0) to Imazu (station-number, 49), namely the western shore region of Lake Biwa, is somewhat worth noticing, because of the increase in gravity values at all stations along this route during 1950 to 1952. As this area is just in the region of large negative Bouguer anomlies with steep gradient, it is speculatively interest-

ing to imagine some connection between the amount of secular variation in gravity and the steepness of distribution in gravity anomalies. But it is questionable as to whether the changes shown in Fig. 3 depend upon real gravity changes or some instrumental and observational errors, for only two surveys were made in this route. The solution of this sort of problem by the repetition of gravity surveys in the succeeding decade or century is greatly to be desired.

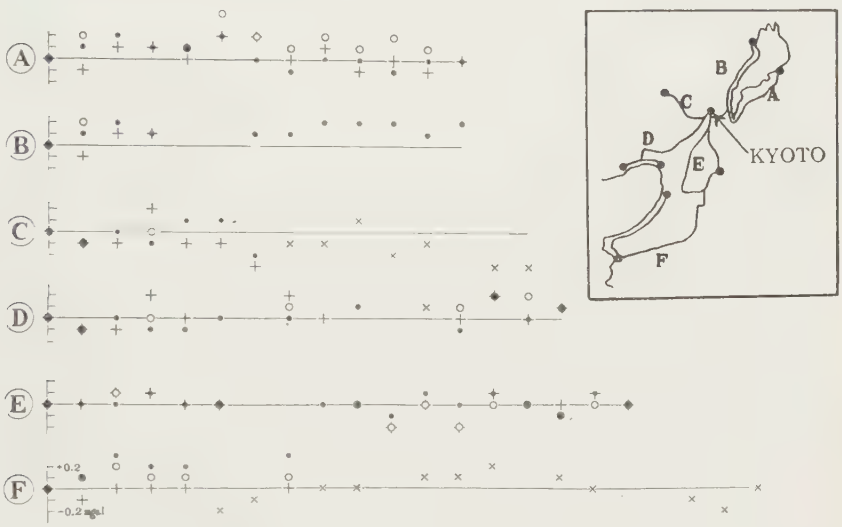

Fig. 3

⁻ : Difference between surveys I–II
● : 〃 〃 〃 I–III
⊥ : 〃 〃 〃 I–IV
× : 〃 〃 〃 III–IV
A : Station numbers, 0, 13, 31, 32, 33, 34, 35, 36, 37, 38, 39, 40, 40.1
B : 〃 〃 , 0, 13, 31, 32, 41, 42, 43, 44, 45, 46, 47, 48, 49,
C : 〃 〃 , 0, 14, 15, 16, 17, 18, 19, 20, 21, 52, 53, 54, 55, 56, 57
D : 〃 〃 , 0, 14, 15, 16, 29, 30, 58, 59, 60, 61, 62, 63, 64, 65, 66, 67
E : 〃 〃 , 0, 6, 7, 8, 9, 10, 11, 69, 70, 71, 72, 73, 74, 75, 76, 76.1, 77, 78
F : 〃 〃 , 0, 79, 80, 81, 82, 83, 84, 85, 86, 87, 88, 89, 90, 91, 92, 93, 94, 95, 96, 97, 98, 99

Concerning the data of Ōsaka City, the observed materials in surveys II, III, and IV will be analyzed, because the survey stations were only two points in survey I. In Figs. 4 and 5, the difference between the gravity values observed in surveys II and III, and in surveys III and IV are plotted respectively. And the amount of ground-subsidence measured in Ōsaka City are also shown in Fig. 6 for comparison with Figs. 4 and 5. From these three figures it is generally understood that the places of large ground-subsidence well coincide with those of large increases in gravity, excepting the case in the small north-western part of City. Ground-subsidence certainly causes an increase of gravity value owing to the approach of the survey

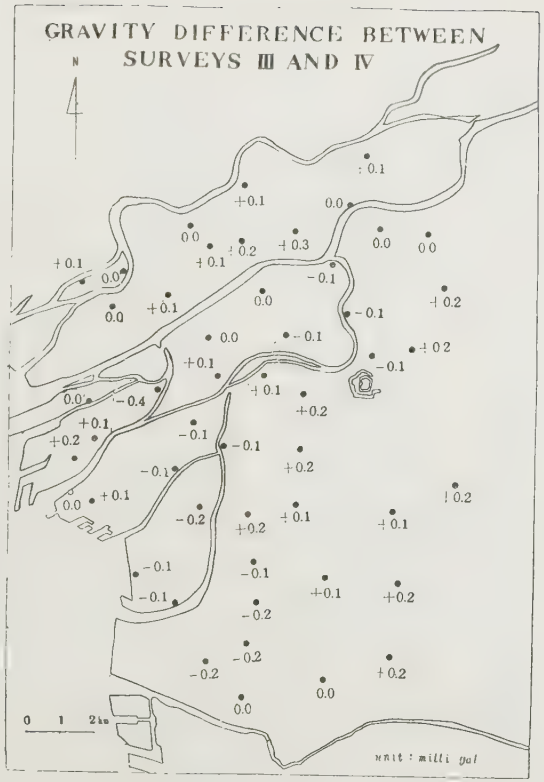

Fig. 5. Gravity difference in Ōsaka City

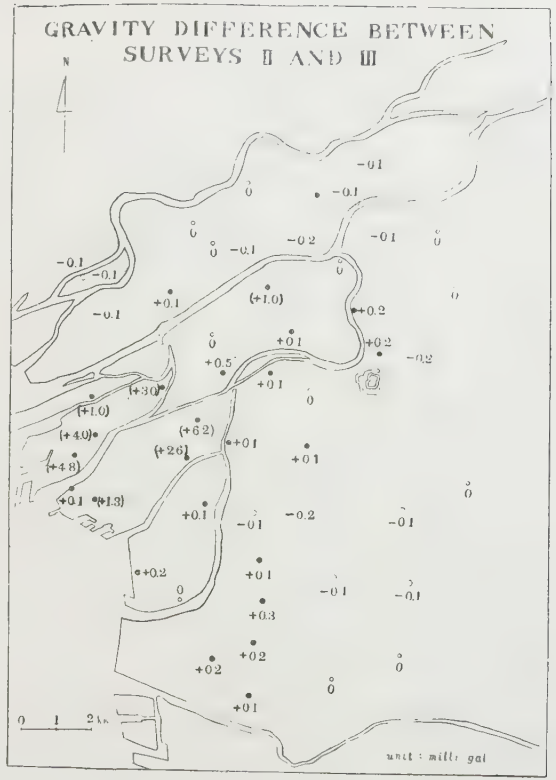

Fig. 4. Cravity difference in Ōsaka City.

Fig. 6. Ground-subsidence in Ōsaka City

station, though small, to the centre of the earth, but, in the case of Ōsaka City, special note should be made of amount of gravity increase. Namely, the maximum subsidence in this case amounted to nearly 10 cm, and consequently the gravity increase by this subsidence was calculated as nearly 0.03 mgal, which is exceedingly small compared with those observed in the present survey, as seen in Figs. 4 and 5. Therefore, if the observed increase in gravity in Ōsaka City is assumed as the real phenomenon, the ground-subsidence would cause the increase of effective density in the subterranean layer which generally contains a great deal of underground-water. And, on the other hand, it has been previously discussed (**12**) that the places of large ground-subsidence generally coincide with the places of negative Bouguer anomalies in gravity in the area of Ōsaka City. Combining this and the above argument, it can be said that, phenomenologically, the gravity value increased largely at the places of negative Bouguer anomalies in Ōsaka City. This relation resembles, in appearance, that discussed in the case of the western shore region of Lake Biwa. But, under practical considerations, the gravity variation of 1 mgal would necessitate a density variation of 0.05 gr/cm^3 in the subterranean layer of 500 m thickness, or 0.24 gr/cm^3 in the layer of 100 m, and these amounts of density variation are generally unthinkable excepting in an unusual instance. Besides, the places of large ground-subsidence are generally on sandy and weak ground where the amplitude of the micro-tremors of the ground excited by various sources is enormously large compared with those of ordinary firm ground. As it is reasonably supposed that the large micro-tremors of ground would greatly disturb the reading of the portable gravimeter, the large change of gravity at the places of large ground-subsidence deduced from the gravity surveys in Ōsaka City may partly be attributable to the erroneous observation of gravity on the weak and restless ground. Especially, anomalously large changes shown

in Fig. 4 may perhaps be interpreted as derived from the observational errors in survey in 1951. On the contrary, the gravity change shown in Fig. 5 is considered to be trustworthy, and this problem on the relation between the ground-subsidence and the change in gravity could be solved by applying the repeated survey of gravity and levelling to the restricted small area of large ground-subsidence.

In the above discussions the following three essential points are naturally assumed:

(a) All values of gravity in the present four surveys are referred to that at the gravity base station of Kyoto, in the old Astronomical Institute, Kyoto University, and the gravity value at the reference station was assumed to have suffered no change during the period of the successive surveys.

(b) In the application of correction for drift to the measured values, the amount of drift was assumed to be in a linear rate with time in any closing circuit of survey.

(c) The sensitivity of the gravimeter was assumed to have remained constant throughout the period of all the surveys.

Regarding the first supposition, as all gravity measurements made in the world are generally so-called relative measurements, any point should tentatively be adopted as a reference station of no change in the treatment of the relative time variation of gravity in the event that there is no base station of absolute measurement as reference. In the case of the present survey, therefore, the absolute amount of gravity variation, if it exists, is undetectable, and it must be noticed that that which is detectable in the present surveys is the time variation of gravity difference between any of the stations and the old Astronomical Institute of Kyoto University. As to the second supposition, this problem is considered to be an extremely essential point for the investigation of the phenomenon of time variation in gravity, perhaps of an exceedingly minute amount, if it exists, by a highly sensitive but labile survey gravimeter. The North American Gravimeter used in the present surveys is somewhat troublesome in the point of artificial heating for regulating the temperature in the equipment, but its rate of drift is extremely small (roughly estimated as 0.05 mgal per day, during the period of the present surveys). As the main spring of the North American Gravimeter, made of an isoelastic alloy, contains in itself a large internal stress in the manufacturing process of the La Coste-winding, only three years' guarantee is generally provided for the stability of the spring. But the Gravimeter AG–1, 108, used has been satisfactory in the points of its sensitivity and small drift since its import in 1949 to the present, its cause being supposed to be partly attributable to the continuous temperature-regulation and the gravity mass-clamping in every time, though cumbersome in manipulation. The Worden Gravimeter, on the contrary, the spring and other principal parts of the instrument being made of fused silica, needs no heating and clamping. But in spite of its easy manipulation, the Worden Gravimeter

belonging to the Geological Institude, Kyoto University, by which the tidal variation of gravity was observed at several stations in the Kinki District by the writer (**13**), showed a large amount of drift about 0.6 mgal per day and moreover a non-linear rate of drift even in the course of continuous reading at one station. Therefore, in the study on the time variation of gravity, a strict examination has to be made as to whether the rate of drift of the used gravimeter maintains the linearity or not.

Regarding the third postulation, the calibration of the sensitivity of the instrument has frequently been made by comparing the gravity value at the basement with that at the roof of the building of the Geological Survey. From these measurements the scale-constant of the instrument was confirmed to have been practically invariable during the past several years, but it needs to be ascertained in other ways as to whether the scale-constant is invariable or not with time in wider ranges as well. On this point it will be checked, as one way of discrimination, by the following procedure; taking the base station (old Astronomical Institute, Kyoto University) as the coordinate origin, and the difference of gravity value between any station and the base station as the abscissa, and plotting the change of gravity during surveys I to II, I to III, and I to IV at the corresponding stations as the ordinate, the diagram as shown in Fig. 7 is obtained. When at any time there happens to be a variation in the gravimeter's scale-constant, even if there is no time variation of gravity at any station, all points thus plotted would range on three straight lines passing through the coordinate origin and producing some angles with the abscissa-axis respectively. And if the rate of change of scale-constant with time is constant from year to year, the three straight lines thus obtained for each difference in surveys I–II, I–III, and I–IV would pass the coordinate origin with angles increasing at a uniform rate to the abscissa-axis. But

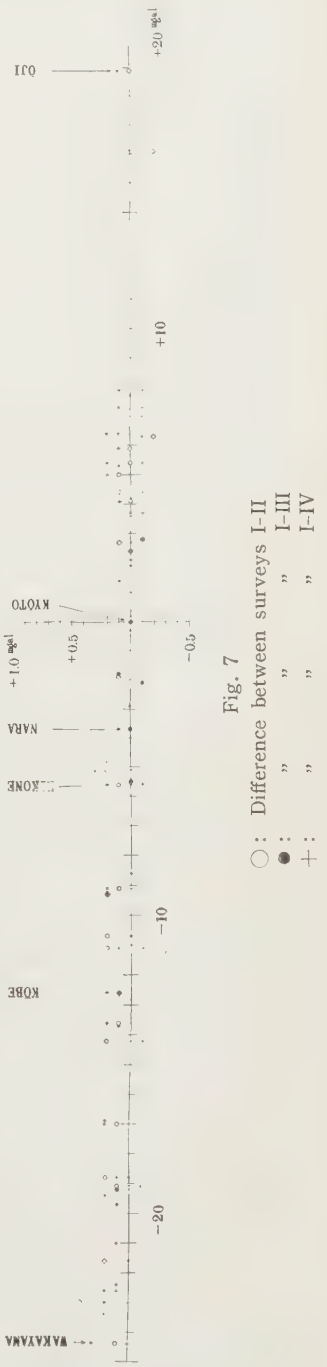

Fig. 7

as seen in Fig. 7, such a tendency is never systematically observed, and, therefore, the scale-constant in the present instrument is considered to have been approximately invariable throughout the whole survey period.

4. Summary

The results of the present surveys of gravity repeatedly operated during the period of 1950–1953 in the Kinki District may be summarized as follows:

1. The change of gravity value in the order of magnitude of 0.1–0.2 mgal in every survey compared with those of the preceding year were observed at a majority of the observation stations. But there were generally no systematic changes of gravity value at the stations in any region excepting the cases in the western shore region of Lake Biwa and Ōsaka City. The apparent changes of gravity value obtained in the present surveys may be attributed mainly to instrumental and observational errors, and this type of investigation for secular variation of gravity is considered to necessitate an assistant named "time" of several decades or centuries for the complete solution of the problem.
2. In the area of the western shore of Lake Biwa, all stations showed a somewhat increasing variation in measured values. If this increase is assumed to be an increase in real gravity value, it provides an interesting speculation on the relation between the time variation of gravity and the area of steep gradient in the Bouguer anomalies of gravity. But its reality should also be ascertained by the repetition of gravity surveys in the future.
3. In Ōsaka City, the tendency was observed that the gravity value increased in the area of markedly large ground-subsidence. The amount of these increases in gravity is not adequately covered by the change of station level and needs to be explained by some another unknown procedure through which both the phenomena of gravity variation and the deformation of weak ground are connected. This problem is also an interesting research item which should be solved by applying the same gravity survey to other area of large ground-subsidence.

In conclusion, the result derived from the present series of gravity surveys is, in a word, that the secular variation in gravity, if it exists, is very minute in quantity, and the errors caused by the instrument, observation, and other unknown sources are far larger than the quantity in question. Nevertheless, the study on the secular variation of gravity should be advanced by reducing the instrumental and observational errors as far as possible, and on the other hand, by spending long series of surveys over several decades or even centuries. The phenomenon of gravity change with time is certainly an attractive and essential research item in geodesy and seismology, especially in regions greatly disturbed by such crustal deformation and strong seismic activity

as found in this country. In our institute, the study on the time variation of gravity is scheduled to be operated by the combined observation with the extremely highly sensitive station gravimeter, frequently checked by the gravity pendulum, along with frequently repeated surveys with the portable gravimeter of high sensitivity and small drift. Finally, it is earnestly hoped that the values of gravity listed in the table at the end of this paper and the various remarks above described may serve, to a certain degree, for the future development of study on the periodic and non-periodic variation of gravity with time.

Acknowledgements

The writer wishes to express his heartfelt gratitude to Dr. K. Sassa, Dr. K. Iida, Dr. M. Hayakawa, Mr. Y. Kotani, and Mr. T. Sugiyama for their generous permission to use for publication the materials of several surveys which the writer had the honour of sharing with them. And the writer is further indebted to Dr. K. Sassa and Dr. E. Nishimura for their kind advices on the analysis of the data throughout this study. The writer is also grateful for the kind help by the members of the Bureau of Public Works of Ōsaka Prefecture and the Bureau of Planning of the Ōsake Municipal Office. The cost of the present study was partly covered by a grant-in-aid for scientific research given by the Ministry of Education.

REFERENCES

1. Tsuboi, C., JŪRYOKU (Gravity), 1944, 212–213. (in Japanese)
2. Browne, B. C. and Bullard, E. C., Comparison of the acceleration due to gravity at the National Laboratory, Teddington and the Bureau of Standards, Washington, D. C., Proc. Roy. Soc. London, A **175** (1940), 110–117.
3. Woollard, G. P., The gravity meter as a geodetic instrument, Geophysics, **15** (1950), 1–29; The earth's gravitational field and its exploitation, Advances in Geophysics, **1** (1952), 281–311.
4. Ishimoto, M. and Tuzi, K., Monthly means of the daily rates of the Riefler clock in the Tôkyô Astronomical Observatory and their bearing on the occurrence of earthquakes, Bull. Earthq. Res. Inst., Tokyo Univ., **6** (1929), 355.
5. Iida, K., Hayakawa, M. and Katayose, K., Changes of gravity difference between Imaichi and Nikkō owing to the "Imaichi Earthquake", Bull. Geol. Surv. Japan, **1** (1950), 136–138. (in Japanese)
6. Iida, K., Hayakawa, M. and Katayose, K., Gravity change according to the eruption of Volcano Mihara, Ooshima Island in 1950 and 1951, Chigaku Zasshi (Journ. Geogr.), 681 (1951), 133–136. (in Japanese)
7. Okuda, T., On the change of local geoid in the south western part of Japan, Bull. Geogr. Surv. Inst., **2** (1951), 239–275.
8. Tsuboi, C., Gravity survey along the precise levels throughout Japan by means of a Worden gravimeter. Part IV. Map of Bouguer anomaly distribution in Japan based on approximately 4.500 measurements., Bull. Earthq. Res. Inst., Tokyo Univ., Supplementary volume IV. Part III, 1954.
9. Matsuda, T., North American Gravimeter, BUTSURI-TANKŌ (Geophysical Exploration),

6 (1953), 210-212. (in Japanese)

10. Sassa, K. and Iida, K., Gravity values in the vicinity of Kyoto, ZISIN (Journ. Seis. Soc. Japan), 2nd. Ser., 4 (1951), 68-70; Gravity measurements in Kansai Districts, ditto, 5 (1952), 136-140. (in Japanese)
11. Ichinohe, T., Bouguer anomalies in the vicinity of Kyoto, ZISIN (Journ. Seis. Soc. Japan) 2nd. Ser., 4 (1951), 71-75. (in Japanese)
12. Hayakawa, M., Kotani, Y. and Ichinohe, T., Interpretation of gravity measurements in Kansai Districts, ZISIN (Journ. Seis. Soc. Japan), 2nd. Ser., 5 (1952), 141-150. (in Japanese)
13. Ichinohe, T. and Nakagawa, I., Observations of the tidal variations of gravity, Sokuchi Gakkai Shi (Journ. Geod. Soc. Japan), 1 (1954), 62-66. (in Japanese)

Description of survey stations

Number

0. Kyoto University, Cellar of the old Astronomical Institute, Gravity base station, on floor (not on stone base).
1. " " , Geophysical Institute, Basement room by the side of stairs, on floor.
1.1. " " , Geophysical Institute, at roof.
2. " " , Geological Institute, International fundamental gravity station, on floor (not on stone base).
3. Kyoto City, Yama-bana trifurcate road, on road of 1 meter east from the guide post of "Daikokuten-michi".
4. " " , Yase, on road near the west edge of Saitō bridge.
5. " " , Kode-ishi trifurcate road, on road in front of a small shrine.
6. " " , Gion-ishidan-shita, on road in front of the stone pillar of the Yasaka shrine.
7. " " , Hon-machi hachi-chōme, B. M. 216. 1.
8. " " , Fushimi-inari, B.M.
9. " " , Fujino-mori, B.M. 217. 1.
10. " " , Momoyama, B.M.
11. " " , Bank of Uji river, B.M.
12. " " , Daigo, on road in front of the gate of Sampō-in.
13. " " , Yamashina, B.M. 214. 1.
14. " " , De-machi, B.M. 241.
15. " " , Kyoto Palace, T.P.
16. " " , In front of the west gate of Honkoku-ji, B.M.
17. " " , Senshō-ji-chō, B.M.
18. " " , Katsura, B.M. 1298.
19. " " , Kataki-bara, B.M. 1297.
20. " " , Tsuka-hara, B.M. 1296.
21. " " , Oino-saka ridge, B.M. 1293.
22. " " , Saga, on road near the north edge of the Togetsu bridge.
23. " " , Uzumasa, T.P.
24. " " , Intersecting point of Sanjō street and Sembon avenue, on ground in front of 40 cm from the monument stone of "Shōgaku-in".
25. " " , North gate of Myōshin-ji, on road in front of 1 meter from the monument stone of "Sakuma Shōzan".
26. " " , Rentai-ji, on pavement in front of 2 meters from the name post of "Rentai-ji".
27. " " , Ōmiya primary school, on ground between the gate pillars.

28. Kyoto City, Minami-shiba-chō trifurcate road, on road in front of the police box.
29. " " , near Rajō-mon stop of the city tram, on pavement in front of 3 meters from the name post of "Kanzeon bosatsu".
30. " " , Tōno-mori, T.P.
31. Ōtsu City, Ōsaka-yama Observatory of Kyoto University, on ground near the entrance of tunnel.
32. " " , Izumi chō, B.M. J. 213.
33. " " , Seta bridge, B.M. 211.
34. Shiga Prefecture, Kusatsu Town, on road in front of Minami dental hospital.
35. " " , Yasu Town, B.M. 207.
36. " " , Shino-hara Village, B.M. 206. 1. (new : on concrete block).
37. " " , Musa Village, B.M. 204.
38. " " , Hie Village, B.M. 201. 1.
39. " " , Takamiya Town, B.M. 200.
40. Hikone City, Hikone Castle, on ground in front of 2 meters from the monument stone of "Enjō Kendō" (new : inside of palisade).
41. 1. " " , Hikone Municipal Office, on ground in front of 1.5 meters from the right hand pillar of porch.
41. Ōtsu City, Karasaki, B.M. 1302.
42. " " , Okoto, B.M. 1305.
43. Shiga Prefecture, Katada Town, B.M. 1307. (new : near side of B.M.).
44. " " , Wani Village, B.M. 1309.
45. " " , Kido Village, B.M. 1312.
46. " " , Komatsu Village, Kita Komatu, Kino-shita shrine, on road in front of 1 meter from the name post of "Kino-shita Shrine"
47. " " , Takashima Town, B.M. 1320.
48. " " , Aiba Village, Kumanomoto, Intersecting point, on road in south-western corner.
49. " " , Imazu Town, B.M. 1326.
50. " " , Ikatachi Village, Kami-ryūge, Fukujuzen-ji, on ground in front of 40cm from the stone steps.
51. " " , Ikatachi Village, Tochū trifurcate road, on road.
52. Kyoto Prefecture, Shino Village, B.M. 1292.
53. " " , Ōi Village, Namikawa, Namikawa station, on concrete block in railway near crossing.
54. " " , Chiyokawa Village, B.M. 1287.
55. " " , Yagi Town, Ōyabu, B.M. 1285.
56. " " , Yagi Town, Yoshitomi, B.M. (new : Yoshitomi primary school, on stepping-stone in front of the gate).
57. " " , Sonobe Town, B.M. 1281.
58. " " , Mukou Town, Mukou shrine, on ground in front of stone steps.
59. Takatsuki City, B.M.
60. Ōsaka Prefecture, Tonda Town, Intersecting point of so-called industrial road, on road near B.M. of Ōsaka Prefecture.
61. Takatsuki City, Abuyama Seismological Observatory of Kyoto University, Basement room, on stone base.

61. 0. " " , " " , Basement.
63. 1. " " , " " , First floor.
61. 2. " " , " " , Second floor.
61. 3. " " , " " , Third floor.

61. 4. Takatsuki City, Abuyama Seismological Observatory of Kyoto University, Fourth floor.
61. 5. " " , " " , Fifth floor.
61. 6. " " , " " , Sixth floor.
62. " " , " " , Pumping room.
63. Ibaraki City, Tobushi, B.M. 225.
64. Suita City, Tarumi, B.M. 411.
65. Itami City, Koya, B.M. 464.
66. Nishinomiya City, B.M.
67. Kōbe City, Mikage chō, on pavement in front of Higashi-nada police station.
67. 1. " " , Uosaki chō, Nada high school, in the porch.
68. Amagasaki City, Amagasaki high school, on ground in front of the porch.
69. Kyoto Prefecture, Yahata Town, South edge of Gokō bridge, on road in front of the guide post.
70. Hirakata City, South edge of Hirakata bridge, on road in front of the stone pillar.
71. Ōsaka Prefecture, Suminodō Town, Suminodō primary school, on ground in front of 1 meter from the name post.
72. " " , Kashihara Town, Ichimura, on road in front of 2 meters from the monument stone of "Hatanaka Ō".
73. Nara Prefecture, Ōji Town, B.M. 1388.
74. " " , Ikaruga Town, Hōryū-ji, on stepping stone in front of the south gate.
75. " " , Kōriyama Town, B.M. 1395.
76. Nara City, Sanjō street, B.M. 1398.
76. 1. " " , Nara Gakugei University, on ground in front of the assembly hall.
77. Kyoto prefecture, Ide Village, East edge of the Tamamizu bridge, Intersecting point on bank, at north-eastern corner.
78. Uji City, Ōkubo, Intersecting point, on road near the guide post.
79. Sakai City, Ayano chō, B.M. J. 246.
80. Ōsaka Prefecture, Takaishi Town, Town office, on ground between the gate pillars.
81. Kishiwada City, B.M. 255.
82. Izumi-sano City, Ichiba, B.M. 259.
83. Ōsaka Prefecture, Ozaki Town, intersecting point, on stone block near a solitary pine-tree.
84. " " , Tan-nowa Village, Izumisaki middle school, on ground between the gate pillars.
85. Wakayama City, Nakanoshima primary school, at a small room by the side of assembly hall.
86. " " , Hon-machi, B.M. J. 273.
87. Wakayama prefecture, Nishi-wasa Village, Hachikenya, B.M. J. 271.
88. " " , Iwade Town, B.M. 1582.
89. " " , Tanaka Village, Kurotsuchi, B.M. 1579.
90. " " , Nade Town, B.M. 1576.
91. " " , Ōtani Village, Shin-zaika, Bank near B.M., on concrete block of a small shrine.
92. " " , Kōyaguchi Town, B.M. 1570.
93. " " , Hashimoto Town, B.M.
94. " " , Suda Village, Matsuchi, on road near the east edge of Ryōgoku bridge.
95. Nara Prefecture, Katsuragi Village, Kotono, at porch of the ruin of isolation hospital.
96. Yamato-takada City, on concrete block by the side of monument stone of "The Emperor Meiji"
97. Nara Prefecture, Yagi Town, Ebisu shrine, on stone base of left hand lantern.
98. " " , Tawaramoto Town, Tsushima shrine, on stone base of the monument

of "Kokui Senyō".

99. Nara Prefecture, Nikaidō Village, Kizuki shrine, at the middle of the dancing-platform.
100. Ōsaka City, Ōyodo ku, Nagara Nakadōri, B.M. J. 229.
101. Higashi Yodogawa ku, Kita Ōmichi chō, Ōsumi shrine, O.B.M. N. 1. (*)
102. » » , Komatsu Nakadōri, Sennen-ji, O,B.M. N .2.
103. » » , Shimo Shinjō chō, B.M. 228.
104. » » , Toyosato Samban chō, Teisembō, O.B.M. N. 4.
105. » » , Toyosato Sugahara chō, O.B.M. N. 5.
106. » » , Shibajima chō, Shibajima shrine, O.B.M. N. 6.
107. » » , Shibajima chō, B.M. 228. 1.
108. » » , Minamikata chō, Shōfuku-ji, O.B.M. N. 8.
109. » » , Mikuni Hon-machi, Mikuni primary school, O.B.M. N. 12.
110. » » , Nishi chō, Kōyō-ji, O.B.M. N. 13.
111. » » , Jūso Higashino chō, Jūso primary school, O.B.M. N. 14.
112. » » , Motoimasato, Hakuaisha kindergarten, O.B.M. N. 16.
113. » » , Mitsuya Nakadōri, Renshō-ji, O.B.M. N. 17.
114. Nishi Yodogawa ku, Nozato chō, Tanaka laboratory, O.B.M. N. 20.
115. » » , Nozato chō, Nozato Sumiyoshi shrine, O.B.M. N. 22.
116. » » , Himejima chō, Himejima shrine, B.M. 10696.
117. » » , Tsukuta chō, Ichi chōme, O.B.M. N. 24.
118. » » , Ōwada chō, Ōwada Higashi primary school, O.B.M. N. 25.
119. » » , Ōno chō, Sumiyoshi shrine, O.B.M. N. 26.
120. » » , Tsukuta chō, B.M. 10697.
121. Miyakojima ku, Nakano chō, B.M. 229. 1.
122. Asahi ku, Ōmiya chō, Ōmiya shrine, O.B.M. E. 2.
123. » » , Akagawa chō, Jōhoku primary school, O.B.M. E. 3.
124. Jōtō ku, Sekime chō, Police school, O.B.M. E. 6.
125. » » , Hanaten chō, B.M. 10746.
126. » » , Shin Kita chō, B.M. 10747.
127. Miyakojima ku, Aioi chō, B.M. J. 232.
128. Ikuno ku, Ōtomo chō, Koji primary school, O.B.M. E. 20.
129. » » , Katsuyama dōri, Ōsaka Meteorological Observatory, B.M. near well.
129. 1. » » , » » , » » » , B.M. in garden.
129. 2. » » , » » , » » » , Seismograph room.
130. Higashi ku, Ōtemaeno chō, Staff's hall of Ōsaka Prefecture, at porch.
131. » » , Morinomiya Higashino chō, Labourer's hall of Ōsaka City, in front of the stone steps.
131. 1. » » , » » » , Hikarino-ma in the third floor.
132. Ōyodo ku, Nakatsu Hon dōri, Nakatsu primary school, O.B.M. M. 8.
133. Fukushima ku, Ebie chō, Nippon Medicine Co., O.B.M. M. 16.
134. » » , Tamakawa chō, Ebisu shrine, O.B.M. M. 13.
135. Kita ku, Sonezaki kami ni chōme, Tsuyu-tenjin shrine, O.B.M. M. 18.
136. Nishi ku, Edobori minami dōri, Nishi Semba primary school, O.B.M. M. 23.
137. Higashi ku, Hon-machi ni chōme, north-eastern corner, O.B.M. M. 27.
138. Minami ku, North edge of Nippon bridge, O.B.M. M. 40.
139. Konohana ku, Shikanjima Ōdōri, Donkai-in, O.B.M. W. 2.
140. » » , Hideno chō, Senshū-ji, O.B.M. W. 10.
141. » » , Shimaya chō, Sumitomo Metal Co., O.B.M. W. 13.
142. » » , Sakurajima Kitano chō, Hitachi shipyard, O.B.M. W. 18.
143. Minato ku, Ichioka Hama dōri, Ichioka commercial high school, O.B.M. W. 27.

144. Minato ku, Yawataya Motomachi, Harbour works section of Ōsaka City, at lowest step of the stairs. (new : in lawn graden in front of the building).
145. 〃 〃, Tempōzan, T.P.
146. Taishō ku, Minami Izuo chō, Izuo Higashi primary school, O.B.M. W. 33.
147. 〃 〃, Funa chō, Nakayama Steel Co. O.B.M. W. 38.
148. 〃 〃, Tsuruhama dōri, Harbour works section of Ōsaka City, O.B.M. W. 40.
149. Nishi ku, Kujō dōri, Kujō small park, O.B.M. W. 45.
150. 〃 〃, Nishi Dōtonbori dōri, B.M. 235. 2.
151. Naniwa ku, Ebisu chō, B.M. 235.
152. Nishinari ku, Nakabiraki chō, Nakabiraki primary school, O.B.M. S. 3.
153. 〃 〃, Tachibana dōri, Tachibana primary school, O.B.M. S. 7.
154. Abeno ku, Hannan chō, Abeno high school, O.B.M. S. 11.
155. Higashi Sumiyoshi ku, Kuizen chō, Ikuwa primary school, O.B.M. S. 12.
156. 〃 〃 〃, Yuzato chō, Minami Kudara primary school, O.B.M. S. 15.
157. Nishinari ku, Tabata dōri, O.B.M. S. 20.
158. Sumiyoshi ku, Shibaya chō, Fujinagata shipyard, O.B.M. S. 22.
159. Nishinari ku, Kohama Nakano chō, Kohama primary school, O.B.M. S. 24.
160. Sumiyoshi ku, Higashi Nagai chō, Nagai primary school, O.B.M. S. 27.
161. 〃 〃, Minami kagaya chō, Sumiyoshi park, O.B.M. S. 34.
162. 〃 〃, Adachi chō, B.M. 245.

(*) O.B.M. : Abbreviation of bench mark made by Ōsaka City

Table

Station number	Latitude (N)	Longitude (E)	Elevation m *1	Bouguer anomaly (mgal) *2	Survey I: Correction to elevation (m) *3	Survey I: g (gal) *4	Survey II: Correction to elevation (m)	Survey II: g (gal)	Survey II: Difference I-II (mgal)	Survey III: Correction to elevation (m)	Survey III: g (gal)	Survey III: Difference II-III (mgal)	Survey III: Difference I-III (mgal)	Survey IV: g (gal)	Survey IV: Difference III-IV (mgal)	Survey IV: Difference II-IV (mgal)	Survey IV: Difference I-IV (mgal)
0	35°01'40	135°46'93	55	−11.6		979.7230				—	979.7230	0.0	0.0	979.7230	0.0	0.0	0.0
1	35°01'39	135°46'93	55.6					979.7230	0.0								
1.1	"	"	55.6+13.67			7228				—	.7228	0.0	0.0	.7228	0.0	0.0	0.0
2	35°01'56	135°47'18				7189		.7228	0.0	—							
3	35°02'84	135°47'56				7208					7210		+0.2	7208	0.2		0.0
4	35°03'80	135°48'62				7199					7199		0.0				
5	35°08'57	135°50'59				7046											
6	35°00'03	135°46'82				6967											
7	34°59'00	135°46'38	31.90			7240											
8	34°57'95	135°46'13	39.32	−11.3	−0.20	7258	−0.26	7268	−1.0		7249	−0.1	−0.1				
9	34°56'89	135°46'11	30.04	−11.6	−0.16	7241				—	7244	−0.1	−0.1	7243	0.1	0.0	−0.1
10	34°56'98	135°46'08	26.73	−9.3	−0.15	7245					7247			7247	0.0		0.0
11	34°54'80	135°44'51	16.39	−8.0	−0.20	7256	−0.20	7258	−0.2		7260	−0.2	−0.3	7260	0.0	0.0	0.0
12	34°56'93	135°49'30		−6.8	−0.10	7252											
13	34°59'28	135°49'37	69.94			7146											
14	35°01'62	135°46'37	53.74	−11.8	+0.20 *5	7177											
15	35°00'92	135°45'90	46.10	−9.8	−0.30	7236	−0.30	7236	0.0		7228	−0.1	−0.1				
				−9.8	−0.10	7236	−0.07	7236	0.0		7236	0.0	0.0				
16	34°59'40	135°45'13	72.75	−10.9	−0.20	7186					7186						
17	34°59'17	135°45'62	21.70	−9.2	−0.25	7236	−0.14	7236	0.0		7241	−0.1	−0.1	7241	0.0	0.0	0.0
18	34°58'65	135°45'73	21.97	−9.7	−0.25	7231					7242						
19	34°58'30	135°44'71	35.9	−9.2	−0.20	7234					7236						
20	34°58'24	135°49'44	78.93		−0.20	7202					7204						
21	34°59'29	135°46'78	193.70								7160						
22	35°00'64	135°49'83															
23	35°00'05	135°42'39	33.9	−9.5	−0.15	7230					7231						
24	35°00'34	135°44'71				7230					7233						
25	35°01'37	135°43'32				7267					7266						
						7281					7282						
26	35°02'06	135°44'32															
27	35°03'34	135°44'94				7226					7230						
28	35°02'88	135°46'19				7225					7226						
29	34°58'56	135°44'79				7250					7252						
30	34°57'00	135°44'21	20.2	−5.7	−0.15	7285					7286						
											7305						
31	34°59'81	135°51'63				7062											
32	35°00'14	135°52'40	91.01	−21.6	−0.20	7041					7044						
33	34°58'19	135°54'50	88.69	−19.2	−0.25	7035	−0.25	7035	0.0		7033	−0.2	−0.2				
34	35°00'81	135°57'75				6998		7002	−0.4		7000	−0.2	−0.4				
35	35°03'64	136°01'41	99.86	−27.0	−0.15	7012	−0.15	7014	−0.2		7012	−0.2	−0.4				
36	35°04'60	136°03'61	102.44	−25.3	−0.20	.7037	−0.20	7038	−0.1	.7036	7036	−0.2	−0.3				
37	35°06'67	136°07'94	106.60	−28.4	−0.20	.7040	−0.20	7042	−0.2	new in III	7040	−0.2	−0.3				
38	35°11'02	136°15'33	100.00	−38.7	−0.15	6998	−0.15	6999	−0.1		6998	−0.1	−0.2				
39	35°13'82	136°15'47	104.73	−32.8	−0.25	.7086	−0.25	7086	0.0		7088	+0.1	−0.1				
40	35°16'44	136°15'57		−32.0		7172		7173	−0.1	.7172	7172	−0.1	−0.2				
40.1	35°16'16	136°15'29				7142				new in III	7142						
41	35°02'65	135°52'56	87.03							0.0	6956						
42	35°05'30	135°53'82	87.41							+0.24	6976						
43	35°07'26	135°55'25	88.04	−35.3	−0.40	.7004				.7004	7005	−0.1					
44	35°09'18	135°55'44	98.21	−35.5	−0.15	.7002				new in III	7003	−0.1					
45	35°11'76	135°55'42	104.55	−36.3	−0.30	.6994					6996	−0.2					
46	35°14'84	135°58'39				.7059					.7061	+0.2					
47	35°17'71	136°00'96	87.15	−46.9	−0.05	.7034					.7036	+0.2					
48	35°21'43	136°01'96				.7446					.7447	+0.1					
49	35°23'80	136°02'32	87.42	−41.3	−0.15	.7180					.7182	+0.2					
50	35°09'39	135°52'84				.6907											
51	35°09'83	135°51'70															
52	34°59'88	135°36'82	116.85			.6774											
53	35°01'67	135°33'46															
54	35°02'57	135°32'84	100.64							-0.28	.7169			7168	−0.1		
55	35°04'51	135°31'52	110.32								7230			7228	−0.2		
										-0.18	.7235			7234	−0.1		
										-0.30	.7282						
56	35°05'08	135°30'83	112.83	—	—	—											
57	35°06'48	135°28'20	131.03	—	—	—				.7312	.7316			7313	−0.3		
58	34°56'50	135°42'13	—	—	—	—				new in IV	.7347			7344	−0.3		
59	34°50'41	135°37'68	7.64	−2.3	−0.20	.7299											
60	34°50'24	135°35'53	—			.7262					.7278	−0.1	0.0	7278	−0.2	−0.1	−0.3
														7282			
61	34°51'56	135°34'40	200+0.28			.7016											
61.0	"	"	200+0.00			.7018					.7019		+0.1				
61.1	"	"	200+3.23			.7008											
61.2	"	"	200+6.84			.6996					.6996		0.0				
61.3	"	"	200+10.55			.6983											
61.4	"	"	200+14.61			.6970					.6970		0.0				
61.5	"	"	200+22.81			.6942											
61.6	"	"	200+29.11			.6921					.6921		0.0				
62	34°51'65	135°34'51				.7106											
63	34°49'10	135°34'91	10.33							-0.05	.7265			7266	−0.1		
64	34°45'65	135°30'69	9.03	+4.1	(+0.20	.7272	0.20	.7273	−0.1		.7271	−0.2	−0.1	.7272	+0.1	0.1	−0.1
65	34°46'74	135°24'28	21.15	−8.5	−0.30	.7135	−0.27	.7137	−0.2		.7137	0.0	−0.2	7137	0.0	0.0	−0.2
66	34°43'84	135°20'09				.7121		.7123	−0.2		.7121	0.2	0.0	7121	0.0	0.2	0.0
67	34°42'86	135°15'62		(−6.4)		.7102		.7103	−0.1		.7103	0.0	−0.1	7102	0.0	0.0	−0.1
67.1	34°42'97	135°16'26						.7074			.7074	0.0		.7074	0.0	0.0	
68	34°42'68	135°25'41				.7092		.7093	−0.1		.7094	−0.1	−0.2	.7094	0.0	−0.1	−0.2
69	34°53'04	135°42'16				.7293											
70	34°48'49	135°38'24				.7270					.7270		0.0				
71	34°42'36	135°37'60				.7173		.7173	0.0		.7173	0.0	0.0				
72	34°34'68	135°37'80				.7291		.7289	−0.2		.7290	−0.1	0.1	7289	−0.1	0.0	−0.2
73	34°35'75	135°42'17	35.87	+38.8	0.05	.7417	0.05	.7417	0.0		.7418	−0.1	−0.1	7417	−0.1	0.0	−0.1
74	34°36'58	135°44'23				.7389		.7387	0.2		.7389	−0.2	0.0	7387	−0.2	−0.2	−0.2
75	34°39'50	135°47'48	56.81	+23.0	−0.15	.7269	0.15	.7269	0.0		.7270	−0.1	+0.1	7270	−0.1	−0.1	−0.1
76	34°40'76	135°50'19	98.48	+23.1	−0.15	.7191	0.15	.7191	0.0		.7191	0.0	0.0				
76.1	34°40'95	135°50'20				.7207		.7206	0.1		.7206	0.0	+0.1	.7207	+0.1	0.1	0.0
77	34°47'75	135°48'36				.7287		.7287	0.0		.7288	+0.1	+0.1	7288	0.0	+0.1	+0.1
78	34°52'35	135°46'95				.7252		.7252	0.0		.7252	0.0	0.0	7252	0.0	0.0	0.0
79	34°35'02	135°29'06	3.52	+11.4	(+0.20	.7210	−0.15	.7211	−0.1		.7211	0.0	+0.1	7209	−0.2	−0.2	−0.1
80	34°31'51	135°26'14				.7177		.7179	−0.2		.7180	−0.1	−0.3	7177	−0.3	−0.2	−0.5
81	34°27'36	135°22'24	3.26	+14.9	−0.20	.7137	0.14	.7138	−0.1		.7139	+0.1	+0.2	7137	−0.2	−0.1	−0.3
82	34°24'07	135°19'50	18.38	+15.1	0.20	.7058	0.20	.7059	−0.1		.7060	+0.1	+0.2	7058	−0.2	−0.1	−0.3
83	34°21'13	135°14'91									.7024			7022	−0.2		
84	34°19'26	135°09'81									.6974			6973	−0.1		
85	34°14'22	135°11'28		(+17.9		.6984		.6985	−0.1		.6987	+0.2	+0.3	6984	−0.3	−0.1	−0.4
86	34°14'32	135°10'61	2.74							0.02	.6978			6978			
87	34°14'54	135°13'12	5.79							0.25	.7028			7028	−0.1		
88	34°15'00	135°19'33	22.97							0.20	.7120						
89	34°15'45	135°22'87	40.21							0.22	.7061			7062	−0.1		
90	34°16'29	135°26'21	58.22							0.15	.7043			7045	−0.1		
91	34°17'37	135°29'62									.7003			7005	+0.2		
92	34°18'10	135°33'08	67.87							0.45	.7000			7011	+1.1		
93	34°18'75	135°36'51	84.84							0.42	.7006			7007	+0.3		
94	34°19'80	135°39'75									.6955			6955	0.0		
95	34°25'54	135°43'40												6970			
96	34°30'62	135°44'88												7207			
97	34°30'54	135°47'83									.7261			7251	−1.0		
98	34°32'97	135°47'73									.7345			7343	−0.2		
99	34°35'70	135°48'00									.7330			7326	−0.4		
100	34°42'85	135°31'08	4.2146	+4.9			0.0	.7254			.7254	0.0		7253	−0.1	+0.1	
101	34°44'85	135°33'22	5.4157	+2.2			+0.20	.7250									
102	34°45'03	135°32'47	5.5086	+4.5			−0.08	.7277									
103	34°44'57	135°31'65	3.6198	+5.5			−0.10	.7285			.7284	−0.1		7285	+0.1	0.0	
104	34°44'30	135°31'43	3.4582	+4.6			+0.10	.7272									
105	34°44'15	135°31'68	2.9874	+5.9			+0.09	.7284									
106	34°43'65	135°31'00	4.5787	+5.8			+0.20	.7271									
107	34°43'77	135°31'37	10.3654	+6.1			−0.10	.7265			.7264	−0.1		7264	0.0	−0.1	
108	34°43'40	135°30'37	3.3339	−2.0			−0.06	.7194			7192	−0.2		7191	−0.1	−0.1	
109	34°44'10	135°29'50	2.4332	−8.2			−0.13	.7144			.7144	0.0		7143	−0.1	−0.1	
110	34°43'65	135°30'02	2.5552	−5.6			+0.09	.7163									
111	34°43'23	135°29'33	1.7706	−8.2	—	—	+0.18	.7133	—	—	.7132	−0.1	—	.7134	−0.2	−0.3	
112	34°43'13	135°28'73	1.2730	−9.4	—	—	+0.80	.7119	—	—	.7119	0.0	—	.7120	−0.1	−0.2	
113	34°43'45	135°28'32	2.4875	−10.1	—	—	+0.26	.7114	—	—	.7114	0.0	—	.7114	0.0	0.0	
114	34°42'77	135°27'97	1.7371	−10.1	—	—	+0.15	.7108	—	—	—	—	—	—	—	—	
115	34°42'43	135°27'88	1.8791	−9.6	—	—	+0.13	.7107	—	—	.7108	+0.1	—	.7109	−0.1	−0.2	
116	34°42'07	135°27'33	1.2154	−9.2	—	—	−0.02	.7108	—	—	—	—	—	—	—	—	
117	34°42'78	135°27'03	2.3946	−10.1	—	—	+0.50	.7103	—	—	.7102	−0.1	—	.7102	0.0	−0.1	
118	34°42'17	135°26'87	0.5545	−9.5	—	—	+0.10	.7107	—	—	.7106	−0.1	—	.7106	0.0	−0.1	
119	34°41'62	135°26'52	1.6246	−8.8	—	—	0.0	.7105	—	—	—	—	—	—	—	—	
120	34°42'53	135°26'30	0.8954	−10.3	—	—	+0.15	.7104	—	—	.7103	−0.1	—	.7104	+0.1	0.0	
121	34°42'13	135°31'35	7.4058	+6.4	—	—	−0.10	.7252	—	—	.7254	+0.2	—	.7253	−0.1	+0.1	
122	34°43'32	135°32'87	3.6701	+3.7	—	—	+0.21	.7249	—	—	.7249	0.0	—	.7249	0.0	0.0	
123	34°43'42	135°31'97	3.1932	+6.0	—	—	+0.02	.7275	—	—	.7274	−0.1	—	.7274	0.0	−0.1	
124	34°42'53	135°33'17	2.4647	+3.1	—	—	+0.19	.7234	—	—	.7234	0.0	—	.7236	+0.2	+0.2	
125	34°41'53	135°34'02	4.1267	+0.5	—	—	+0.01	.7191	—	—	—	—	—	—	—	—	
126	34°41'55	135°32'58	3.7462	+5.1			+0.04	.7238			.7236	+0.2		7236	−0.2	−0.2	
127	34°41'45	135°31'82	4.6735	+6.3			−0.18	.7247			.7249	−0.2		7248	−0.1	−0.3	
128	34°39'43	135°33'52	4.0270	+2.1			−0.12	.7178			.7178	0.0		7178	−0.2	−0.2	
129	34°39'03	135°32'38					−0.14	.7183			.7182	−0.1		7180	−0.2	−0.3	
129.1	"	"					−0.12	.7184						7184		−0.1	
129.2	"	"						.7186									
130	34°41'00	135°31'28				.7209		.7210	−0.1		.7210	0.0	+0.1	7210	0.0	0.0	+0.1
131	34°40'63	135°32'08						.7230			.7228	−0.2		7228	−0.2	−0.2	
131.1	"	"						.7208									
132	34°42'45	135°29'72	2.0817	−7.2			−0.07	.7131			.7131	+1.0		.7131	0.0	(+1.0)	
133	34°41'70	135°28'67	1.6020	−7.8			−0.07	.7116			.7116	0.0		.7116	0.0	0.0	
134	34°41'12	135°28'88	1.9294	−7.1			−0.17	.7114			.7119	+0.5		.7120	+0.1	+0.6	
135	34°41'78	135°30'20	3.6558	−3.6			−0.25	.7153			.7154	+0.1		.7153	−0.1	0.0	
136	34°41'12	135°29'80	3.5417	−4.8			−0.11	.7134			.7135	+0.1		.7136	+0.1	+0.2	
137	34°40'82	135°30'37	5.3761	−0.7			−0.29	.7168			.7168	0.0		.7170	+0.2	+0.2	
138	34°39'98	135°30'55	5.4836	−2.8			−0.19	.7189			.7190	+0.1		.7192	+0.2	+0.3	
139	34°40'85	135°27'82	2.2406	−9.2			−0.18	.7080			.7080	0.0		.7080	0.0	0.0	
140	34°40'67	135°26'52	1.2391	−8.0			−0.15	.7094			.7116	+2.2		.7116	+2.2	+2.2	
141	34°40'08	135°26'35	1.1240	−10.1			−0.10	.7097			.7113	−1.6		.7113	−0.3	−1.9	
142	34°39'77	135°26'22	1.4845	−10.7			−0.40	.7055			.7061	+0.6		.7061	−0.2	+0.4	
143	34°39'60	135°28'03	1.0047	−6.5			−0.17	.7128			.7128	0.0		.7128	0.0	0.0	
144	34°39'08	135°26'35						.7099		7.04	.7100	+1.1		.7100	−0.1	+1.0	
145	34°39'30	135°26'10	7.2		0.0	7091	−0.16	.7099	+1.2	new in IV	.7103	+0.4	+1.6	.7102	+0.1	+0.5	+1.6
146	34°39'05	135°28'63	1.1721	−2.6			−0.19	.7137			.7140	−0.3		.7140	0.0	−0.3	
147	34°37'53	135°28'20	2.4847	−0.7			−0.12	.7145			.7134	+1.1		.7138	−0.4	+0.7	
148	34°37'93	135°27'38	2.0361	−2.2			−0.10	.7111			.7113	−0.2		.7113	0.0	−0.2	
149	34°40'15	135°28'45	0.8776	−11.3			−0.24	.7081			.7084	−0.3		.7083	+0.1	−0.2	
150	34°39'97	135°29'05	1.0051	−3.4			−0.27	.7150			.7154	−0.4		.7153	−0.1	−0.3	
151	34°39'12	135°30'52	3.6837	+3.6			−0.44	.7189			.7187	+0.2		.7188	−0.1	+0.1	
152	34°38'92	135°29'58	2.0960	+1.3			−0.45	.7164			.7166	−0.2		.7167	−0.1	−0.3	
153	34°38'18	135°29'67	3.1574	+2.3			−0.26	.7167			.7166	+0.1		.7166	0.0	+0.1	
154	34°37'97	135°31'03	14.6970	−5.5			−0.04	.7164			.7164	0.0		.7165	−0.1	−0.1	
155	34°37'88	135°32'45	5.6525	−4.8			−0.06	.7129			.7128	+0.1		.7128	0.0	−0.1	
156	34°36'68	135°32'30	7.3871	+8.1			−0.15	.7160			.7161	−0.1		.7161	0.0	−0.1	
157	34°37'58	135°29'73	3.6278	+4.0			−0.27	.7147			.7144	+0.3		.7145	−0.1	+0.2	
158	34°37'20	135°28'10	3.0514	−1.4			−0.13	.7142									
159	34°36'88	135°29'54	3.2631	+6.6			−0.35	.7185			.7186	−0.1		.7187	−0.1	−0.2	
160	34°36'47	135°31'02	12.8134	+10.2			−0.01	.7196			.7196	0.0		.7197	−0.1	−0.1	
161	34°36'58	135°28'92	2.9724	+5.4			−0.01	.7170			.7173	−0.3		.7173	0.0	−0.3	
162	34°36'08	135°29'52	3.6134	+0.7			−0.25	.7257			.7258	−0.1		.7258	0.0	−0.1	

Notices on Table

*1. Elevations of the stations of from No. 0 to No. 99 are obtained from the map published by the Geographical Survey Institute and those of from No. 100 to No. 162 are referred to the results of precise levelling. O.P. is adopted as reference level, made by the Bureau of Planning of Ōsaka Municipal Office in 1931.

*2. The international formula is adopted as the reference gravity formula.

*3. This column means the elevation difference between the top of bench mark and the lower end of the gravimeter stand.

*4. The calculation of the absolute value of gravity at each station is based on the assumption that the absolute gravity value at the old Astronomical Institute of Kyoto University is 979.7230 gal and this value is invariable with time.

*5. All values in bracket are considered to be uncertain.

Memoirs of the College of Science, University of Kyoto, Series A,
Vol. XXVII, No. 3, Article 5, 1955

SOME REMARKS ON THE OPERATION OF THE SELF-CONTROLLING INFRA-RED SPECTROPHOTOMETER

BY

Hisao YAGI

Department of Physics

(*Received July 11, 1955*)

ABSTRACT

In order to operate the infra-red spectrophotometer automatically, proper attention should be given to the facts that the resolving power, scanning speed of wavelength and the signal-to-noise ratio of the spectrometer are not mutually independent but are related in a complicated manner. It will be shown, however, that their mutual dependence can be expressed by a somewhat simple formula.

1. Introduction

The sources of limitations in the resolving power of a recording monochromator may be divided into two groups; namely, those concerning with the optical conditions of the monochromator, which are present even at infinitely narrow slit-width, and those relating to the electrical conditions, such as the signal-to-noise ratios of the receiving system and the scanning speed of wavelength of the recording spectrophotometer.

The optical factors have already been discussed in detail by Brodersen (**1**). Moreover, in practice a considerably wide slit-width has to be chosen in order to maintain a certain value of the signal-to-noise ratio of receiving system, so that there is no meaning to pursue along this way indefinitely.

Therefore, the second group, i. e. electrical conditions will be mainly discussed in the following pages in order to get conditions for good resolution and recording accuracy.

2. Condition for wavelength scanning

The most important condition for driving a monochromator is to scan the wavelength with constant time T per spectral slit-width. Let the dispersed image of the entrance slit be moved past the exit slit at a linear speed of $fd\phi/dt$, where $d\phi/dt$ is the rate of rotation of the scanning Littrow mirror and f the focal length of collimator (see Fig. 1).

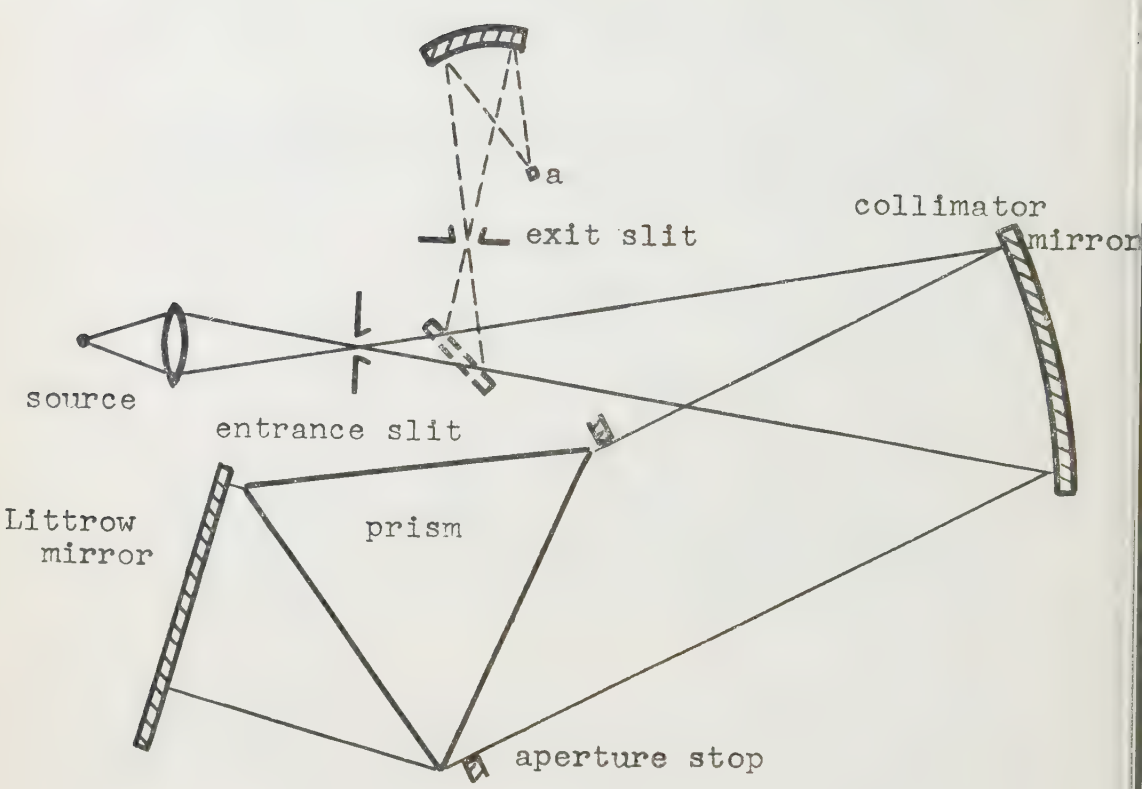

Fig. 1. Optical layout of infra-red monochromator.

The spectral slit-width s is proportional to the ratio of the geometrical slit-width W_λ to the linear dispersion L_λ of the prism taken as constant over the wavelength interval concerned in the plane of the exit slit, namely:

$$s=a_1 W_\lambda / L_\lambda , \tag{1}$$

where a_1 is a constant. Since, however,

$$L_\lambda = a_2 D_\lambda f , \tag{2}$$

where D_λ is the angular dispersion and a_3 is another constant, the spectral slit-width becomes

$$s=\frac{a_1 W_\lambda}{a_2 D_\lambda f} . \tag{3}$$

For the angle $\Delta\phi$ through which the scanning system must be turned in order to scan a spectral slit-width s, we have

$$\Delta\phi = a_3 D_\lambda s , \tag{4}$$

which, by (3), becomes

$$\Delta\phi = a_4 W_\lambda / f , \tag{5}$$

where a_3 and a_4 are both constants.

Therefore, in order to get a constant scanning time T per spectral slight-width, we should have

$$\frac{d\phi}{dt} = \frac{\Delta\phi}{T} = \frac{a_4 W_\lambda}{f T} , \tag{6}$$

namely, the rate of drive $d\phi/dt$ of dispersing system must be proportional to the geometrical slit-width, independently of dispersion.

3. Relation between wavelength scanning time T and response of electronic system

Tet τ be the response time of the receiving system, including the associated circuits, and $\Delta\lambda$ be the wavelength interval scanned in a time P. Then, the smallest wavelength interval $d\lambda$ by which two signals can be separated and clearly resolved, is determined by

$$\frac{d\lambda}{\tau} = \frac{\Delta\lambda}{P} .$$

Using the conventional optical definition for resolving power it follows that the resolving power R_{scan} in the scanning system is given by

$$R_{\text{scan}} = \frac{\lambda}{d\lambda} = \frac{\lambda P}{\tau \Delta\lambda} . \tag{7}$$

Since, on the other hand, $\Delta\lambda/P = f d\phi/dt$, we get, using (6),

$$R_{\text{scan}} = \alpha \frac{\lambda T}{\tau W_\lambda} , \tag{8}$$

where α is a constant of proportionality.

Thus, we see that the resolving power in the scanning system is proportional to wavelength λ and scanning time T and inversely proportional to response time τ and geometrical slit-width W_λ. It seems that this resolving power can be raised by decreasing both τ and W_λ, but one cannot decrease τ indefinitely not only from the practical standpoint but also for the reason that the signal-to-noise ratio decreases in proportion to $\tau^{\frac{1}{2}}$ (**2**). Also, the slit-width W_λ cannot be decreased indefinitely, because the slit-width is controlled automatically in order to keep the energy passing through the second slit approximately constant in the recording spectrophotometer.

In this connection, therefore, the relation between the slit-width and the signal-

to-noise ratio is important. Referring to Fig. 1, which shows the optical design factors, the energy flux in the spectral band $d\lambda$ passing through the entrance slit and the aperture stop is given by $\pi J_\lambda hWN^2 d\lambda$, where J_λ is the source radiation per cm^2 per steradiation per unit $\Delta\lambda$ at wavelength λ, h the height of the slit, W the width of the slit and N the numerical aperture of the collimator and aperture stop. The dispersing element spreads this spectral band over a width $fD_\lambda d\lambda$ in the plane of the exit slit, but the portion falling on the second slit passes to the receiver. Thus, the flux which generates the signal in the receiver is given by

$$E_s = \frac{W}{fD_\lambda d\lambda} \times \emptyset \pi J_\lambda hWN^2 d\lambda ,$$

where an optical transmission factor $\emptyset$ has been added in order to account for losses due to absorption and unwanted reflections. Since the real slit-width W is proportional to the geometrical slit-width W_λ, we may finally put

$$E_s = \beta \frac{J_\lambda W_\lambda^2}{D_\lambda} , \tag{9}$$

where β is a constant of proportionality.

Empirically the thermal agitation noise E_n in the receiver of optimum design is given by (2)

$$E_n = ka^{\frac{1}{2}} , \tag{10}$$

where a is the area of receiver, E_n is expressed in terms of the incident flux required to produce a signal voltage equal to the RMS value of the noise voltage, and k is a constant depending on the type of construction, materials employed and the speed of response of measuring system. Dividing (9) by (10), we obtain

$$\frac{E_s}{E_n} = \frac{\delta J_\lambda W^2}{D_\lambda k \sqrt{a}} , \tag{11}$$

where δ is a constant of proportionality. Since, as mentioned before, E_s/E_n decreases in proportion to $\tau^{\frac{1}{2}}$, we may ultimately put the relation between the slit-width and the signal-to-noise ratio in the form:

$$\frac{E_s}{E_n} = \kappa \frac{\tau^{\frac{1}{2}} W_\lambda^2}{D_\lambda} , \tag{12}$$

where κ is a constant of proportionality. We see from this equation that the signal-to-noise ratio becomes large when W_λ is large, but, according to Eq. (8) R_{scan} becomes small in this case.

Taking the above two formulae (8) and (12) into consideration, we obtain the following conditions for operation of recording spectrophotometer.

(a) High resolution is obtained by slow scanning speed, fast response time and narrow slit-width.

(b) Accurate transmission value is obtained by slow response time and wide slit-width.

These two conditions are not consistent with each other, however. The optimum solutions may be obtained by widening the slit of the spectrometer until the optical and electrical resolving power become equal to each other for a particular scanning time T. So, the most desirable condition for the user, i. e., high resolution, fast scanning as well as accurate transmission value may be established only by the suitable arrangement of T, τ, W_λ and moreover signal amplifier gain factor G as in the case of the Beckman Spectrophotometer IR-2T, which will be described precisely in the next paragraph.

3. Application to the Beckman Spectrophotometer

We had the opportunity to handle with thd Beckman IR-2T Infra-red Spectrophotometer and examined its construction in detail. Now, we shall begin with the main feature of this instrument.

The Beckman Infra-red Spectrophotometer is a single beam monochromator instrument employing "*Memory Standardization*" to obtain direct transmittancy recordings on the pen recorder. The 100% reference level for direct transmittancy recording is automatically determined by making a "standardization run" against the definite light source, especially containing the empty or solvent filled sample cell in the optical path of the monochromator. The automatic slit control system maintains the amplified photoreceiver signal E_λ at a constant value E_0, and is so arranged that the electric signal for the function of the slit-width versus wavelength is recorded on a tape recorder. Thus, the following relation for E_λ is obtained:

$$E_\lambda = E_0 = \gamma W_\lambda G F(W_\lambda), \tag{13}*$$

where G is the thermocouple signal amplifier gain factor and γ is a constant.

On subsequent "play back", the signal from the tape recorder controls the slit and wavelength servo-motors, precisely reproducing the standardizing conditions so that absorption spectra from a sample are recorded in transmittancy when the sample is inserted into the optical path of the spectrometer at "play back run". So, in the case of the Beckman Spectrophotometer, high resolution and accurate transmission

---

* $F(W_\lambda)$ is the correction term of G as introduced according to the following reason. In the Beckman IR-2T control system, it is necessary to drive an adjustable attenuator with the slit-motor, so that the percent error per revolution of the slit-motor is constant regardless of slit setting, since the slit-width versus rotation is non-linear. The factor is automatically controlled according to the slit-width.

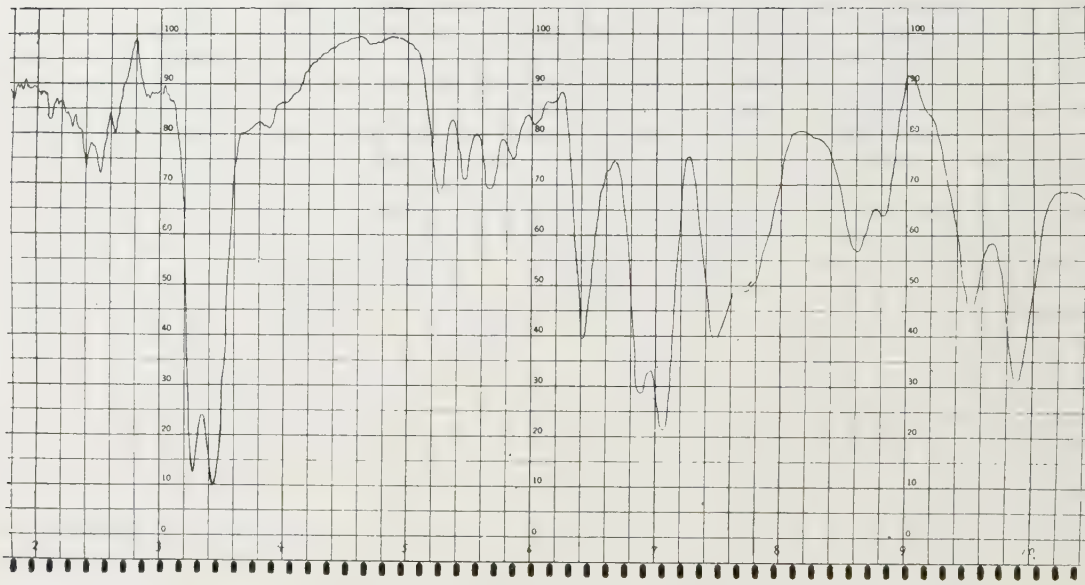

Fig. 2. Infra-red absorption of polystyrene film taken by the Beckman

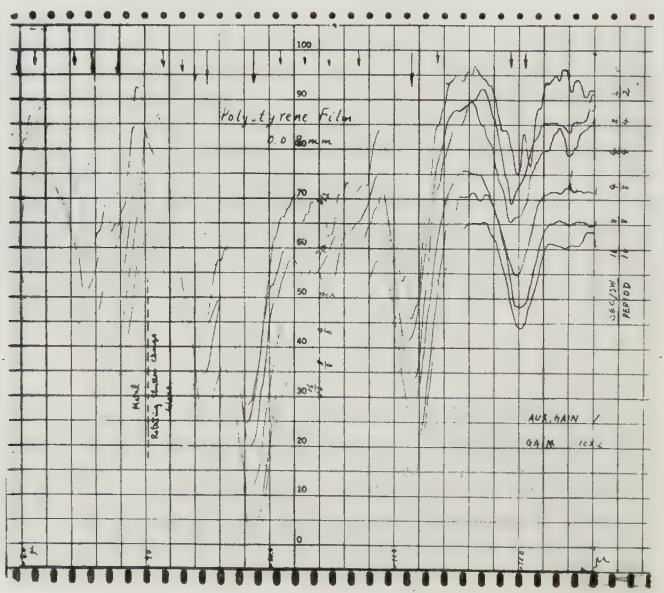

Fig. 3. Infra-red absorption curves of polystyrene film taken with the gain factor 1, 2, 7 and 10.

are obtained, considering the above-described formulae (8), (12) and (13).

By using the Beckman Infra-red Spectrophotometer IR-2T, we measured the absorption spectra of polystyrene film at various values of the scanning speed T, the

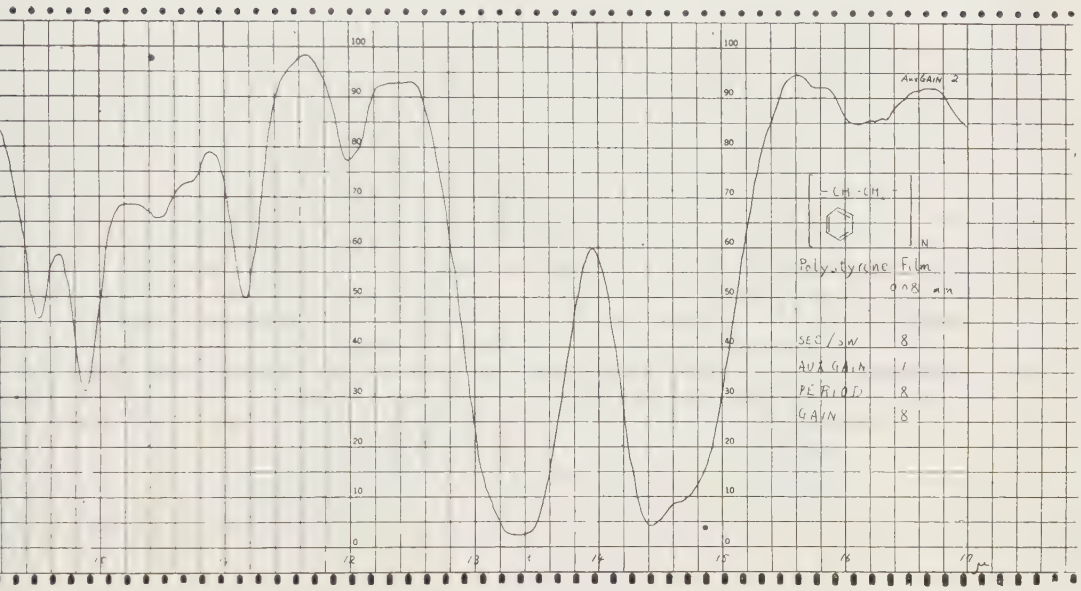

Infra-red Spectrophotometer IR-2T (using KBr 60° prism).

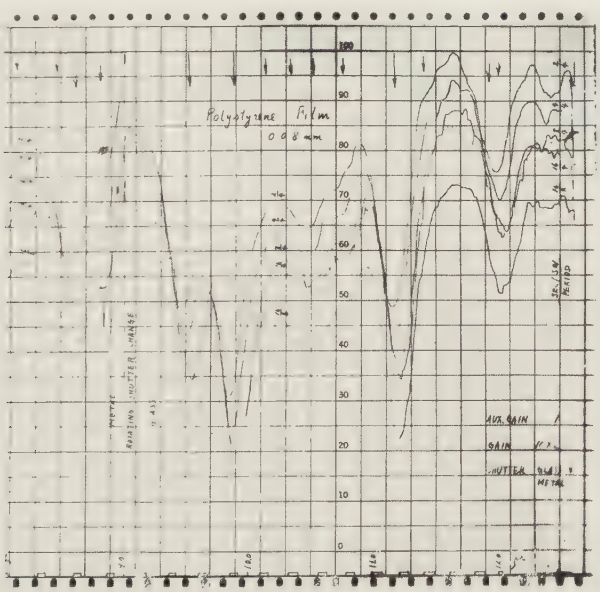

Fig. 4. Infra-red absorption curves of polystyrene taken with Sec./SW Period $= \frac{16}{8}, \frac{16}{4}, \frac{8}{4}, \frac{4}{4}$ and $\frac{2}{4}$.

response time τ and the gain G. The results are shown in Figs. 2, 3, 4 and 5, as well as in Tables 1, 2 and 3. In these tables are given the absorption values of the polystyrene film, which have been measured from Figs. 3, 4 and 5.

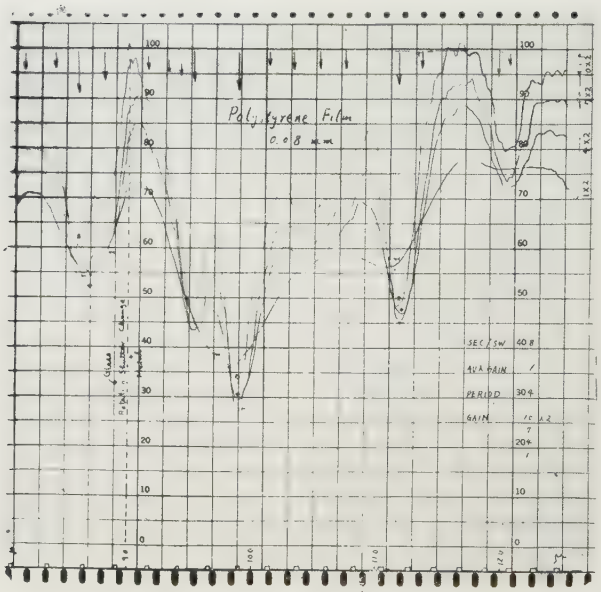

Fig. 5. Infra-red absorption curves of polystyrene taken with $\frac{\text{Sec./SW}}{\text{Period}} = \frac{16}{16}, \frac{8}{8}, \frac{4}{8}, \frac{4}{4}, \frac{2}{4}$ and $\frac{2}{2}$.

Table 1. Absorption of polystyrene film (0.08 mm)

Wavelength in microns	Gain			
	1	4	7	10
8.6	18	28	30	31.5
8.8	—	—	14	16.5
9.5	30	23.5	29.7	32.5
9.9		25	33	37.5
		6.3	—	—
10.5	—	—	10	15
			3	6
11.1	12	31.8	40.3	43.7
12	1.1	14.9	17.6	18.1

Aux. Gain $\frac{1}{2}$, Sec./SW(T) 8, Period (τ) 4.

Table 2. Absorption of polystyrene film (0.08 mm)

Wavelength in microns	T/τ				
	16/8	16/4	8/4	4/4	2/4
8.6	35	33	34	32.5	29.5
8.8	16.5	15	20.3	16.5	15.7
9.5	33.5	34	33.5	30	27.5
9.9	35.5	37.5	36.5	35	38
	2	—	2	1	—
10.5	11.5	11.5	12.5	10.5	10.5
	5	4	5	4	3
11.1	42.7	42	43.7	42.7	41.5
12	20.5	20.7	20.5	22	22.5

Aux. Gain $\frac{1}{2}$, Gain 10.

From these results it can obviously be seen that the user of the infra-red spectrophotometer must control the three variables: (1) resolution, (2) signal-to-noise ratio, and (3) speed of scanning over wide ranges, in order to obtain full power and flexibility from the spectrophotometer.

Resolution R_{scan} is the first of the three important variables. We need high resolution if we wish to study highly detailed spectra. If we scan fast at high

Table 3. Absorption of polystyrene film (0.08 mm)

Wavelength in microns	T/τ					
	16, 16	8/8	4/8	4/4	2/4	2/2
8.6	36.5	34	31.5	34.5	28	30
8.8	16	15.5	14.7	16.5	13.5	18
9.5	30.5	34.5	28.5	33.5	26.5	30
9.9	35	36.5	29.5	35.9	29	37.5
		—	—	3	—	5
10.5	10.5	10	8.5	12.5	12	15
	4	3	—	4	—	7
11.1	43	41	40	46.5	42.5	44.5
12	19	20	18.5	22	19.5	21.5

Aux. Gain $\frac{1}{2}$, Gain 10.

resolution (i.e., R_{scan} is large and T is small in the formula (8)), we must accept a chart record with relatively inaccurate transmission value, because the record will be noisy (i.e., τ is small and then E_s/E_n becomes small in (12)). In Fig. 4, the record is very noisy when T/τ is equal to 16/4. If we scan slowly at high resolution (i.e., both R_{scan} and T are large in (8)), the chart record will be free of noise and will have accurate transmission values, but it will take somewhat longer time to make the spectrogram (see Fig. 5). These compromises will be made with any spectrophotometer.

The signal-to-noise ratio E_s/E_n is the second of the three important variables. If the signal is large compared with the noise, the chart record will be smooth and successive spectrograms of the same sample will match each other closely, and so we can obtain accurate transmission readings or the highest resolution (see Table 1). We cannot have all these advantages at high scanning speed. Accurate transmission readings combined with high scanning speed give rise to the loss of resolution, because E_s/E_n is large and T is small and hence R_{scan} is small: high resolution combined with high scanning speed results in a noisy record and hence results in the loss of accuracy in transmission readings, as described before. In Figs. 4 and 5, the values of T/τ are compared with each other, and these relations may be understood easily.

Scanning speed T is the last of the three important variables, and refers to the time required for the light of any particular wavelength to traverse the exit slit as the infra-red spectrum sweeps across the slit plates. The scanning speed for a series of runs is measured in seconds per spectral slit-width. The instrument automatically changes the speed of the wavelength drive as the slit-width changes to give the selected speed in seconds per slit-width. This allows us to traverse each slit-width in the time proportional to the response period of the recording system, where the proportional constant depends on the nature of the spectrum. Such scanning rates will give maximum efficiency (**3**).

Moreover, we lose accuracy if the response period is longer than the time taken to scan one spectral slit-width, because the chart will not be able to follow the changes in absorption fast enough. Empirically, in our instrument, when for sharp spectra

as in the case of gases the proportional constant T/τ is equal to unity, we have good recording (see Fig. 5). For broad spectra as in the case of liquids, T/τ is equal to 2, except in regions of strong sharp back ground absorption where the constant is equal to unity.

Then, in addition to the three important variables mentioned above, we must especially refer to the relations between amplifier gain factor G and slit-width W_λ according to the formula (13).

In order to keep high resolution, we must use narrow slit, high amplifier gain and a short response period of the recording system, according to formulae (8) and (13). The combination of high amplifier gain and short response periods causes noisy or randomly irregular chart record.

We can obtain a quiet chart record, i. e., accurate transmission values, by using low amplifier gain together with either of wide slit and long response periods of the recording system or together with these two, according to the formulae (12) and (13). Wide slits, though giving quiet records, reduce resolution (see Fig. 3). Thus it is evident that we lose resolution or accuracy of transmission readings if we go to the case of extremely fast scanning. Nevertheless, if we are more interested in finding the main absorption peak of the sample than in exact transmission values or resolution and want to obtain results in a hurry, rapid scanning may be most useful.

5. Summary

(1) Resolution is automatically kept to a maximum as determined by the chosen amplification G, response period τ and scanning speed T.

(2) Transmittancy recording accuracy is limited only by signal-to-noise ratio and linearity of the used amplifier in the single beam optical system such as the Beckman IR-2T Spectrophotometer.

(3) Recording speed may automatically be maintained at a maximum consistent with the resolving power of the spectrophotometer and chosen recording condition.

To get versatility in the infra-red spectrophotometer, its user must change the speed of scanning T, the response time τ and the gain factor G over wide range and must set the spectrophotometer in the best condition as stated above.

The planning of this work was stimulated when the opportunity was given to the writer to handle with the Beckman Infra-red Spectrophotometer purchased for Professor Yôichi Uchida with a grant-in-aid for scientific research of the Ministry of Education. The writer wishes to express his cordial thanks to Professor Uchida for his kind advices during the course of this work.

REFERENCES

1. S. Brodersen, J. O. S. A. **43** (1953), 877.
2. B. W. Bullock and S. Silverman, J. O. S. A. **39** (1949), 200 ; **40** (1950), 608.
   D. F. Horning, Rev. Sci. Inst. **18** (1947), 474.
3. R. R. Brattain, Phys. Rev. **60** (1941), 164.
4. G. E. Valley and H. Wallman, *Vacuum Tube Amplifier* (McGraw-Hill, 1948).

CONTENTS

The Influence of Vortices upon the Drag experienced by an Elliptic Cylinder moving through an Inviscid Liquid

By *S. Tomotika and H. Fujikawa* 227

Seismometric Investigation of the Earth's Interior. Part II. On the Structure of the Earth's Crust

By *Yoshimichi Kishimoto* 243

Study on Change of Gravity with Time. Part I. On the Tidal Variation of Gravity

By *Tokio Ichinohe* 289

Study on Change of Gravity with Time. Part II. Repeated Gravity Surveys in the Kinki District

By *Tokio Ichinohe* 317

Some Remarks on the Operation of the Self-controlling Infra-red Spectrophotometer

By *Hisao Yagi* 335

Printed by NIPPON INSATSU SHUPPAN

Fukushima, Osaka